AEDC-TR-70-26

copy 2

INTERNAL MHD CHANNEL FLOWS INCLUDING HALL EFFECT AND VARIABLE FLUID PROPERTIES

William T. Snyder and James R. Maus

The University of Tennessee Space Institute
Tullahoma, Tennessee

February 1970

ARNOLD ENGINEERING DEVELOPMENT CENTER
AIR FORCE SYSTEMS COMMAND
ARNOLD AIR FORCE STATION, TENNESSEE

NOTICES

When U. S. Government drawings specifications, or other data are used for any purpose other than a definitely related Government procurement operation, the Government thereby incurs no responsibility nor any obligation whatsoever, and the fact that the Government may have formulated, furnished, or in any way supplied the said drawings, specifications, or other data, is not to be regarded by implication or otherwise, or in any manner licensing the holder or any other person or corporation, or conveying any rights or permission to manufacture, use, or sell any patented invention that may in any way be related thereto.

Qualified users may obtain copies of this report from the Defense Documentation Center.

References to named commercial products in this report are not to be considered in any sense as an endorsement of the product by the United States Air Force or the Government.

INTERNAL MHD CHANNEL FLOWS INCLUDING HALL EFFECT AND VARIABLE FLUID PROPERTIES

William T. Snyder and James R. Maus

The University of Tennessee Space Institute
Tullahoma, Tennessee

FOREWORD

The work reported herein was sponsored by Arnold Engineering Development Center (AEDC), Air Force Systems Command (AFSC), Arnold Air Force Station, Tennessee, under Program Element 6240533F, Project 8950, Task 12.

The results of research presented were obtained by The University of Tennessee Space Institute under Contract F40600-67-C-0001, Task I. The manuscript was submitted for publication on November 26, 1969.

The reproducibles used for the reproduction of this report were supplied by the authors.

This technical report has been reviewed and is approved.

Thomas G. Horn
2d Lt, USAF
Research Division
Directorate of Plans
and Technology

Harry L. Maynard
Colonel, USAF
Director of Plans
and Technology

ABSTRACT

An analysis is presented of MHD channel flow with Hall effect and variable fluid properties. Because of the highly nonlinear nature of the governing conservation equations, a straight numerical analysis of the equations is followed based on the implicit finite difference method. The analysis considers the two-dimensional flow in the electric field plane in which the channel walls are electrode surfaces. Because of the presence of the Hall effect, a transverse pressure gradient is induced in the flow which necessitates the use of two equations of motion in the longitudinal and transverse directions. The analysis model employed is the so-called slender channel model in which the boundary layer forms of the equations of motion are applied across the entire channel width. Because the boundary layer equations are parabolic, it is possible to integrate the equations in a forward marching manner by starting with initially prescribed velocity and enthalpy profiles at the channel entrance. Numerical results are presented for the velocity and enthalpy profile development from initially assumed profiles of velocity and enthalpy at the channel entrance. Initial velocity and enthalpy profiles which are typical of both laminar and turbulent flows are considered. In addition to the calculation of profiles, the voltage drop across electrodes is calculated by integration of the conductivity profile across the channel.

TABLE OF CONTENTS

LIST OF ILLUSTRATIONS

Figure

NOMENCLATURE

B_z	Applied magnetic field
E_x, E_y	Electric field components
f,g	Functions illustrating finite difference formulae, Eqs. (25)-(31)
h	Enthalpy
h_{w1}, h_{w2}	Enthalpy at lower and upper walls, respectively
Ha	Hartmann number, Eq. (13)
I_x	Total electric current, Eq. (20)
J_x, J_y	Current density components
m,n	Grid point notation, Figure 2
P	Pressure
Pr	Prandtl number
Re	Reynolds number, Eq. (13)
u,v	Velocity components
w	Channel height, Figure 1
x,y	Space coordinate, Figure 1
γ	Heat capacity ratio
η	Dimensionless space coordinate, Eq. (11)
μ	Viscosity
ρ	Density
σ	Electrical conductivity
σ_o	$\frac{\sigma}{1 + (\omega\tau)^2}$
Φ	Electrical potential, Eq. (8)
Φ_x, Φ_y	Dimensionless electric field, Eq. (13)
$\omega\tau$	Hall parameter

SECTION I

INTRODUCTION

Two promising areas of engineering applications of magnetohydrodynamics (MHD) have been defined in recent years, namely MHD power generation and MHD acceleration. The accelerator application has received serious study for several years as a technique for augmenting the performance of aerodynamic test facilities. The principal advantages of an MHD augmented test facility such as a shock tunnel are: (1) energy is added to a moving stream resulting in test section flows with stagnation pressure and temperature which would exceed those achievable in a reservoir because of material limitations, and (2) the energy is added as directed kinetic energy rather than thermal energy.

In order to design MHD augmented accelerators with specified performance characteristics, the prediction of the gas conditions in the accelerating and test regions is essential. Because of the extremely complex physical phenomena occurring in MHD devices, it is safe to say that at this stage of development, a complete theoretical description of the flow is not possible. Because of questions raised recently concerning the role of instabilities on the performance of MHD devices, it is at best an open question as to whether the traditional analytical tools of the fluid mechanician, namely the continuum partial differential conservation equations coupled with the electromagnetic field equations, are adequate to describe the flow in principle. In addition to the question of instabilities, other physical phenomena which make the analysis of MHD flows difficult are (1) the variation of thermodynamic and transport properties resulting in a strong coupling between the fluid mechanics and electromagnetic equations, (2) the two dimensionality of most flows of practical interest (small aspect ratio internal channel flows are actually three-dimensional), (3) the high nonlinearity of the governing equations, and (4) the possibility of turbulence occurring for sufficiently high Reynolds numbers.

Any analytical investigation of such complex physical phenomena as MHD flows requires the adoption of models which do not include all of the physical phenomena involved. For an analytical model to be useful, it must retain the features of those phenomena one wishes to focus attention on. For example, a knowledge of the rate of growth of wall boundary layers in MHD acceleration devices is important in evaluating

the performance of the device as well as determining the extent of the flow with reasonably uniform properties which could be used as a wind tunnel test flow.

The boundary layer equations themselves can be considered as an analytical model which focuses attention on that region of the flow in which the inertia and viscous terms are of equal importance. Given the boundary layer equations, there are then available several approaches for extracting the information on the boundary layer flow region contained in the equations. These methods include similarity solutions, integral methods, finite difference methods, and linearization methods of the Oseen approximation type. Still another method which has recently been applied by the authors (Ref. 1) to MHD boundary layer flows in internal channels is the slender channel model. In this method, the internal channel flow is not divided into a boundary layer - core flow region in which different equations are to be applied. Instead, the boundary layer form of the equations of motion are applied across the entire channel width with boundary conditions being applied at the channel walls. This method was also recently applied by Kitowski (Ref. 2) to analyze MHD flow in the entrance region of a parallel plate channel.

In the present investigation, the slender channel model is used to analyze MHD flow in the E-plane (the plane containing the electric field vector) of a two-dimensional channel including Hall effect. The channel walls thus correspond to the electrode walls of an MHD generator or accelerator. The emphasis is placed on the acceleration mode of operation in the present study.

SECTION II

PREVIOUS WORK

The interaction of an electrically conducting fluid media with applied electric and magnetic fields has been the subject of intense study over the past several years. A brief summary will be given of those investigations most pertinent to the present study.

The original theoretical investigation of magneto-hydrodynamic channel flow was conducted by Hartmann (3). This study was concerned with the fully developed flow of an incompressible fluid between parallel plane walls with a uniform magnetic field applied perpendicular to the flow. This is, of course, the basic Faraday generator or pump geometry and a number of authors have used this model to study in detail the effect of various modifications of the Hartmann problem. Eraslan (4) and Young (5) have examined the effect of variable electrical profiles. Snyder (6) used an Oseen linearization technique to explore the development of the flow in the entrance region of a parallel plate channel.

The equations for compressible, inviscid MHD channel flow were formulated by Resler and Sears (Ref. 7) using a quasi-one-dimensional approximation. Since the quasi-one-dimensional model involves more unknowns than equations, the streamwise variation of some of the independent variables must be specified before a solution can be obtained. Special cases for prescribed variations of electric field, magnetic field, channel area, etc. have been calculated.

The results of the quasi-one-dimensional analysis of compressible MHD channel flow provides free stream conditions that can be used in an analysis of the viscous layer adjacent to the channel walls.

The boundary layer flow adjacent to the electrodes in an MHD accelerator was studied by Kerrebrock (8). This investigation was concerned with compressible boundary layer flow and the effect of variable fluid properties was included. Similar solutions were obtained for a certain class of accelerator flows with constant free stream temperature. The solution showed that the heat transfer rates were much greater than would be the case for non-MHD flow.

The slender channel model differs from the usual boundary layer approach in that the boundary layer equations are applied across the entire channel rather than just in the vicinity of the wall. In this method the streamwise variation of the velocity, pressure, and temperature are given by the solution of the equations rather than by a separate inviscid analysis. This technique was first applied by Williams (9) to ordinary compressible, viscous flow in two-dimensional and axisymmetric slender channels.

The method was extended by Sonnerup (10) to MHD flows. Sonnerup investigated the two-dimensional, fully developed flow of a compressible, electrically conducting fluid in a slowly diverging channel. The confining boundaries of the channel were the electrode surfaces of an MHD generator. By a proper choice of channel geometry, the electromagnetic forces and the pressure forces were made to cancel. This, in turn, permitted the momentum equation to be uncoupled from the energy equation and reduced to an ordinary differential equation. An exact solution to this equation was obtained for the self-similar velocity profiles. The corresponding temperature profiles were generally non-similar.

Kubin and Smolin (11) investigated the two-dimensional, isothermal flow of an electrically conducting fluid in the presence of crossed electric and magnetic fields. The form of the governing equations was very similar to those of Williams (9). By tailoring the electric and magnetic field distributions, self similar velocity solutions were obtained.

The velocity and temperature distribution for magneto-gasdynamic acceleration flow was examined by Snyder and Maus (1). The governing equations were formulated in polar coordinates for steady, two-dimensional, laminar flow between slightly diverging insulator walls. The assumption was made that the dependent variables could be expressed in a separable form. This allowed the governing partial differential equations to be reduced to a pair of coupled, non-linear, ordinary differential equations. These equations were then integrated numerically to yield the velocity and temperature profiles. For certain ranges of the electromagnetic and gas dynamic parameters, the temperature distribution exhibited a marked excess near the wall. This was caused by the large joule heating and viscous dissipation effects in the region.

Kitowski (2) investigated the two-dimensional, compressible MHD flow in the entrance region of a parallel

plate channel. The slender channel model was used and the boundary layer equations were written in an implicit finite difference form developed by Flugge-Lotz and Blottner (12). The analysis was concerned with the flow between insulating walls and included the variation of transport properties. The finite difference equations were solved numerically to yield velocity and static enthalpy profiles along the channel.

None of the studies discussed to this point have included the Hall effect where an electrical current component is induced in the streamwise direction due to the electron velocity. This Hall current results in a much tighter coupling of the basic governing equations and thus complicates considerably the mathematical problem associated with the MHD flow.

The previous investigations on MHD flow including Hall effects can generally be classified into two categories according to whether the main emphasis of the study is on the electrodynamics or the fluid mechanics. In the former approach the gas dynamical variables are considered apecified and solutions are sought for the electric potential and current density distributions. These variables are governed by elliptic partial differential equations derivable from Maxwell's equations and the generalized Ohm's law. On the other hand, in the latter approach, solutions are sought for the fluid mechanical equations with the electrodynamic variables specified. It is the latter approach that is taken in the present investigation.

The studies of Celinski and Fischer (13) and Oliver and Mitchner (14) are examples of analyses where the electrodynamics of the MHD flow is emphasized. Celinski and Fischer examined the effect of finite size electrodes on the distribution of electrical parameters in MHD generators for a wide range of Hall parameter $\omega\tau$. The gas dynamical quantities, velocity and temperature were assumed constant throughout the channel. Numerical solutions were obtained to the partial differential equations describing the electric potential and current density distributions. The analysis of Oliver and Mitchner is somewhat similar to that of Celinski and Fischer except that the variation of the electrical conductivity was included.

Thw work of Sherman and Sutton (15) was one of the earliest fluid dynamic studies of MHD channel flow including Hall effects. This investigation dealt with the fully developed, incompressible flow between parallel

insulating wall, i.e., Hartmann flow with Hall effects. The results of this study showed that the streamwise velocity distribution changed from the characteristic Hartmann profile to a Poissuelle-like profile with increasing Hall parameter.

Snyder and Eraslan (16) studied the MHD flow of an incompressible fluid in the entrance region of a parallel plate channel including Hall effects. This analysis was an extension of Ref. 6 and used the same linearizing technique employed in that study. The results of this investigation showed that the entrance length increased with increasing values of the Hall parameter, $\omega\tau$.

Hale and Kerrebrock (17) were the first to consider both compressibility and the Hall effect in treating the boundary layer on the insulating wall of an MHD accelerator. Two models for the electrical conductivity variation were employed: an equilibrium model where the degree of ionization is determined by the local gas temperature and pressure, and a non-equilibrium model in which the electrical conductivity is strongly coupled to the electric field strength.

It was found that similar solutions could be obtained only for very restrictive conditions and local similarity was assumed. The partial differential equations of motion were thus reduced to ordinary differential equations. Some numerical difficulty was encountered in dealing with the resulting two point boundary value problem and for certain cases satisfactory convergence at the edge of the boundary layer was not obtained.

The results obtained by Hale and Kerrebrock indicated that the general effect of increasing the Hall parameter was to increase the average current near the wall leading to a thinner boundary layer, increased heat transfer, shear stress, and electrical losses.

Hunter (18) in a recent study, analyzed the boundary layer on the insulating walls of an MHD generator including Hall effects. The governing equations were written in modified Levy-Lees variables and non-similar solutions were obtained by numerically integrating the equations using an implicit finite difference method. The effect of the boundary layer growth on the inviscid flow field was accounted for through a displacement thickness correction.

The results of this investigation showed that the Hall effect has a rather pronounced influence on the flow in MHD

generators. It was found that the Hall current tends to cause boundary layer separation further upstream for the decelerating flow in a constant area generator. The energy dissipation due to joule heating was underpredicted when the Hall effect was not included.

SECTION III

FORMULATION OF THE PROBLEM

3.1 GOVERNING EQUATIONS

The geometry for the two-dimensional MHD flow in the E-plane is shown in Figure 1. The channel dimension in the z-direction is assumed to be infinite thus reducing the problem to a two-dimensional flow. The channel height, W(x), is assumed to be a specified function of x, and the magnetic field, B_z, is constant and is in the z-direction.

The assumption of small magnetic Reynolds number is made which implies that the equations of motion and the magnetic field equation are uncoupled. Thus the induced magnetic field effect on the equations of motion is neglected. Using the slender channel assumption means that the complete equations of motion, which are elliptic, are reduced to parabolic, boundary layer form. This means that the equations may be integrated in a marching fashion by starting with initial profiles.

With the inclusion of the Hall effect in the equations of motion, the transverse equation of motion must be included because of the Hall current induced transverse pressure gradient. The governing equations may be written as follows.

$$\rho^*\left(u^* \frac{\partial u^*}{\partial x^*} + v^* \frac{\partial u^*}{\partial y^*}\right) = - \frac{\partial P^*}{\partial x^*} + \frac{\partial}{\partial y^*}\left(\mu^* \frac{\partial u^*}{\partial y^*}\right) + J_y^* B_z^* \tag{1}$$

$$\rho^*\left(u^* \frac{\partial v^*}{\partial x^*} + v^* \frac{\partial v^*}{\partial y^*}\right) = - \frac{\partial P^*}{\partial y^*} + \frac{\partial}{\partial y^*}\left(\mu^* \frac{\partial v^*}{\partial y^*}\right) - J_x^* B_z^* \tag{2}$$

$$\rho^*\left(u^* \frac{\partial h^*}{\partial x^*} + v^* \frac{\partial h^*}{\partial y^*}\right) = u^* \frac{\partial P^*}{\partial x^*} + \frac{\partial}{\partial y^*}\left(\frac{\mu^*}{Pr} \frac{\partial h^*}{\partial y^*}\right)$$

$$+ \mu^*\left(\frac{\partial u^*}{\partial y^*}\right)^2 + \frac{J_x^{*2} + J_y^{*2}}{\sigma^*} \tag{3}$$

$$\frac{\partial(\rho^* u^*)}{\partial x^*} + \frac{\partial(\rho^* v^*)}{\partial y^*} = 0 \tag{4}$$

Equations (1)-(4) are respectively the two equations of motion, the energy equation, the continuity equation. These conservation equations must be supplemented with an equation of state, Ohm's law for the electric current, and a specification of viscosity, μ^*, conductivity, σ^*, Hall parameter, $\omega\tau$, and Prandtl number, Pr, as a function of pressure and temperature. In the present analysis, the Prandtl number and the heat capacity ratio, γ, will be taken as constant. An ideal gas equation of state will be assumed.

The equation of state and the components of electric current from Ohm's law can be written as

$$p^* = \left(\frac{\gamma-1}{\gamma}\right)\rho^* h^* \tag{5}$$

$$J_x^* = \frac{\sigma^*}{1 + (\omega\tau)^2}\left[(E_x^* - \omega\tau E_y^*) + B_z^*(v^* + \omega\tau u^*)\right] \tag{6}$$

$$J_y^* = \frac{\sigma^*}{1 + (\omega\tau)^2}\left[(E_y^* + \omega\tau E_x^*) + B_z^*(\omega\tau v^* - u^*)\right] \tag{7}$$

The electric current components given by Eqns. (6) and (7) introduce the electric field components as additional unknowns. An equation for the electric field potential can be derived from the relations

$$E_x^* = -\frac{\partial\Phi^*}{\partial x^*} \quad , \quad E_y^* = -\frac{\partial\Phi^*}{\partial y^*} \tag{8}$$

$$\frac{\partial J_x^*}{\partial x^*} + \frac{\partial J_y^*}{\partial y^*} = 0 \tag{9}$$

Equation (9) is the conservation of electric charge equation (current continuity). Combining Eqns. (6)-(9) gives

$$\frac{\partial^2\Phi^*}{\partial x^{*2}} + \frac{\partial^2\Phi^*}{\partial y^{*2}} = -\frac{\partial\Phi^*}{\partial x^*}\left[\frac{\partial\omega\tau}{\partial y^*} + \frac{1}{\sigma_o^*}\frac{\partial\sigma_o^*}{\partial x^*} + \frac{\omega\tau}{\sigma_o^*}\frac{\partial\sigma_o^*}{\partial y^*}\right]$$

$$+ \frac{\partial\Phi^*}{\partial y^*}\left[\frac{\partial\omega\tau}{\partial x^*} - \frac{1}{\sigma_o^*}\frac{\partial\sigma_o^*}{\partial y^*} + \frac{\omega\tau}{\sigma_o^*}\frac{\partial\sigma_o^*}{\partial x^*}\right]$$

$$+ B_z^*\left[\frac{\partial}{\partial x^*}(v^* + \omega\tau u^*) + \frac{\partial}{\partial y^*}(\omega\tau v^* - u^*)\right]$$

$$+ B_z^*(v^* + \omega\tau u^*)\frac{1}{\sigma_o^*}\frac{\partial\sigma_o^*}{\partial x^*}$$

$$+ B_z^*(\omega\tau v^* - u^*)\frac{1}{\sigma_o^*}\frac{\partial\sigma_o^*}{\partial y^*} \qquad (10)$$

where

$$\sigma_o^* = \frac{\sigma^*}{1 + (\omega\tau)^2}$$

Equation (10) is an elliptic equation describing the electric field potential and use of this equation requires the specification of boundary conditions for Φ^* or its normal derivative on a closed boundary. The terms on the right side of Eqn. (10) involve the fluid properties and thus there is a strong coupling of the electric field equations and the fluid mechanics equations. It is seen that the right side of Eqn. (10) becomes zero only if all fluid properties including velocity are constant. In this case, the equation reduces to Laplace's equation which is still elliptic. In order to solve the fluid mechanics and electric field equations simultaneously, an iteration procedure must be used in which a tentative solution to the fluid mechanics equations is obtained based on an assumed electric field distribution. From this solution, the fluid property dependent terms in Eqn. (10) may be evaluated and a solution for the electric field potential obtained. With this corrected solution to

the electric field, the fluid mechanics equations can then be solved again with the process being repeated as many times as desired.

Such an iteration procedure would be very time consuming, and was not used in the present investigation. An approximate method was used which will be discussed in detail later.

To account for the divergence of the channel walls as illustrated in Figure 1, a dimensionless transverse coordinate η is defined as

$$\eta = \frac{y^*}{w^*(x^*)} \tag{11}$$

Transforming from (x^*,y^*) coordinates to (x^*,η) coordinates can be done by utilizing the partial differential operators

$$\left(\frac{\partial}{\partial x^*}\right)_{y^*} = \left(\frac{\partial}{\partial x^*}\right)_{\eta} - \frac{\eta}{w^*}\frac{dw^*}{dx^*}\left(\frac{\partial}{\partial \eta}\right)_{x^*}$$

$$\left(\frac{\partial}{\partial y^*}\right)_{x^*} = \frac{1}{w^*}\left(\frac{\partial}{\partial \eta}\right)_{x^*} \tag{12}$$

Dimensionless variables are defined as follows.

$$\rho = \frac{\rho^*}{\rho_o} \quad x = \frac{x^*}{w_o} \quad u = \frac{u^*}{u_o} \quad v = \frac{v^*}{u_o} \quad w = \frac{w^*}{w_o}$$

$$\mu = \frac{\mu^*}{\mu_o} \quad h = \frac{h^*}{u_o^2} \quad Re = \frac{\rho_o u_o w_o}{\mu_o} \quad P = \frac{P^*}{\rho_o u_o^2} \tag{13}$$

$$\Phi_x = \frac{E_x^*}{u_o B_z^*} \quad \Phi_y = \frac{E_y^*}{u_o B_z^*} \quad \sigma = \frac{\sigma^*}{\sigma_o} \quad H_a = w_o B_z^* \frac{\sigma_o}{\mu_o}$$

The quantities subscripted with o are constant reference values to be specified later. Rewriting the governing equations in dimensionless form and introducing the transformations of Eqn. (12) gives

$$\rho u\left[\frac{\partial u}{\partial x} - \frac{\eta}{w}\frac{dw}{dx}\frac{\partial u}{\partial \eta}\right] + \frac{\rho v}{w}\frac{\partial u}{\partial \eta} = -\frac{\partial P}{\partial x} + \frac{1}{Rew^2}\frac{\partial}{\partial \eta}\left(\mu\frac{\partial u}{\partial \eta}\right)$$

$$+ \frac{Ha^2}{Re}\frac{\sigma}{1 + (\omega\tau)^2}\left[(\Phi_y + \omega\tau\Phi_x) + (\omega\tau v - u)\right] \tag{14}$$

$$\rho u\left[\frac{\partial v}{\partial x} - \frac{\eta}{w}\frac{dw}{dx}\frac{\partial v}{\partial \eta}\right] + \frac{\rho v}{w}\frac{\partial v}{\partial \eta} = -\frac{1}{w}\frac{\partial P}{\partial \eta} + \frac{1}{Rew^2}\frac{\partial}{\partial \eta}\left(\mu\frac{\partial v}{\partial \eta}\right)$$

$$- \frac{Ha^2}{Re}\frac{\sigma}{1 + (\omega\tau)^2}\left[(\Phi_x - \omega\tau\Phi_y) + (v + \omega\tau u)\right] \tag{15}$$

$$\rho u\left[\frac{\partial h}{\partial x} - \frac{\eta}{w}\frac{dw}{dx}\frac{\partial h}{\partial \eta}\right] + \frac{\rho v}{w}\frac{\partial h}{\partial \eta} = u\frac{\partial P}{\partial x} + \frac{1}{Rew^2}\left[\frac{\partial}{\partial \eta}\left(\frac{\mu}{Pr}\frac{\partial h}{\partial \eta}\right) + \mu\left(\frac{\partial u}{\partial \eta}\right)^2\right]$$

$$+ \frac{Ha^2\,\sigma}{Re\left[1 + (\omega\tau)^2\right]^2}\left\{\left[(\Phi_x - \omega\tau\Phi_y) + (v + \omega\tau u)\right]^2\right.$$

$$\left. + \left[(\Phi_y + \omega\tau\Phi_x) + (\omega\tau v - u)\right]^2\right\} \tag{16}$$

$$\frac{\partial \rho u}{\partial x} - \frac{\eta}{w}\frac{dw}{dx}\frac{\partial \rho u}{\partial \eta} + \frac{1}{w}\frac{\partial \rho v}{\partial \eta} = 0 \tag{17}$$

$$P = \left(\frac{\gamma - 1}{\gamma}\right)\rho h \tag{18}$$

Equations (14)-(18) are a set of five coupled, nonlinear

equations for the five unknown quantities P, ρ, h, u, v. The equations are parabolic which means that numerical integration can be carried out in a forward marching manner by starting with initially specified profiles at a given x position in the channel. Suitable boundary conditions, to be described in the next section, must be prescribed.

3.2 BOUNDARY CONDITIONS

The range of the dimensionless transverse coordinate η is $0 \leq \eta \leq 1$. Thus boundary conditions must be specified along $\eta = 0$ and $\eta = 1$. The velocity boundary conditions are the usual nonslip conditions. The boundary conditions on h can be specified either as constant heat flux or constant enthalpy. The latter conditions were used in the present study. Thus the velocity and enthalpy boundary conditions may be written as follows.

$$\begin{aligned} &\eta = 0 \quad u = 0 \quad v = 0 \quad h = h_{w1} = \text{constant} \\ &\eta = 1 \quad u = 0 \quad v = 0 \quad h = h_{w2} = \text{constant} \end{aligned} \tag{19}$$

The electrical boundary conditions are more difficult to handle than the velocity and enthalpy conditions. As described earlier, Equation (10) which describes the electric field potential is elliptic which would require a specification of boundary conditions on a closed boundary. Due to the strong coupling between the fluid mechanics and electrical equations, a complex and time consuming iteration procedure would have to be used to solve the coupled equations. An approximate but physically reasonable method of handling the electric field distribution was used in the present investigation.

The total Hall current flowing in the channel is given by the expression

$$I_x^* = w_o w \int_0^1 J_x^* \, d\eta \tag{20}$$

Substituting for J_x^* from Equation (6) and introducing dimensionless quantities gives

$$\frac{I_x^*}{\sigma_o u_o w_o w B_z^*} = \int_0^1 \frac{\sigma \Phi_x}{1 + (\omega\tau)^2} \left(1 - \omega\tau \frac{\Phi_y}{\Phi_x}\right) d\eta$$

$$+ \int_0^1 \frac{\sigma}{1 + (\omega\tau)^2} (v + \omega\tau u) d\eta \qquad (21)$$

At this point two additional assumptions are introduced. The first is that the ratio Φ_y/Φ_x is a constant which would be a valid condition for a channel of diagonal wall construction. The second assumption is that Φ_x, which is a variable across the channel, will be replaced by an average value which depends only on x but not η. Solving for $\Phi_x(x)$ from Equation (21) gives

$$\Phi_x(x) = \frac{\frac{I_x^*}{\sigma_o u_o w_o w B_z^*} - \int_0^1 \frac{\sigma}{1 + (\omega\tau)^2} (v + \omega\tau u) d\eta}{\int_0^1 \frac{\sigma}{1 + (\omega\tau)^2} \left(1 - \omega\tau \frac{\Phi_y}{\Phi_x}\right) d\eta} \qquad (22)$$

The total Hall current, I_x^*, and Φ_y/Φ_x are taken as constant parameters of the analysis. After profiles at each station have been calculated, a value of $\Phi_x(x)$ is then calculated at that station using Equation (22).

3.3 ANALYSIS OF PRESSURE DISTRIBUTION

In applying the first order boundary layer equations to an external flow, the pressure distribution as given by the axial pressure gradient dP/dx is known or at worst can be obtained by solving the inviscid equations of motion for the given body shape independent of the boundary layer equations. The situation is more complex for an internal channel flow because the pressure distribution must be determined concurrently with the solution to the boundary layer equations. This is because of the constraint of overall mass conservation in which the total mass flow rate is the same at each x-location. By contrast, the unconfined nature of an external boundary layer flow means that the inviscid pressure distribution is not affected by the growth of the boundary layer

and consequent increase in boundary layer mass flow.

A considerable effort was necessary to develop a method for calculating the transverse pressure distribution at grid column m+1 in terms of known variables at column m. A first approximation was made by neglecting the inertia and viscous terms in Equation (15), the transverse equation of motion. The body force term was evaluated in terms of the known quantities at column m, and the pressure distribution was calculated at m + 1/2, the station halfway between stations m and m+1. Thus,

$$P(\eta)]_{m+1/2} = w \int_0^{\eta} F_y]_m \, d\eta + P(0)]_{m+1/2} \tag{23}$$

where $F_y]_m$ is the y component of body force evaluated at column m. Assuming the pressure at m + 1/2 to be the arithmetic average of the pressures at m and m+1 then gives

$$P(\eta)]_{m+1} = 2P(\eta)]_{m+1/2} - P(\eta)]_m \tag{24}$$

The pressure at the lower wall, $P(0)]_{m+1/2}$ appearing in Equation (23) is unknown, however. An iteration must be performed as follows to determine the correct value of $P(0)]_{m+1/2}$. An initial guess of $P(0)]_{m+1/2}$ is made by setting $P(0)]_{m+1/2} = P(0)]_m$. This initial estimate of the wall pressure then allows the static pressure distribution at station m+1 to be calculated from Equation (24). Knowing the pressure, enthalpy, and velocity profiles at station m+1 then allows the total mass flow rate to be calculated. If the calculated mass flow rate does not agree with the known mass flow rate based on the initial profiles, an adjustment of the wall pressure $P(0)]_{m+1/2}$ is made and the procedure repeated until convergence of the mass flow rate is obtained. In practice it was found that two such iterations were sufficient.

In carrying out the numerical analysis, the iteration was actually performed on the unknown value of wall density $\rho(0)]_{m+1/2}$ instead of wall pressure. This is because

Equations (14), (16), (18) were solved simultaneously for ρ, u, h at station m+1 and a wall value of density must be assumed to initiate the numerical calculation.

3.4 FINITE DIFFERENCE FORMULAE

Because of the strong coupling and nonlinearity of Equations (14)-(18), an implicit finite difference method was used to obtain an approximate solution to the equations at discrete points across the channel. For this purpose, the two-dimensional region in the (x,η) plane is divided into a grid as illustrated in Figure 2. The partial differentiation operators in the governing equations are then replaced by difference quotients. This allows the governing equations to be represented approximately by a set of difference equations. Solutions to the difference equations are obtained at intersection points of the grid lines. A general nodal point is represented by a double subscript (m,n).

There are several types of finite difference quotients which may be used to approximate the partial derivatives. Only implicit finite difference quotients are used in the present investigation since the stability of the finite difference method is enhanced by using implicit differences. With the implicit difference method, solutions along a grid column m+1 can be obtained by simultaneous solution of a system of linear algebraic equations, utilizing known values of the variable at the previous m column. The system of equations is of tridiagonal form which means an efficient algorithm can be utilized not involving the inversion of a large matrix.

Two finite difference schemes may be used to construct the difference equations: the ordinary implicit method and the Crank-Nicolson method. The ordinary implicit scheme is developed by using backward difference quotients to approximate partial derivatives at m+1,n. The Crank-Nicolson implicit scheme utilizes central difference quotients to approximate partial derivative operators at m+1/2,n. The truncation error is smaller for the Crank-Nicolson method than for the ordinary implicit method. If f and g represent two arbitrary dependent variables, the Crank-Nicolson differences may be written as follows.

$$\frac{\partial f}{\partial x} = \frac{f_{m+1,n} - f_{m,n}}{\Delta x} + \frac{1}{24}(\Delta x)^2 f_{xxx} + \ldots \qquad (25)$$

$$\frac{\partial f}{\partial \eta} = \frac{1}{4\Delta\eta}\left(f_{m,n+1} - f_{m,n-1} + f_{m+1,n+1} - f_{m+1,n-1}\right)$$

$$- \frac{1}{8}(\Delta x)^2 f_{xx\eta} - \frac{1}{6}(\Delta\eta)^2 f_{\eta\eta\eta} + \ldots \tag{26}$$

$$\frac{\partial^2 f}{\partial \eta^2} = \frac{1}{2\Delta\eta^2}\left(f_{m,n+1} - 2f_{m,n} + f_{m,n-1} + f_{m+1,n+1}\right.$$

$$\left. - 2f_{m+1,n} + f_{m+1,n-1}\right) - \frac{1}{8}(\Delta x)^2 f_{xx\eta\eta}$$

$$- \frac{1}{12}(\Delta\eta)^2 f_{\eta\eta\eta\eta} + \ldots \tag{27}$$

$$\left(\frac{\partial f}{\partial \eta}\right)^2 = \frac{\left(f_{m,n+1} - f_{m,n-1}\right)}{2\Delta\eta}\,\frac{\left(f_{m+1,n+1} - f_{m+1,n-1}\right)}{2\Delta\eta}$$

$$+ \frac{(\Delta x)^2}{4}\left(f_{x\eta} - f_\eta f_{xx\eta}\right) - \frac{(\Delta x)^2}{3} f_\eta f_{\eta\eta\eta} + \ldots \tag{28}$$

$$\frac{\partial f}{\partial \eta}\,\frac{\partial g}{\partial \eta} = \frac{1}{2}\left[\frac{\left(f_{m,n+1} - f_{m,n-1}\right)}{2\Delta\eta}\,\frac{\left(g_{m+1,n+1} - g_{m+1,n-1}\right)}{2\Delta\eta}\right.$$

$$\left. + \frac{\left(g_{m,n+1} - g_{m,n-1}\right)}{2\Delta\eta}\,\frac{\left(f_{m+1,n+1} - f_{m+1,n-1}\right)}{2\Delta\eta}\right]$$

$$- \frac{(\Delta x)^2}{8}\left(f_\eta g_{xx\eta} - 2f_{x\eta} g_{x\eta} + g_\eta f_{xx\eta}\right)$$

$$- \frac{(\Delta\eta)^2}{6}\left(f_\eta g_{\eta\eta\eta} + g_\eta f_{\eta\eta\eta}\right) + \ldots \tag{29}$$

$$f \frac{\partial g}{\partial x} = f_{m,n} \frac{(g_{m+1,n} - g_{m,n})}{\Delta x} + \ldots \tag{30}$$

$$f \frac{\partial g}{\partial \eta} = f_{m,n} \frac{1}{4\Delta\eta} (g_{m,n+1} - g_{m,n-1} + g_{m+1,n+1} - g_{m+1,n-1}) + \ldots \tag{31}$$

The finite difference approximations of Equations (25)-(31), when substituted into Equations (14), (16), (18), result in a set of linear algebraic equations for the unknown values of u, h, and ρ at column m+1. The matrix of coefficients for this set of equations is the tridiagonal form, and the development of the algorithm for solving the set of equations is contained in the Appendix.

After solving for the u, h, ρ, profiles at column m+1, the pressure distribution in the transverse direction was calculated from Equation (25). Additionally, the v profile at column m+1 is calculated from Equation (17), the continuity equation.

SECTION IV

DISCUSSION OF RESULTS

A total of 17 different computer runs were made for various combinations of the parameters. The ranges of physical parameters for which numerical results were obtained are shown in Table I and Table II. For each combination of parameters, three sets of curves are presented. These three sets of curves show respectively (1) the centerline distributions of enthalpy, velocity, and pressure, (2) velocity and enthalpy profiles at $x/w_o = 4.8$, and (3) velocity and enthalpy profiles at $x/w_o = 9.8$.

The Group I runs compare the influence of initial profiles of velocity and enthalpy on the flow development. Initial condition 1 corresponds to parabolic profiles of velocity and enthalpy at inlet and initial condition 2 corresponds to quartic profiles of velocity and enthalpy at inlet. The quartic profiles are flatter profiles than the parabolic profiles and would simulate turbulent initial profiles.

For each computer run, the calculations were done from the channel entrance to a downstream distance of approximately 10 channel widths. This distance was sufficient to establish the trends of the calculations and represents a compromise of the computer time that was available between computing for a small number of cases over a large channel distance and a large number of cases over a short channel distance. A few runs were made over a distance of over 100 channel widths with no difficulties encountered in the program.

It was found that the method of handling the electrical boundary conditions described earlier became very time consuming. Since the amount of computer time available was limited, all calculations were performed assuming constant values of the transverse and Hall currents, J_y and J_x respectively.

The results for the Group I calculations will be discussed first. A detailed study of the Group I results contained in Figures 3-32 revealed that the following conclusions may be drawn.

1) The Hall current had essentially no effect on the centerline distribution of velocity, enthalpy, and pressure.

TABLE I

RANGE OF PHYSICAL PARAMETERS FOR GROUP I RUNS

Fixed Values: $Ha = 100$ $R_e = 0.12 \times 10^6$

$M = 2.0$ $P_r = 0.73$

$\gamma = 1.4$ $J_y = 0.1$

Case	J_x	H_{w1}	H_{w2}	Initial Conditions*
1	0	0.04	0.04	1
2	0.05	0.04	0.04	1
3	0.10	0.04	0.04	1
4	0.05	0.08	0.08	1
5	0.05	0.04	0.08	1
1a	0	0.04	0.04	2
2a	0.05	0.04	0.04	2
3a	0.10	0.04	0.04	2
4a	0.05	0.08	0.08	2
5a	0.05	0.04	0.08	2

*Initial condition 1 corresponds to parabolic profiles of velocity and enthalpy at inlet.

Initial condition 2 corresponds to quartic profiles of velocity and enthalpy at inlet.

TABLE II

RANGE OF PHYSICAL PARAMETERS FOR GROUP II RUNS

Fixed Values: $H_{w1} = 0.04$ $H_{w2} = 0.04$

$J_x = 0.05$ $J_y = 0.10$

$\gamma = 1.4$

INITIAL PROFILE 1

Case	Ha	Re	Pr	M
6	50	1.2×10^5	0.73	2.0
7	100	1.2×10^5	0.73	2.0
8	100	0.6×10^5	0.73	2.0
9	100	0.55×10^5	0.73	2.0
10	100	1.2×10^5	0.50	2.0
11	100	1.2×10^5	1.00	2.0
12	100	1.2×10^5	0.73	3.0

2) The shapes of the initial velocity profiles were essentially preserved over the distance of 10 channel widths for which the calculations were performed. Even though the velocity increased and the enthalpy decreased on the centerline, the initially parabolic profiles still had a parabolic shape after 10 channel widths and similarly for the initially quartic profiles.

3) A slightly larger acceleration occurs for initial profiles which are parabolic compared to initially quartic profiles. This difference was slight, however, amounting to about 2 to 3 percent over a distance of 10 channel widths.

4) The pressure drop increases slightly as the wall enthalpy increases for both initially parabolic and quartic profiles. The pressure drop is larger for an initially parabolic profile than for an initially quartic profile. Also, the centerline enthalpy decreases faster for an initially parabolic profile than for a quartic initial profile.

The results for the Group II calculations are contained in Figures 33-53. A detailed study of these curves indicates that the following conclusions are valid.

1) The acceleration on the centerline increases with increasing Hartmann number as one would expect. For example, with all other conditions the same, a Ha value of 100 gives a 14 percent increase in centerline velocity over 10 channel widths compared to a 4.5 percent increase for a Ha value of 50.

2) A smaller value of Reynolds number results in a greater acceleration on the centerline.

3) The variation of Prandtl number over the range $0.73 \leq Pr \leq 1.0$ had essentially no effect on the acceleration characteristics of the flow. No readable change in centerline values of velocity, enthalpy, pressure can be observed over this range of Prandtl number.

4) Increasing the Mach number results in a decrease of acceleration on the centerline.

REFERENCES

1. Snyder, W. T. and J. R. Maus, "Fully Developed Magnetogasdynamic Flow Between Diverging Plane Walls." AEDC-TR-67-80, April 1967.

2. Kitowski, J. V. "Theory of Viscous Compressible Flow in a Slender Channel with Crossed Electric and Magnetic Fields," Ph.D. dissertation, The University of Tennessee Knoxville, Tenn. 1968.

3. Hartmann, J. "Theory of Laminar Flow of an Electrically Conducting Liquid in a Homogeneous Magnetic Field," Kgl. Danske Videnskabernes Selskab, Math.-Fys. Med., 15(6), 1937.

4. Eraslan, A. H., "Nonuniform Conductivity MHD Channel Flow Solution by B. G. Galerkin Method." AIAA J. 4: 1759-1766, 1966.

5. Young, J. D., "A Fredholm Integral Equation Solution for Variable Conductivity Magnetohydrodynamic Channel Flow." M.S. Thesis, The University of Tennessee, Knoxville, 1965.

6. Snyder, W. T. "Magnetohydrodynamic Flow in the Entrance Region of a Parallel Plate Channel." AIAA J. 3:1833, 1965.

7. Resler, E. L., Jr. and W. R. Sears. "Magnetogasdynamic Channel Flow." ZAMP, 96:509-518, 1968.

8. Kerrebrock, J. L. "Electrode Boundary Layers in Direct Current Plasma Accelerators." J. Aerospace Sci. 28:631, 1961.

9. Williams, J. C. "Viscous Compressible and Incompressible Flow in Slender Channels." AIAA J. L:186-195, 1963.

10. Sonnerup, B. O. U. "Theory of Viscous Magnetogasdynamic Flow in Slowly Diverging Two-Dimensional Channels." AFOSR 1332, ASTIA, Arlington, Virginia, 1961.

11. Kubin, I. K. and G. G. Smolin. "Two-Dimensional Flow of Electrically Conducting Liquids and Gases in Channels in the Presence of Electric and Magnetic Fields," High Temperature, 4:65-73, 1966.

12. Flugge-Lotz, I. and F. G. Blottner. "The Solution of Compressible Laminar Boundary Layer Problems by a Finite Method." Stanford University Division of Engineering Mechanics Report Number 131, Stanford, California, 1962.

13. Celinski, Z. N. and F. W. Fischer. "Two-Dimensional Analysis of MHD Generators with Segmented Electrodes." AIAA J. 4:421, 1966.

14. Oliver, D. A. and M. Mitchner. "Nonuniform Electrical Conduction in MHD Channels." AIAA J. 5:1424, 1967.

15. Sherman, A. and G. W. Sutton. "The Combined Effect of Tensor Conductivity and Viscosity on an MHD Generator with Segmented Electrodes." Proceedings 4th Biennial Gas Dynamics Symposium. Northwestern University Press, 1962.

16. Snyder, W. T. and A. H. Eraslan. "The Influence of Hall Effect and Initial Velocity Profile on MHD Flow in the Entrance Region of a Parallel Plate Channel." AEDC-TR-67-79, April 1967.

17. Hale, F. J. and J. L. Kerrebrock. "Insulator Boundary Layers in Magnetohydrodynamic Channels." AIAA J. 2:461-469, 1963.

18. Hunter, L. G. "Non-Similar MHD Boundary Layers on Insulating Walls." Ph.D. dissertation, The University of Tennessee, Knoxville, 1969.

APPENDIX
ILLUSTRATIONS

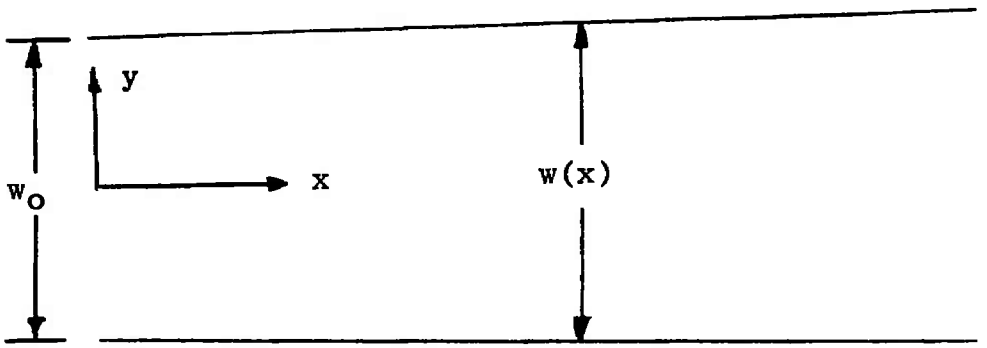

Applied B Field is in the z-Direction.

Figure 1. E-Plane MHD Channel Flow Geometry

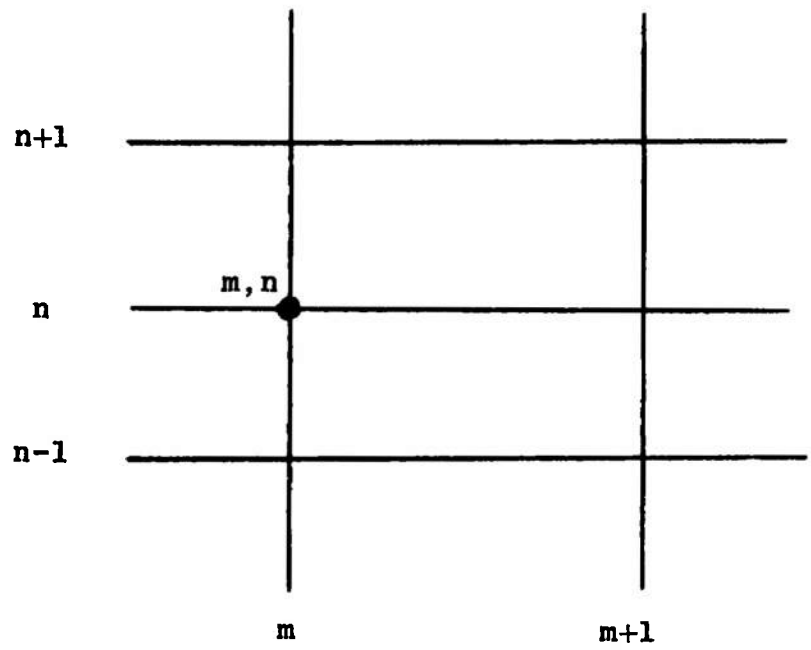

Figure 2. Finite Difference Grid Geometry.

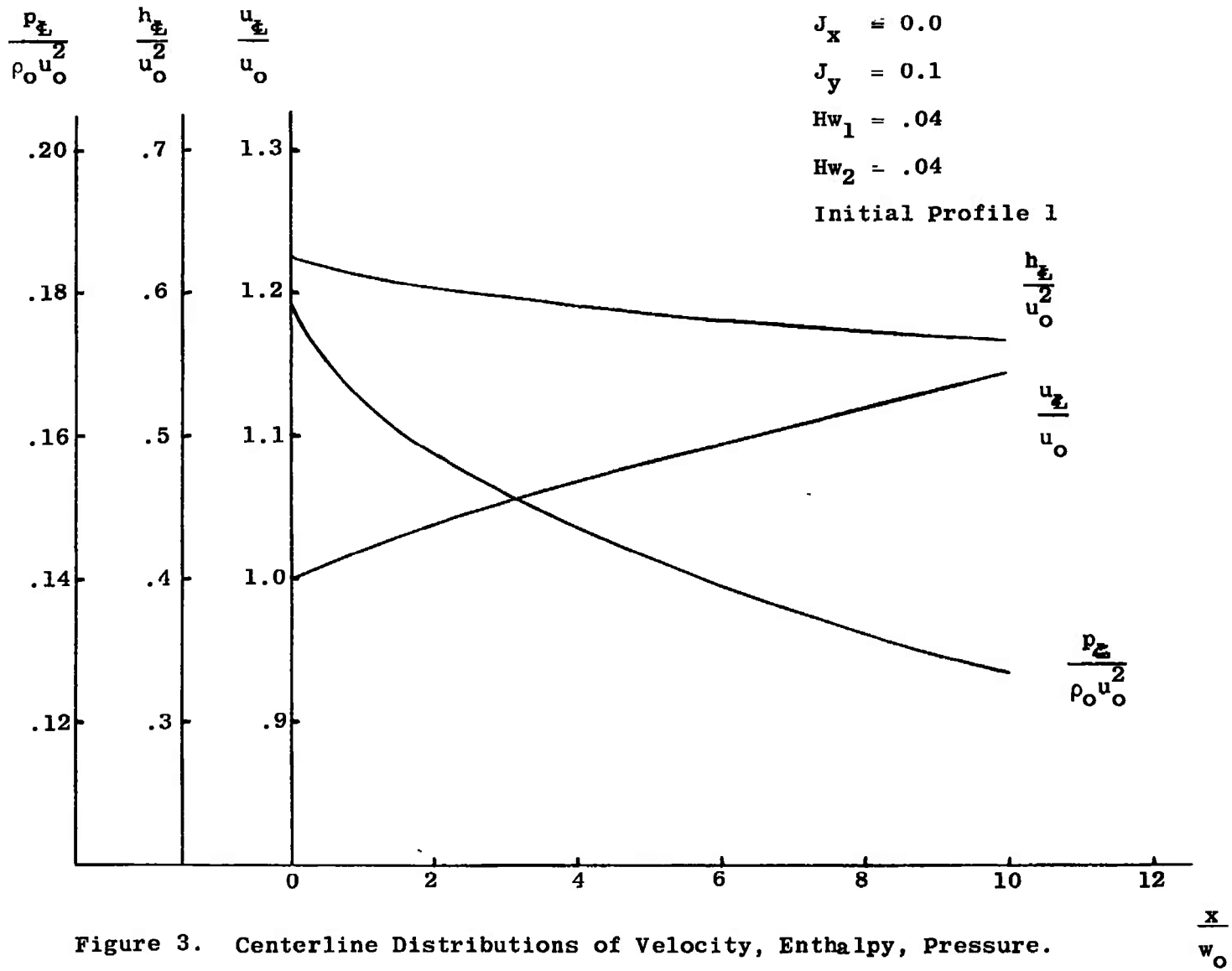

Figure 3. Centerline Distributions of Velocity, Enthalpy, Pressure.

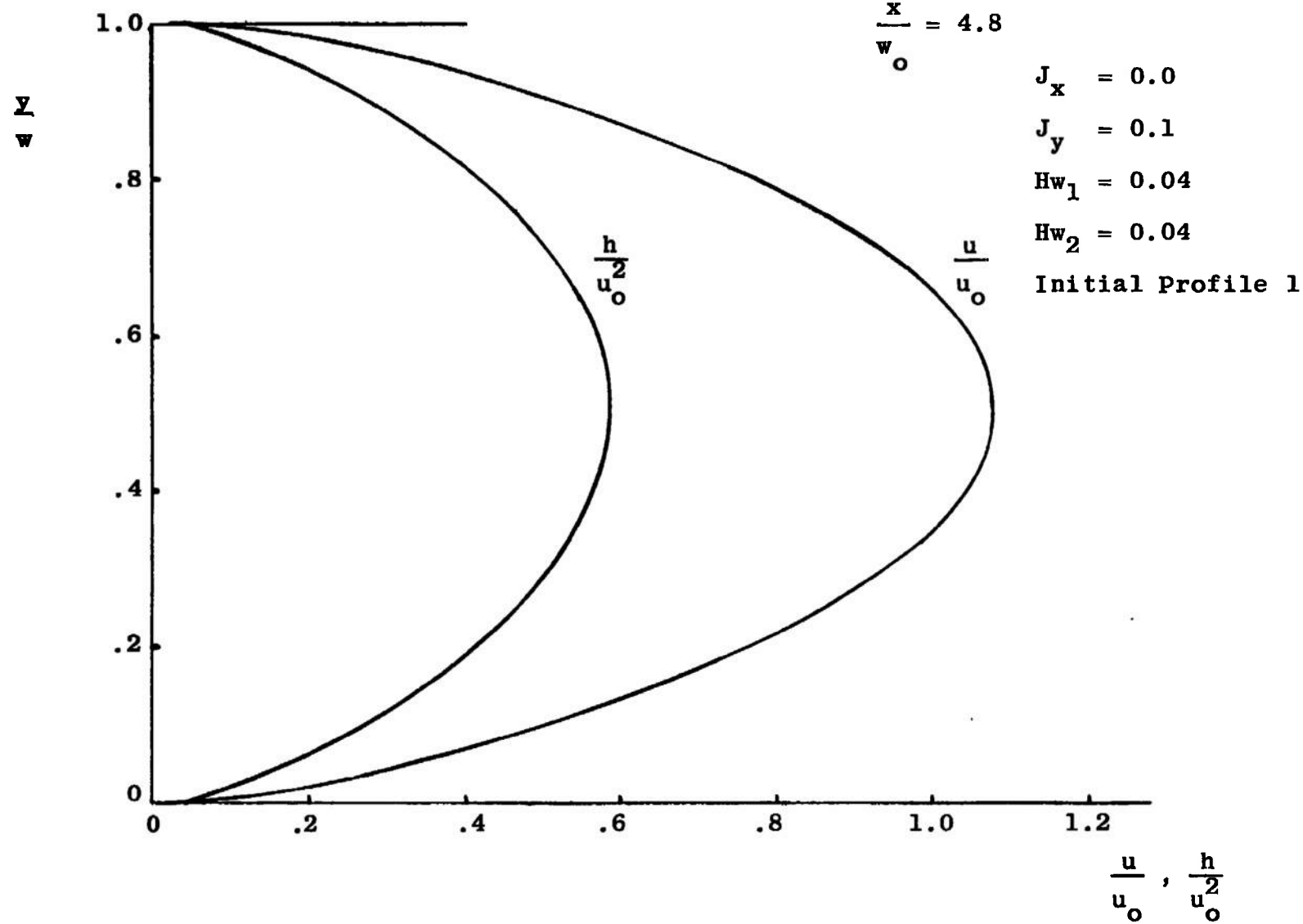

Figure 4. Velocity and Enthalpy Profiles at x/w_o = 4.8.

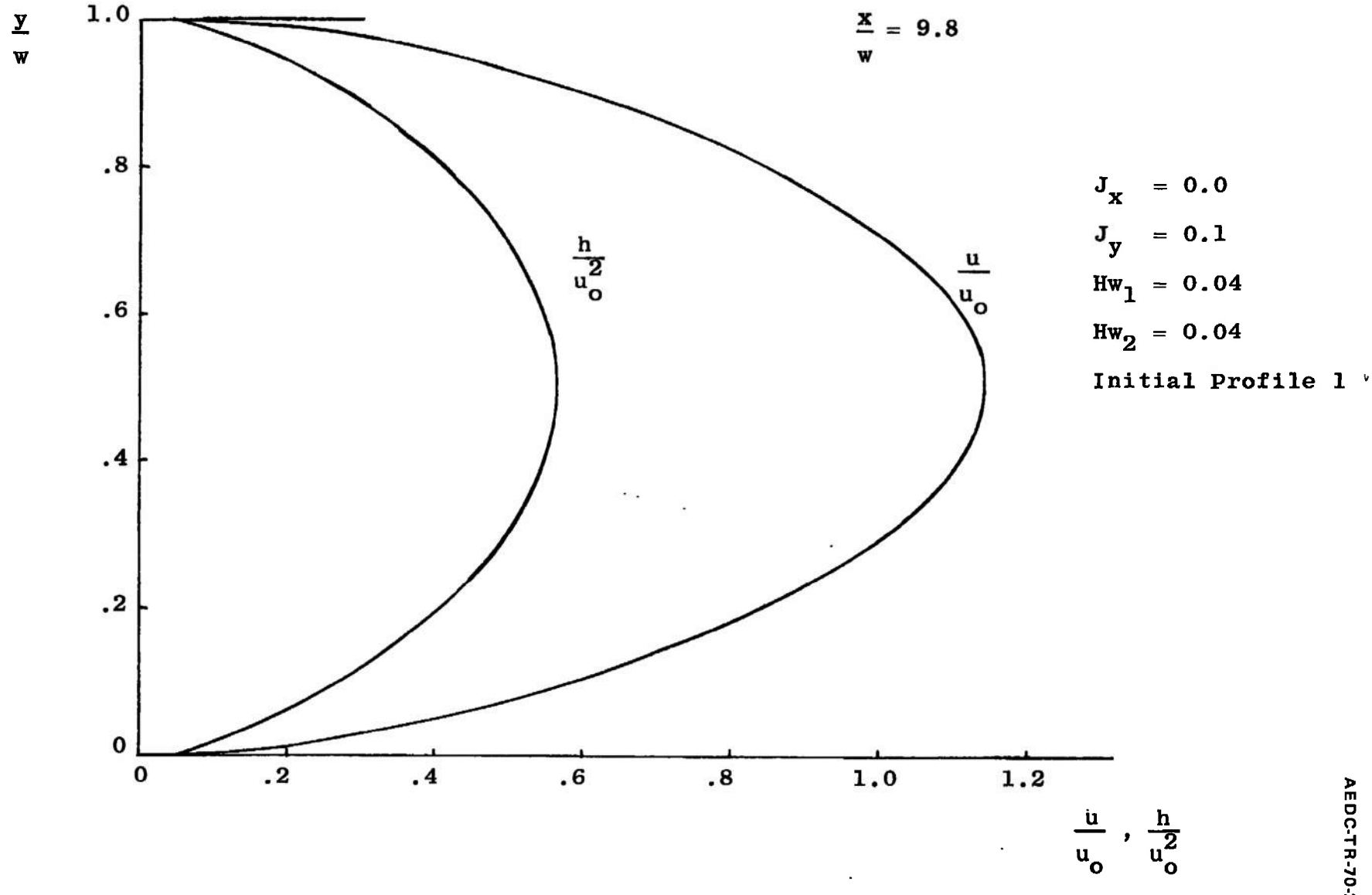

Figure 5. Velocity and Enthalpy Profiles at $x/w_o = 9.8$

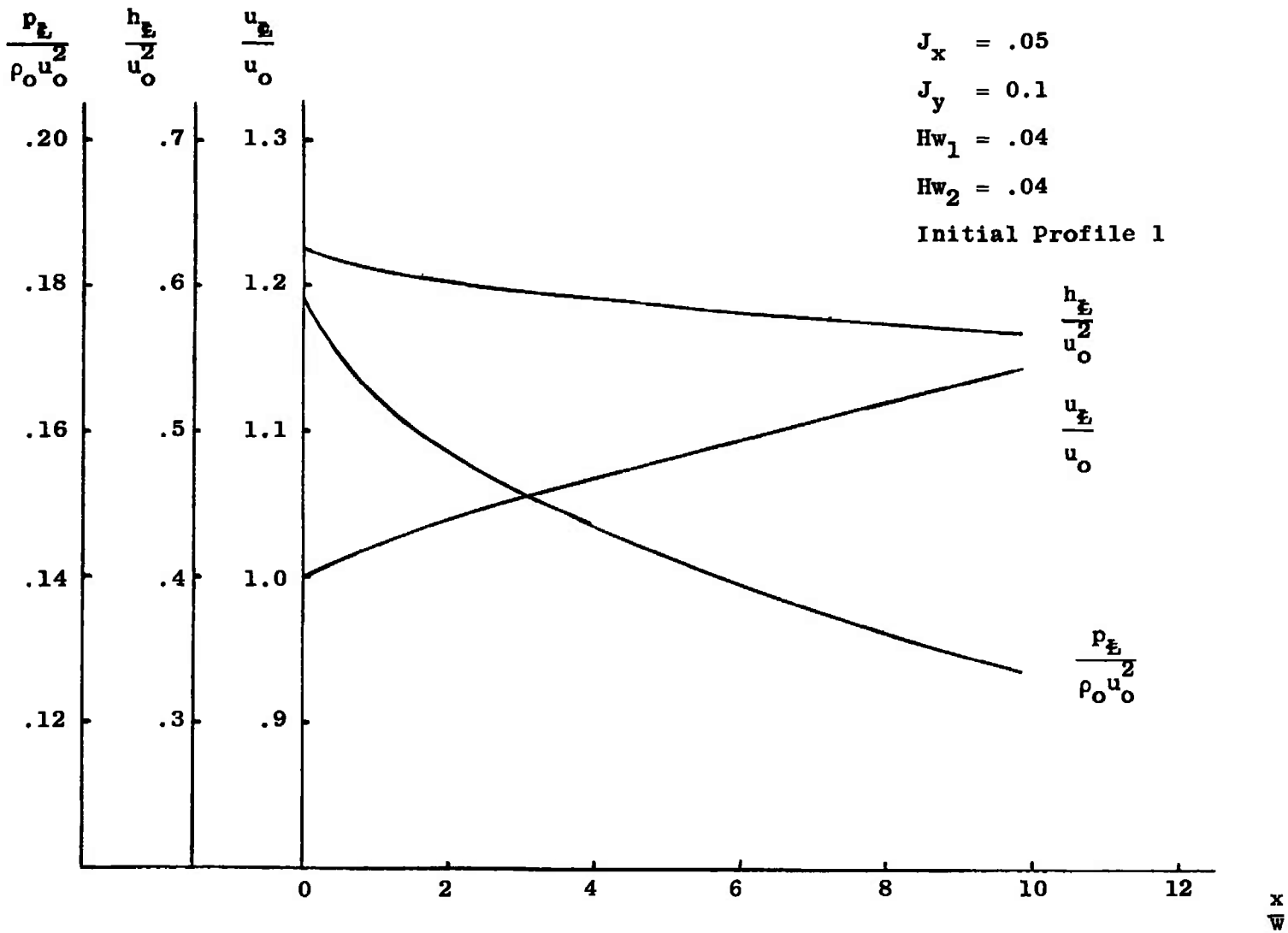

Figure 6. Centerline Distributions of Velocity, Enthalpy, Pressure.

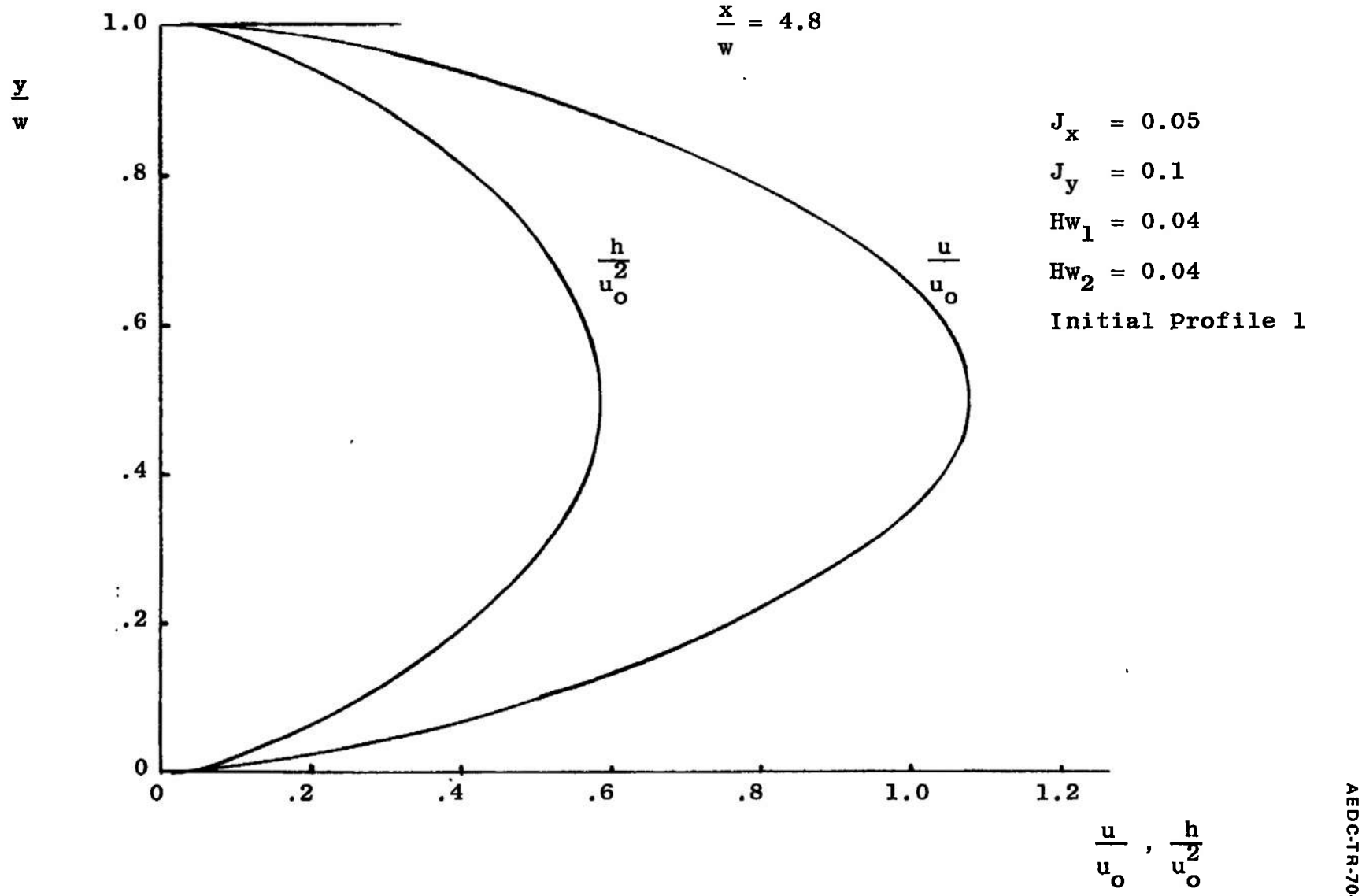

Figure 7. Velocity and Enthalpy Profiles at $x/w_o = 4.8$.

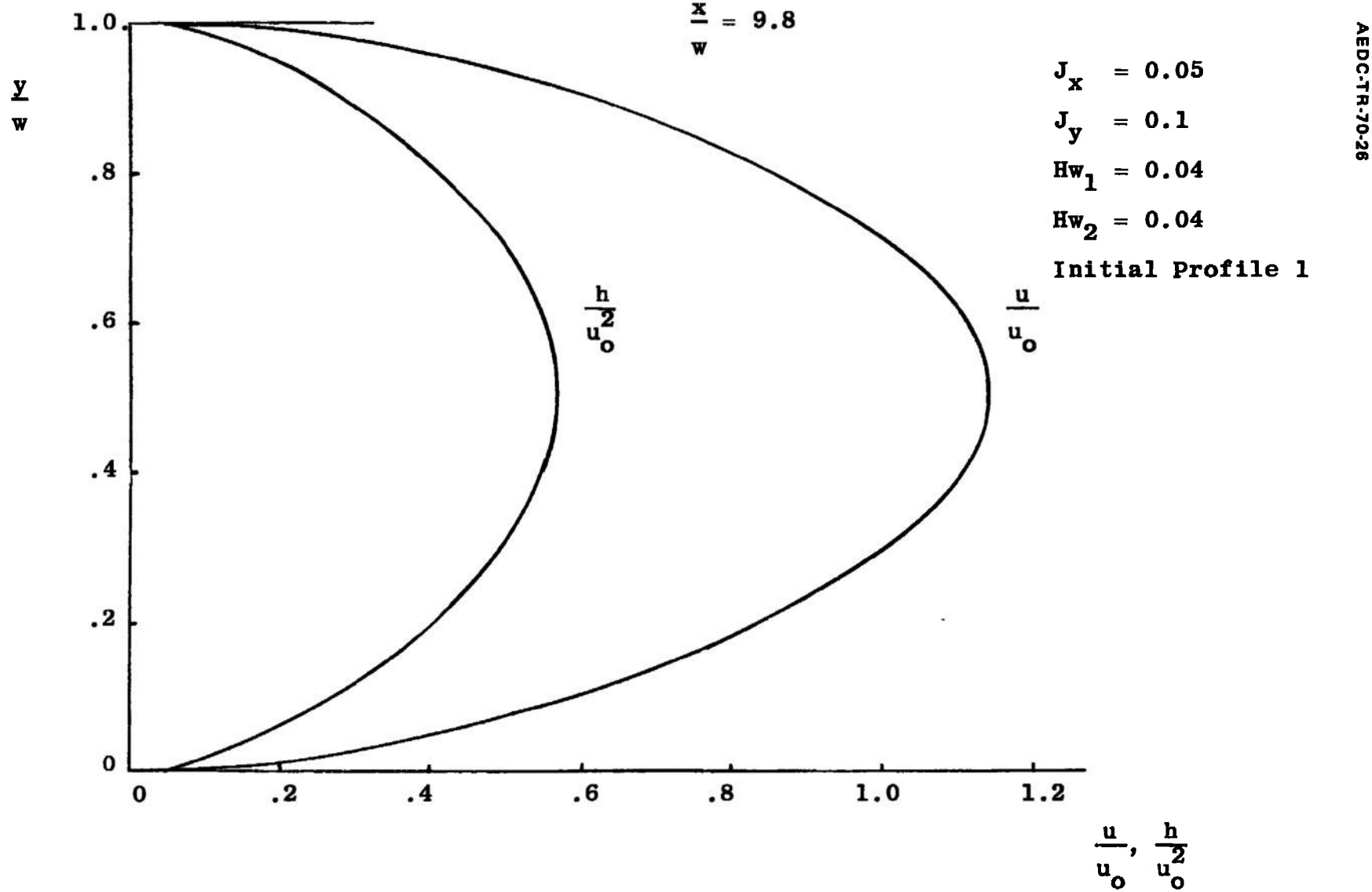

Figure 8. Velocity and Enthalpy Profiles at $x/w_o = 9.8$.

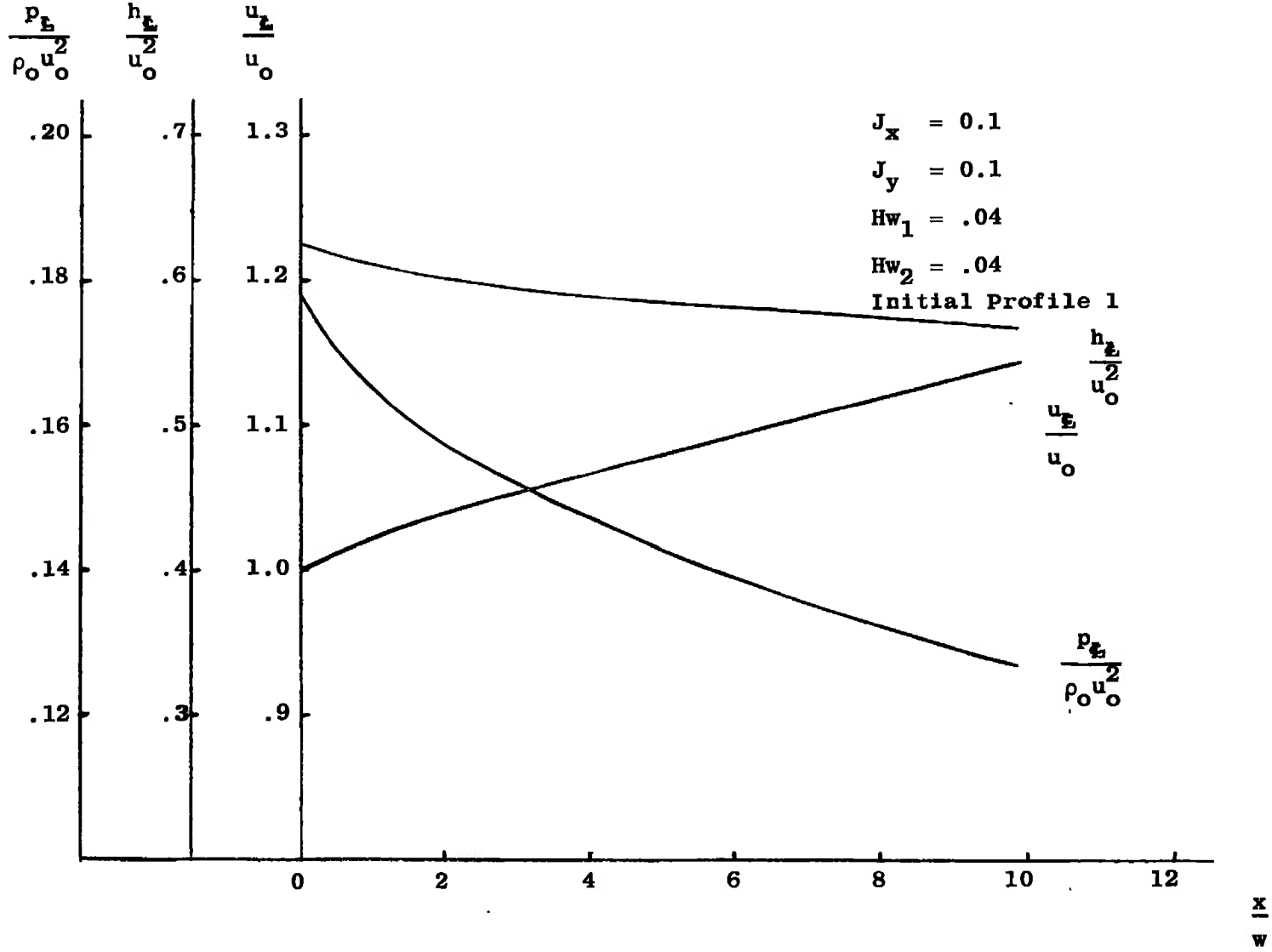

Figure 9. Centerline Distributions of Velocity, Enthalpy, Pressure.

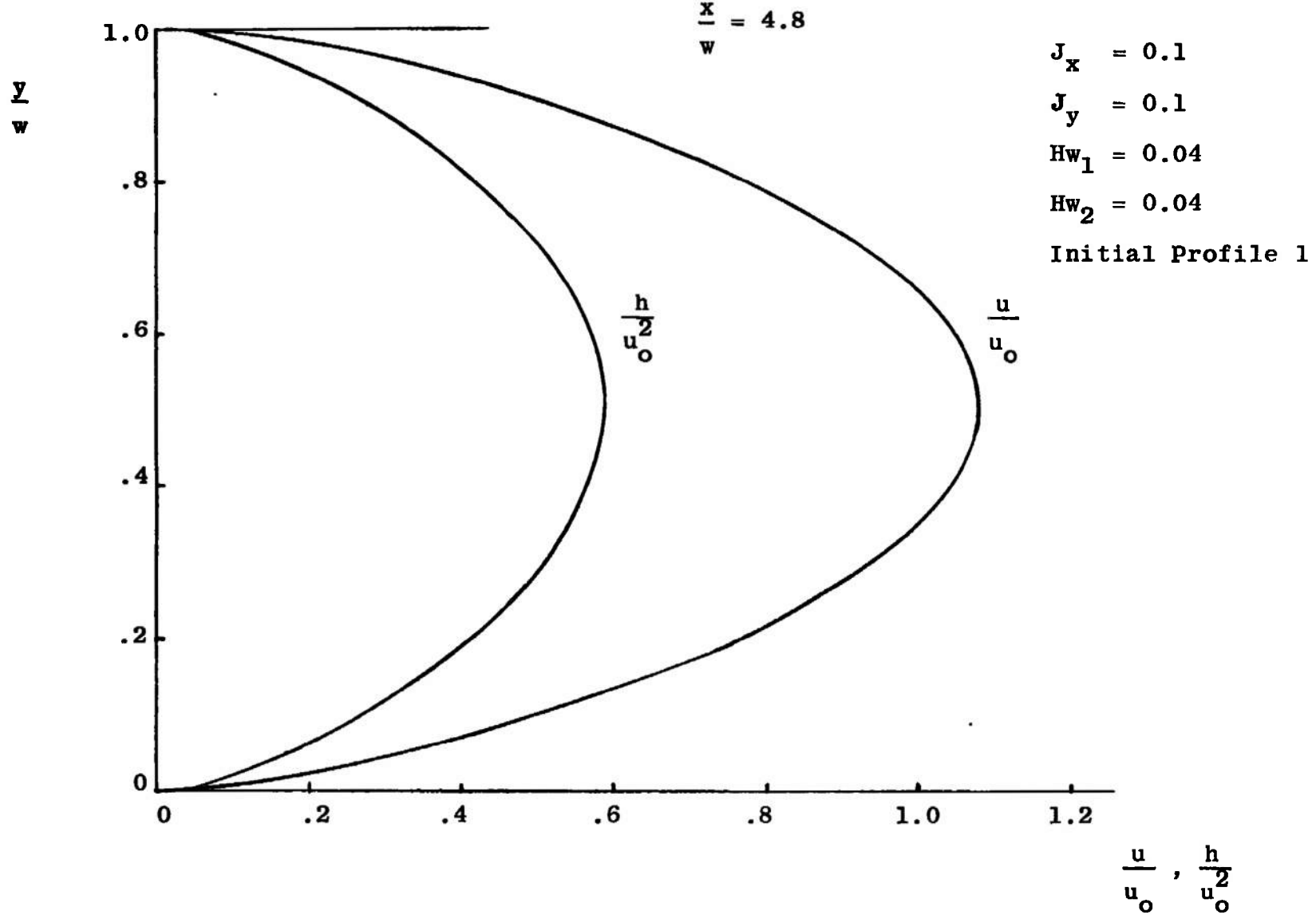

Figure 10. Velocity and Enthalpy Profiles at x/w_o = 4.8.

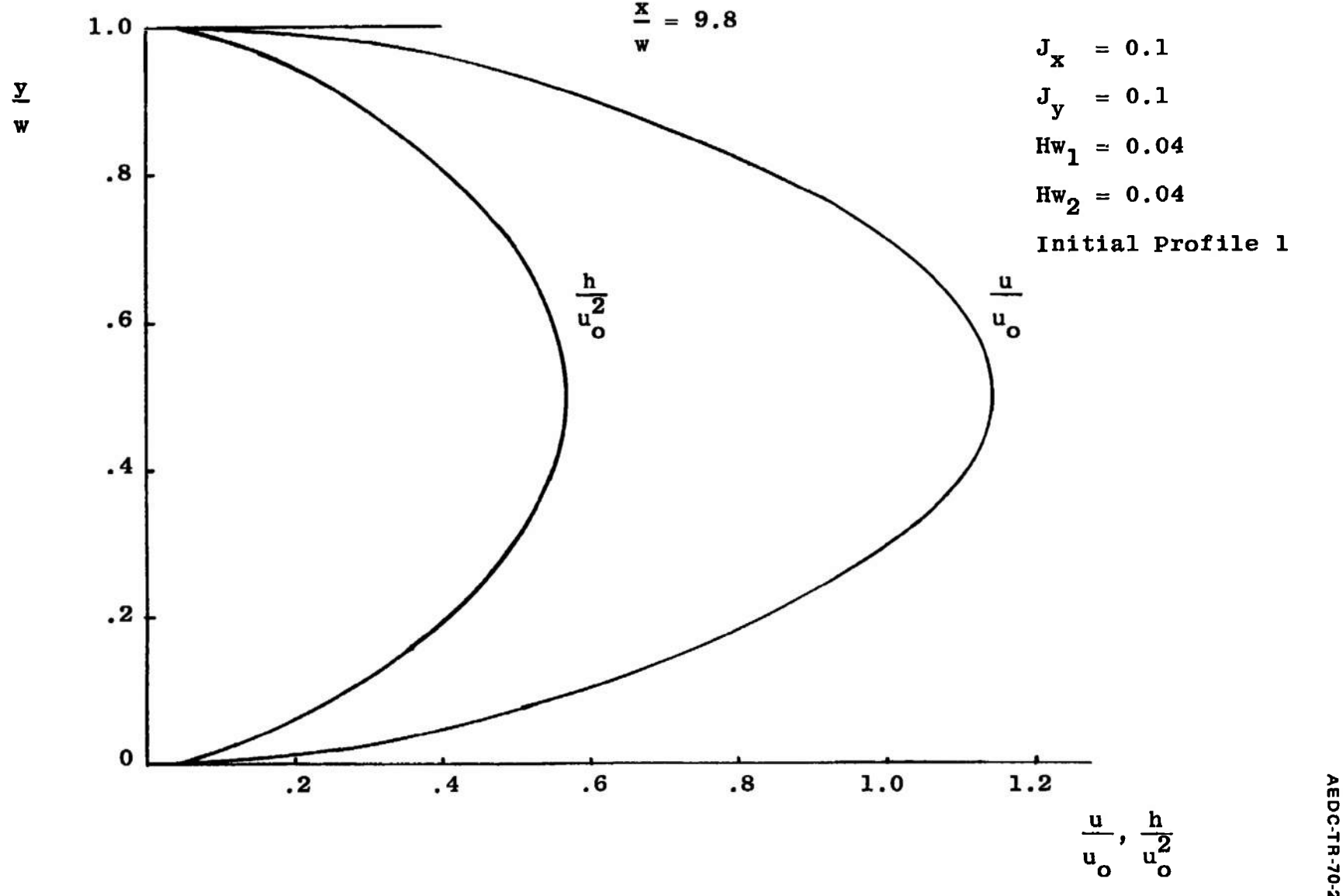

Figure 11. Velocity and Enthalpy Profiles at $x/w_o = 9.8$.

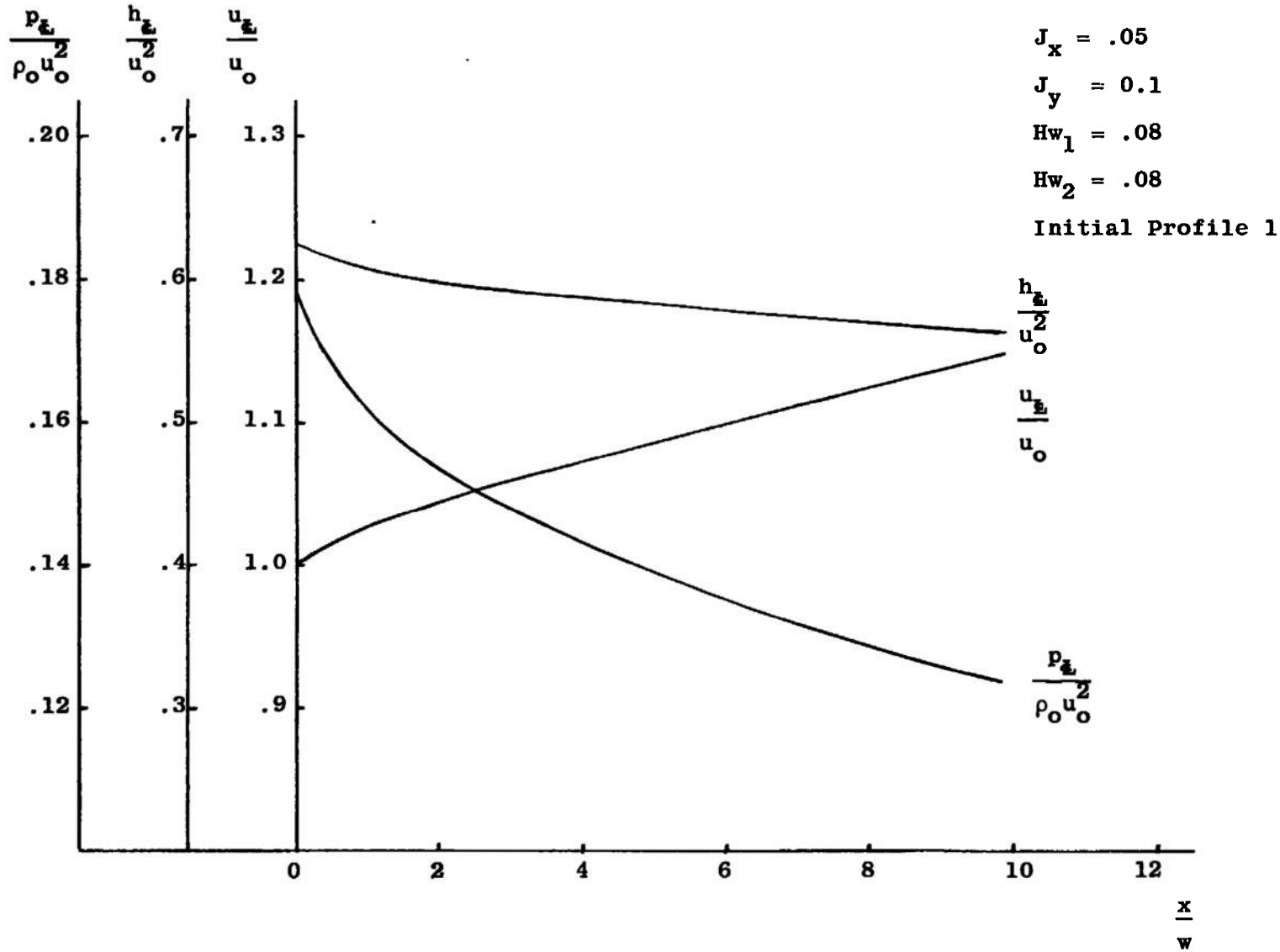

Figure 12. Centerline Distributions of Velocity, Enthalpy, Pressure.

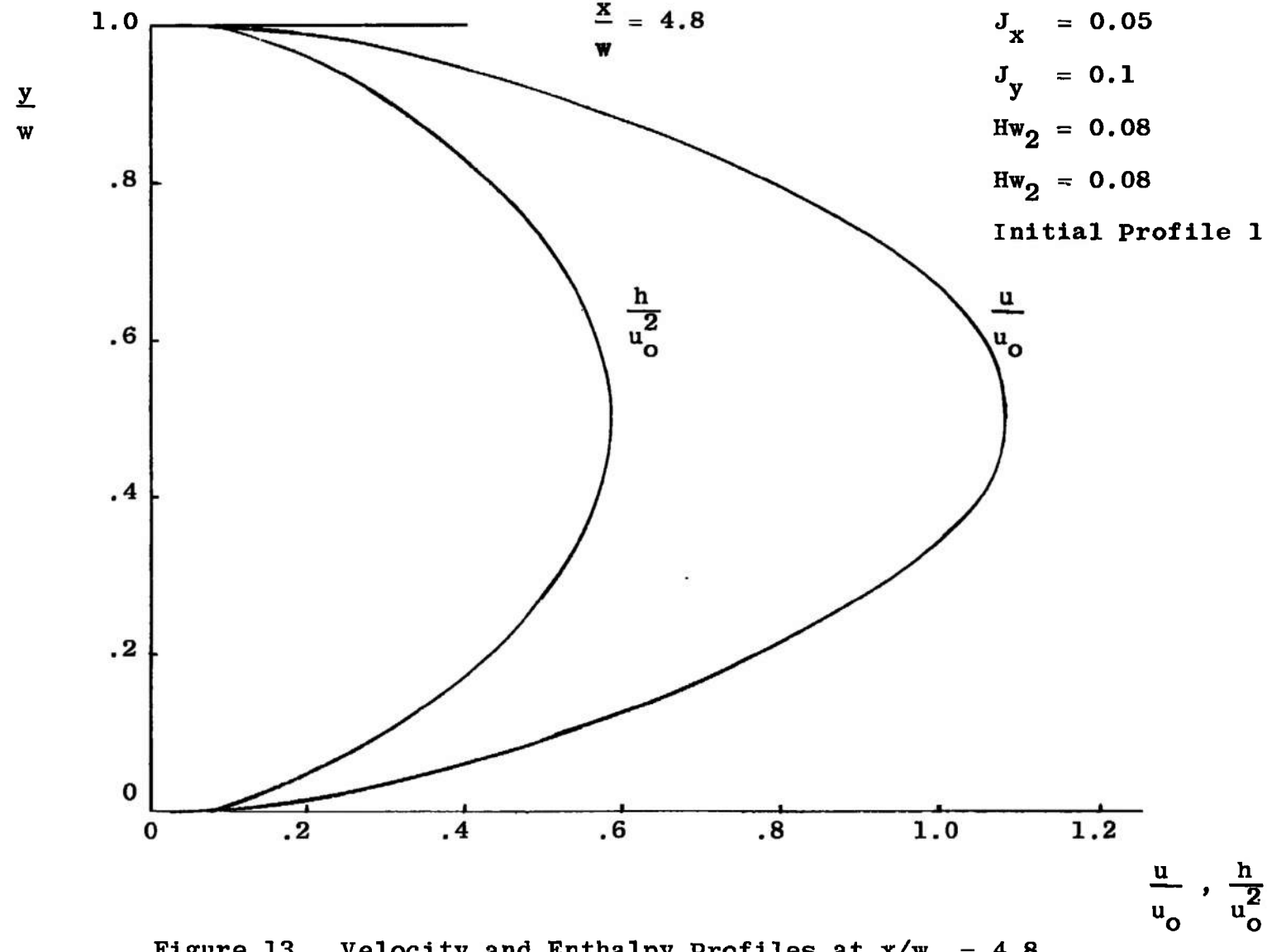

Figure 13. Velocity and Enthalpy Profiles at $x/w_o = 4.8$.

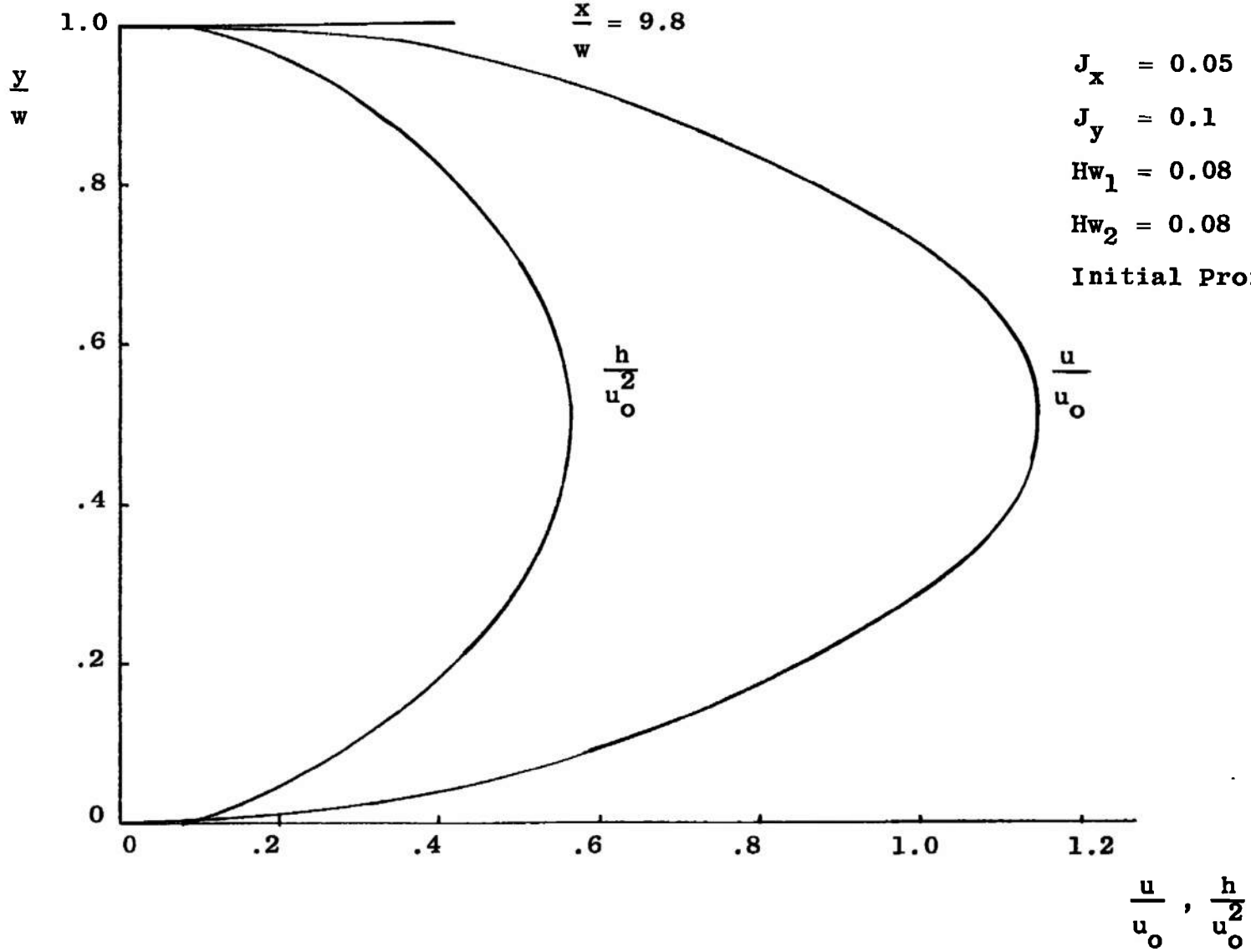

Figure 14. Velocity and Enthalpy Profiles at $x/w_o = 9.8$.

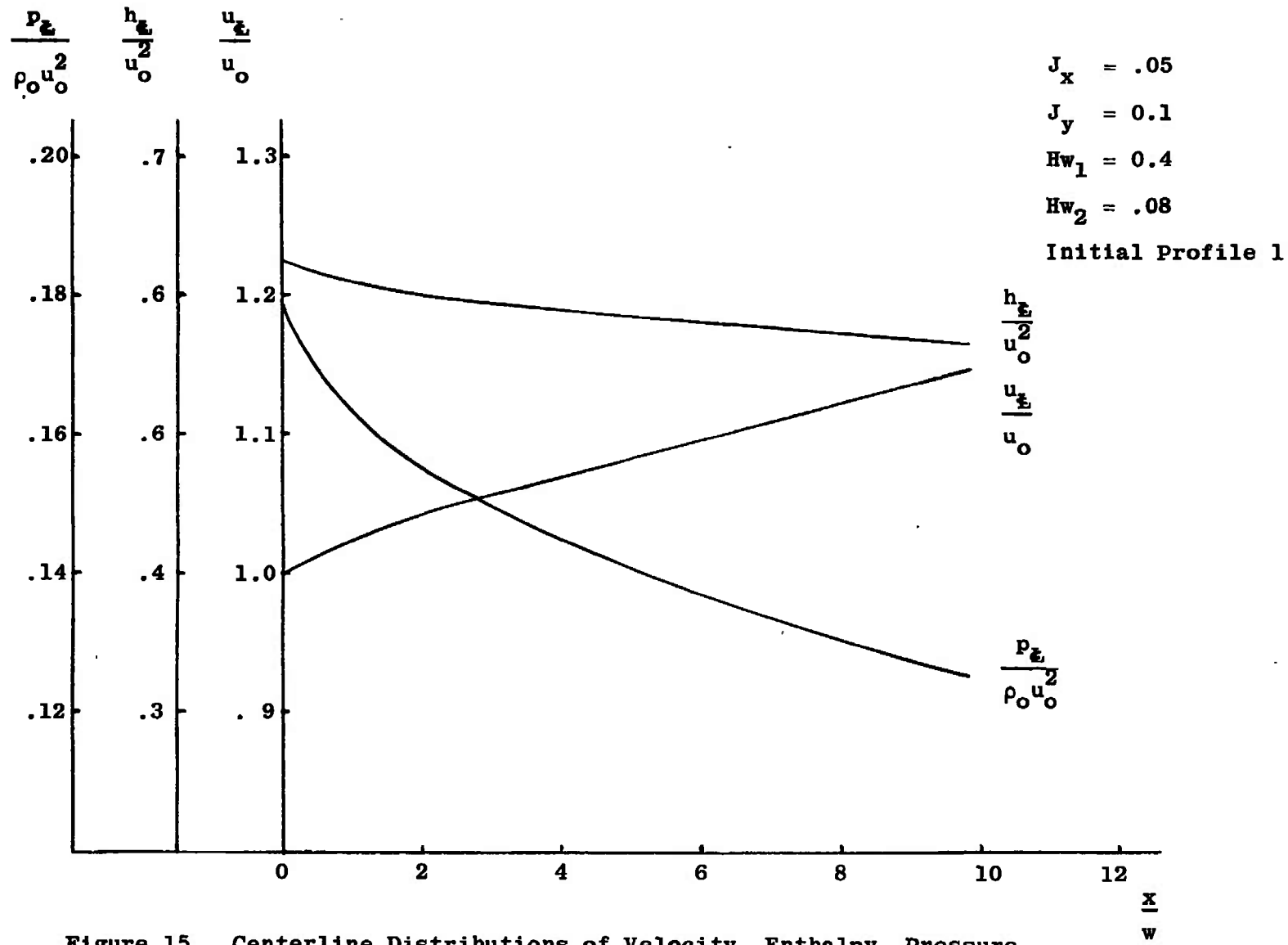

Figure 15. Centerline Distributions of Velocity, Enthalpy, Pressure.

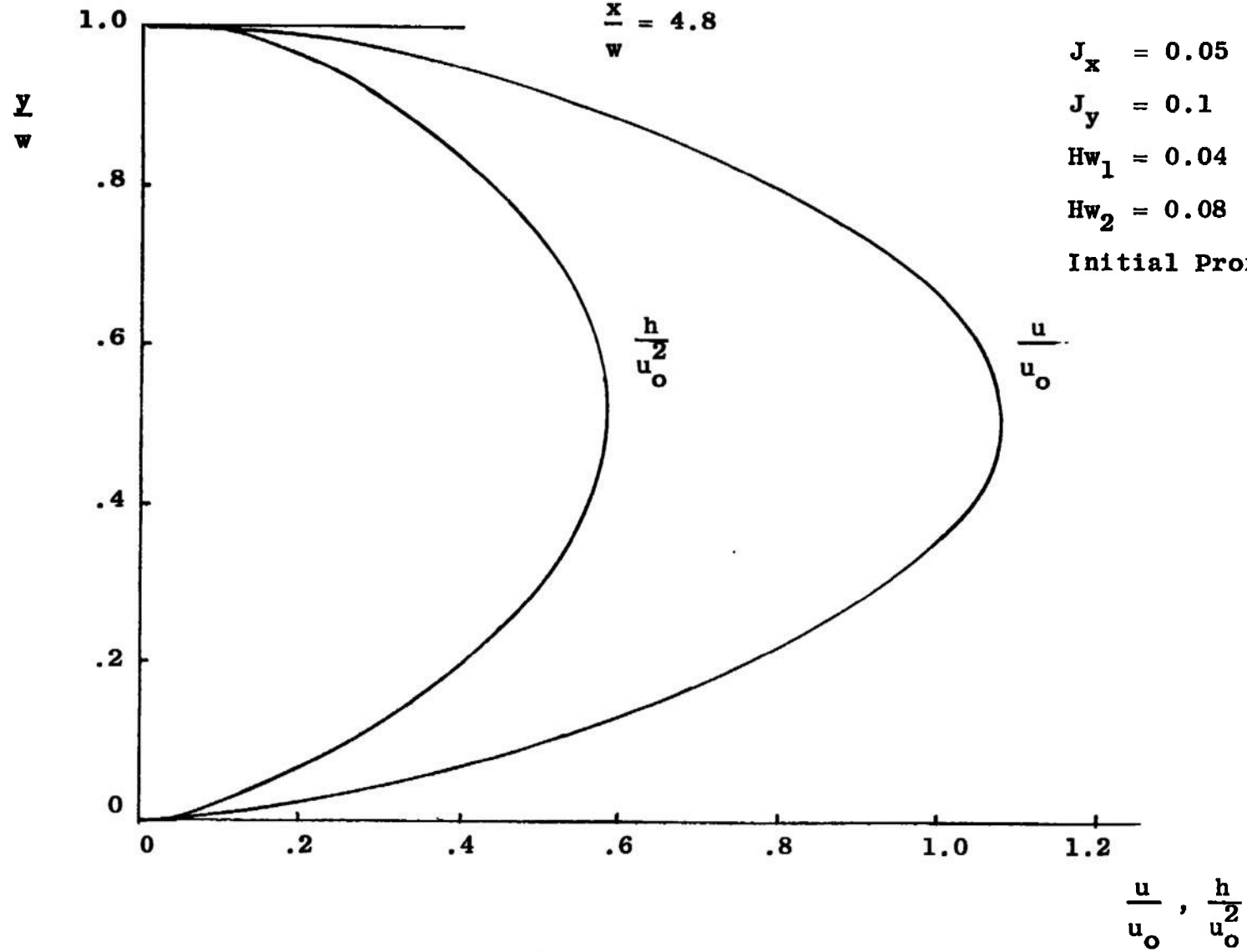

Figure 16. Velocity and Enthalpy Profiles at $x/w_o = 4.8$

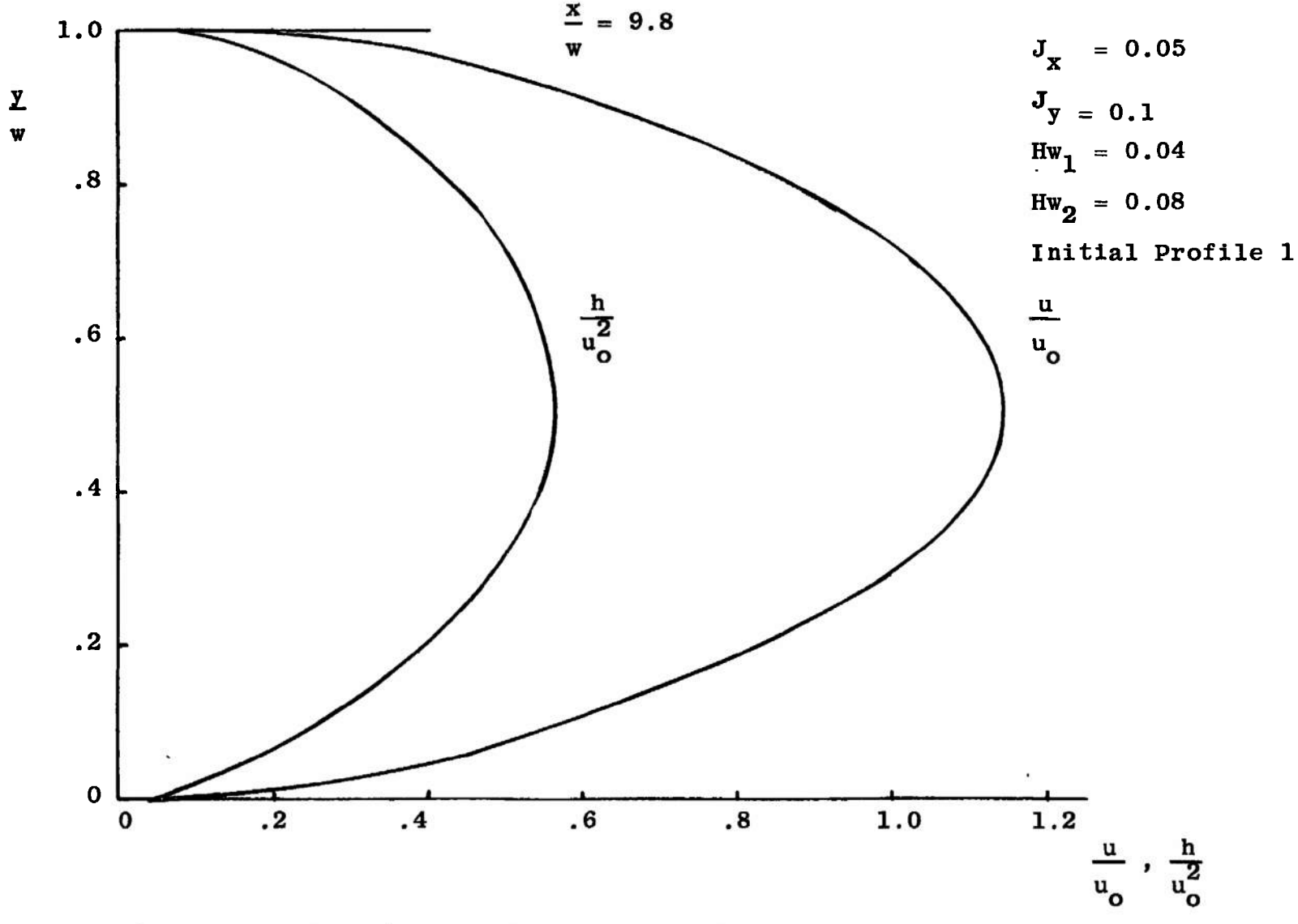

Figure 17. Velocity and Enthalpy Profiles at $x/w_o = 9.8$.

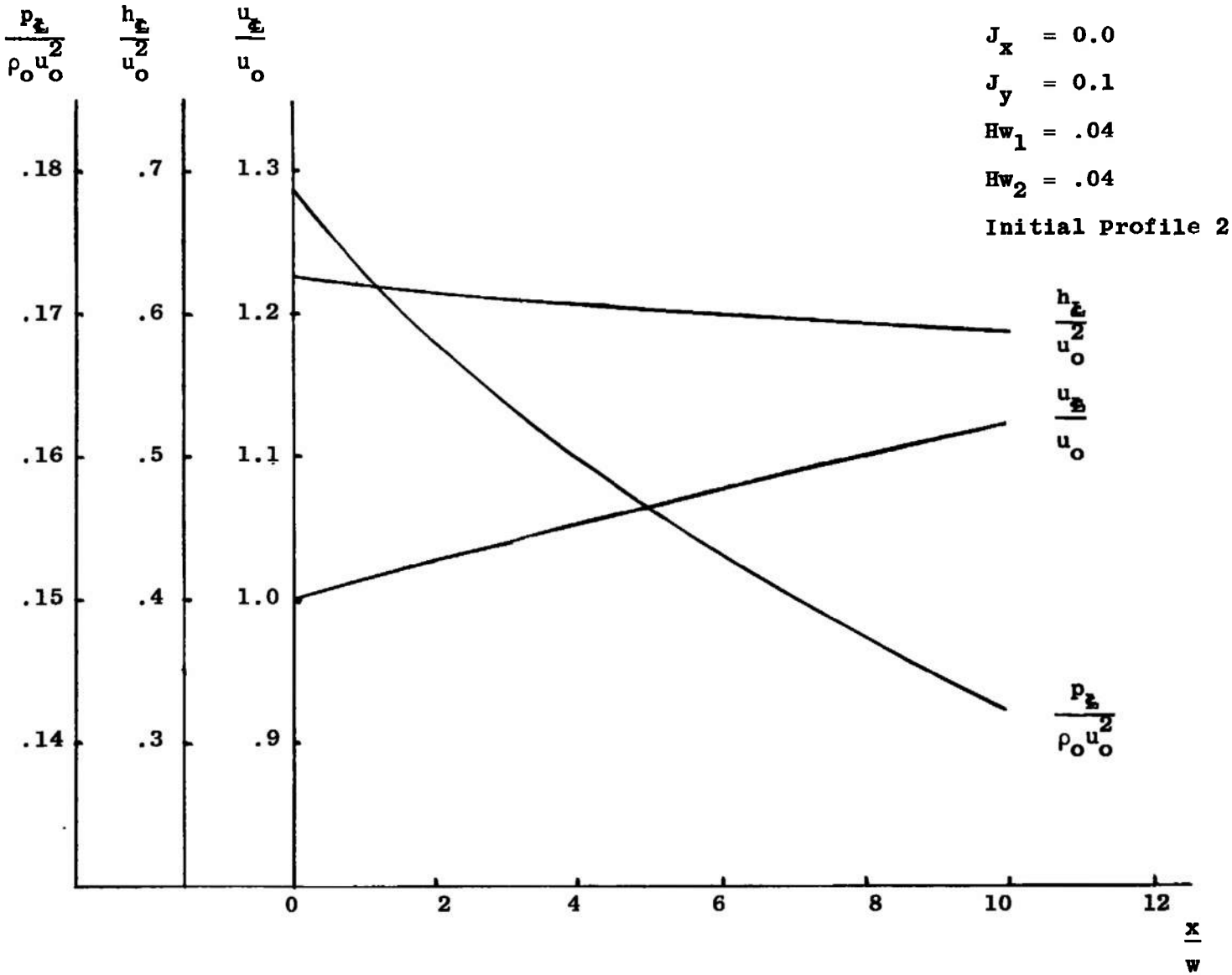

Figure 18. Centerline Distributions of Velocity, Enthalpy, Pressure.

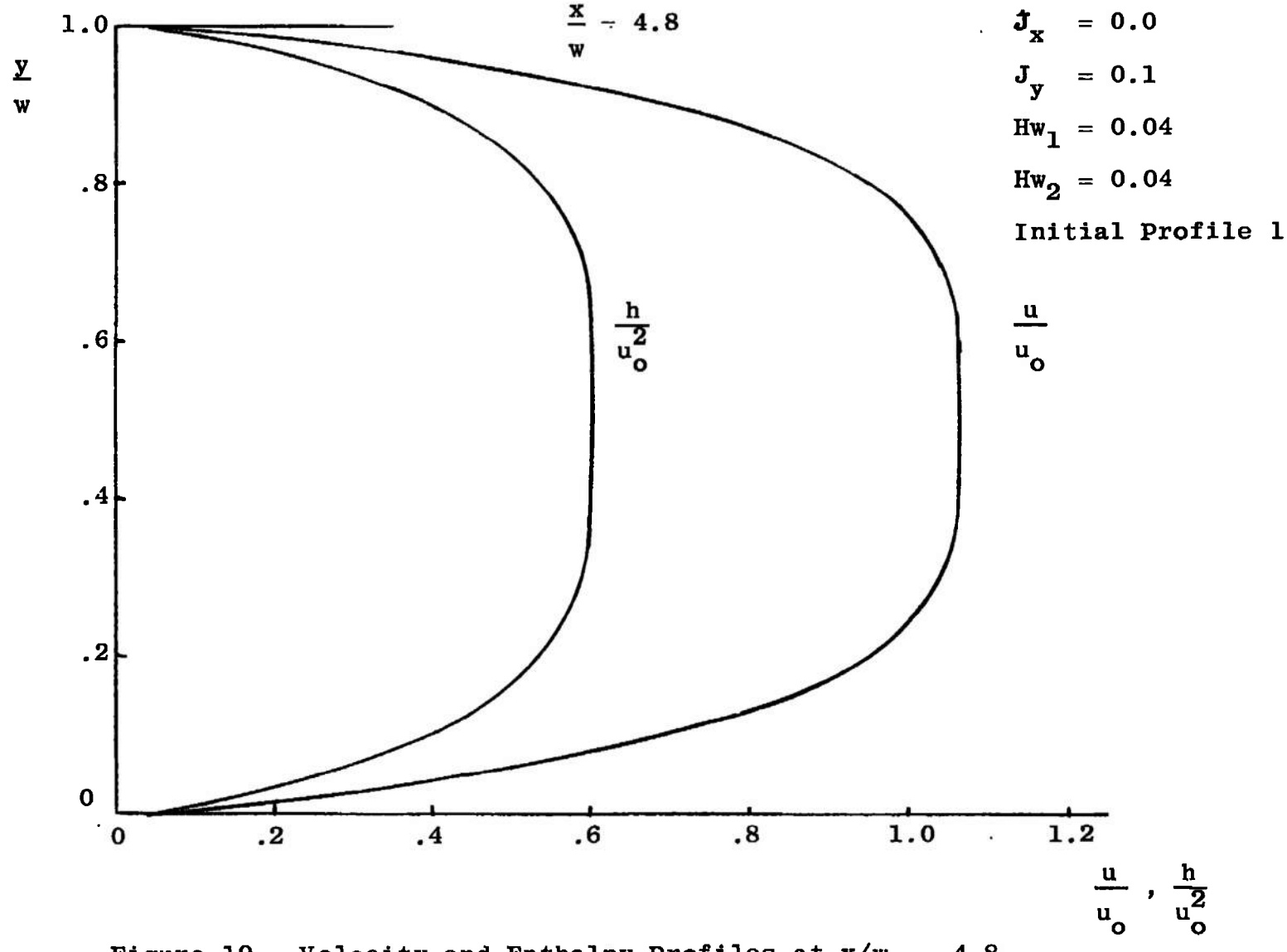

Figure 19. Velocity and Enthalpy Profiles at $x/w_o = 4.8$.

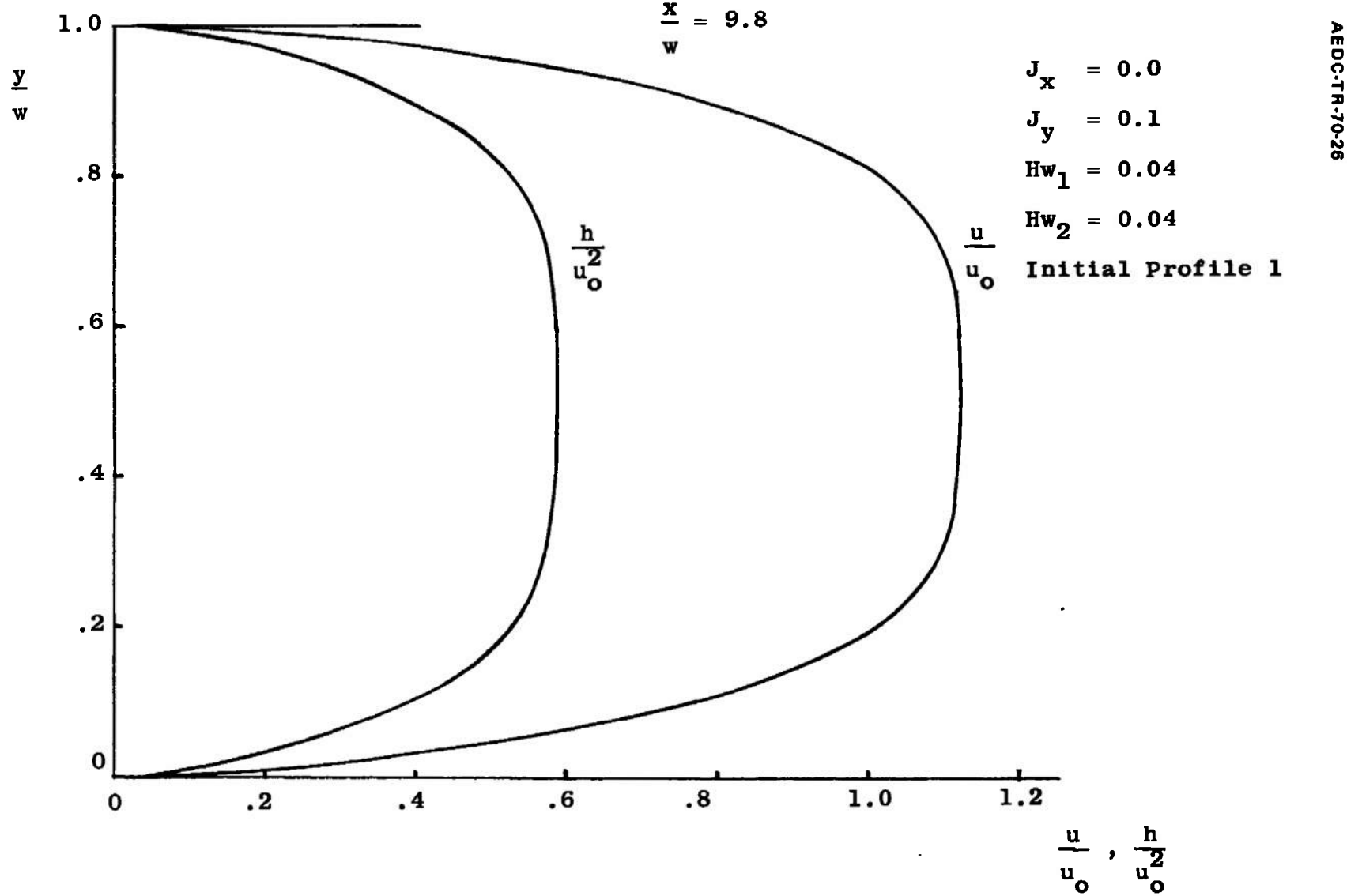

Figure 20. Velocity and Enthalpy Profiles at $x/w_o = 9.8$.

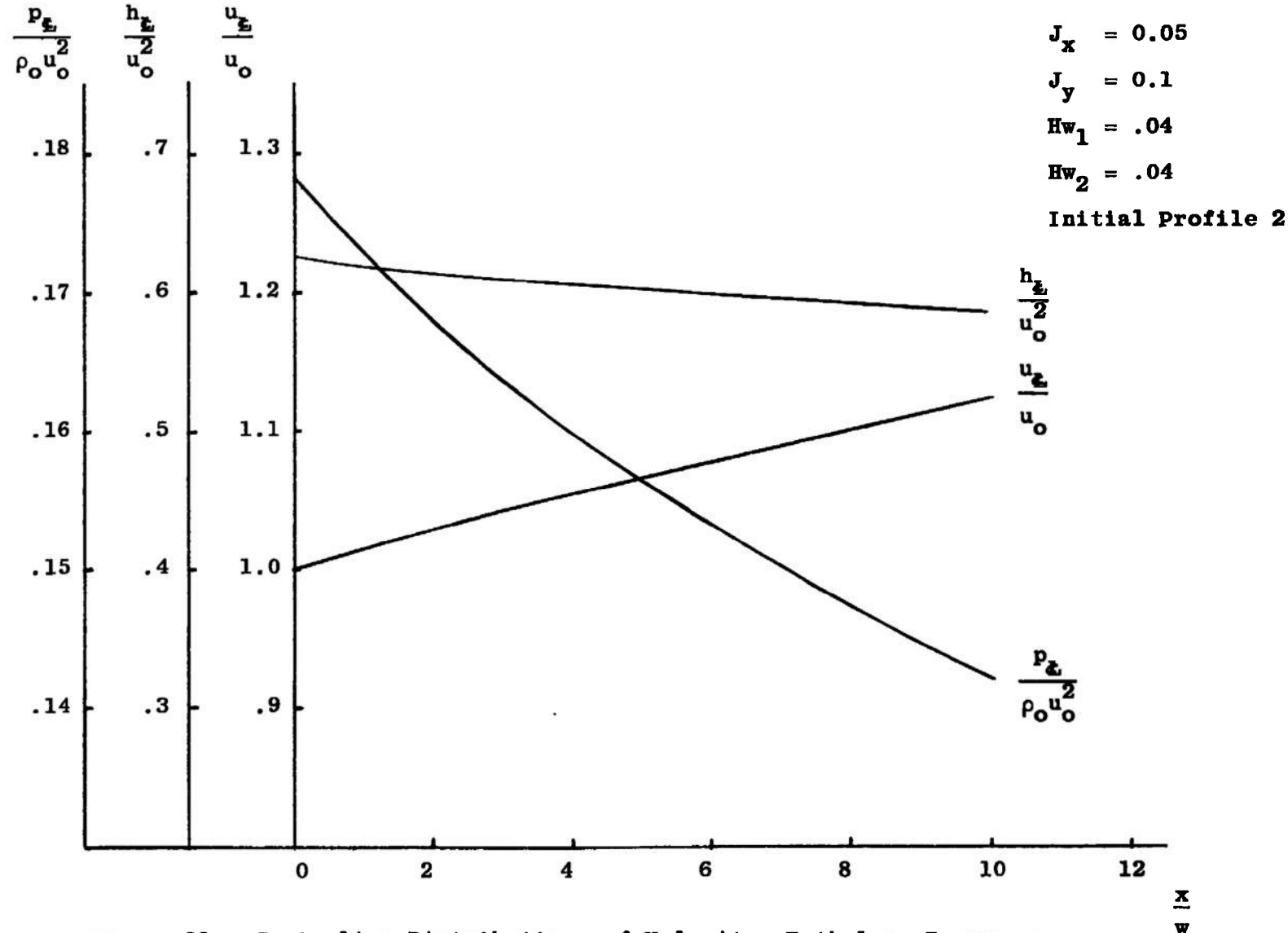

Figure 21. Centerline Distributions of Velocity, Enthalpy, Pressure.

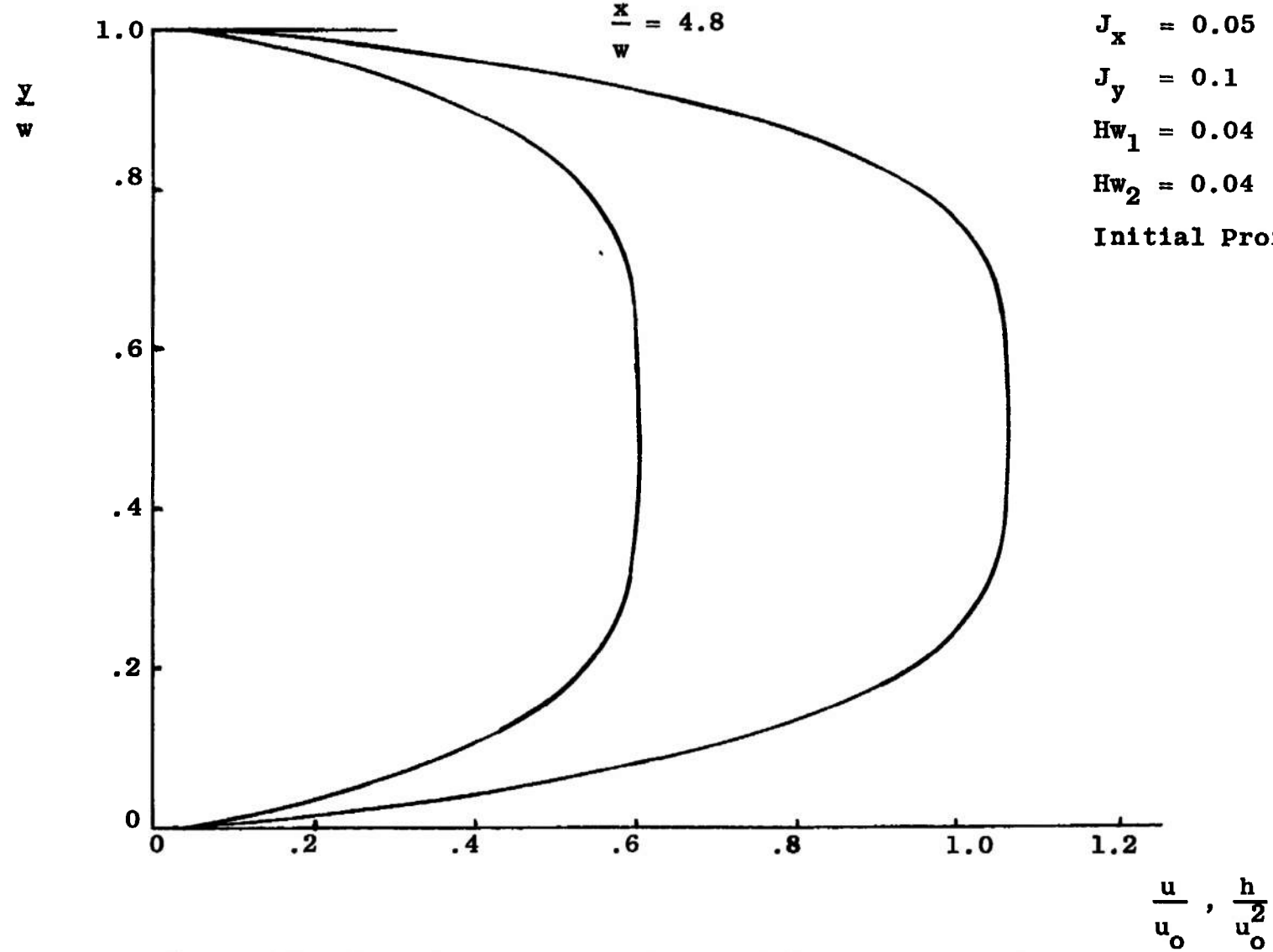

Figure 22. Velocity and Enthalpy Profiles at $x/w_o = 4.8$

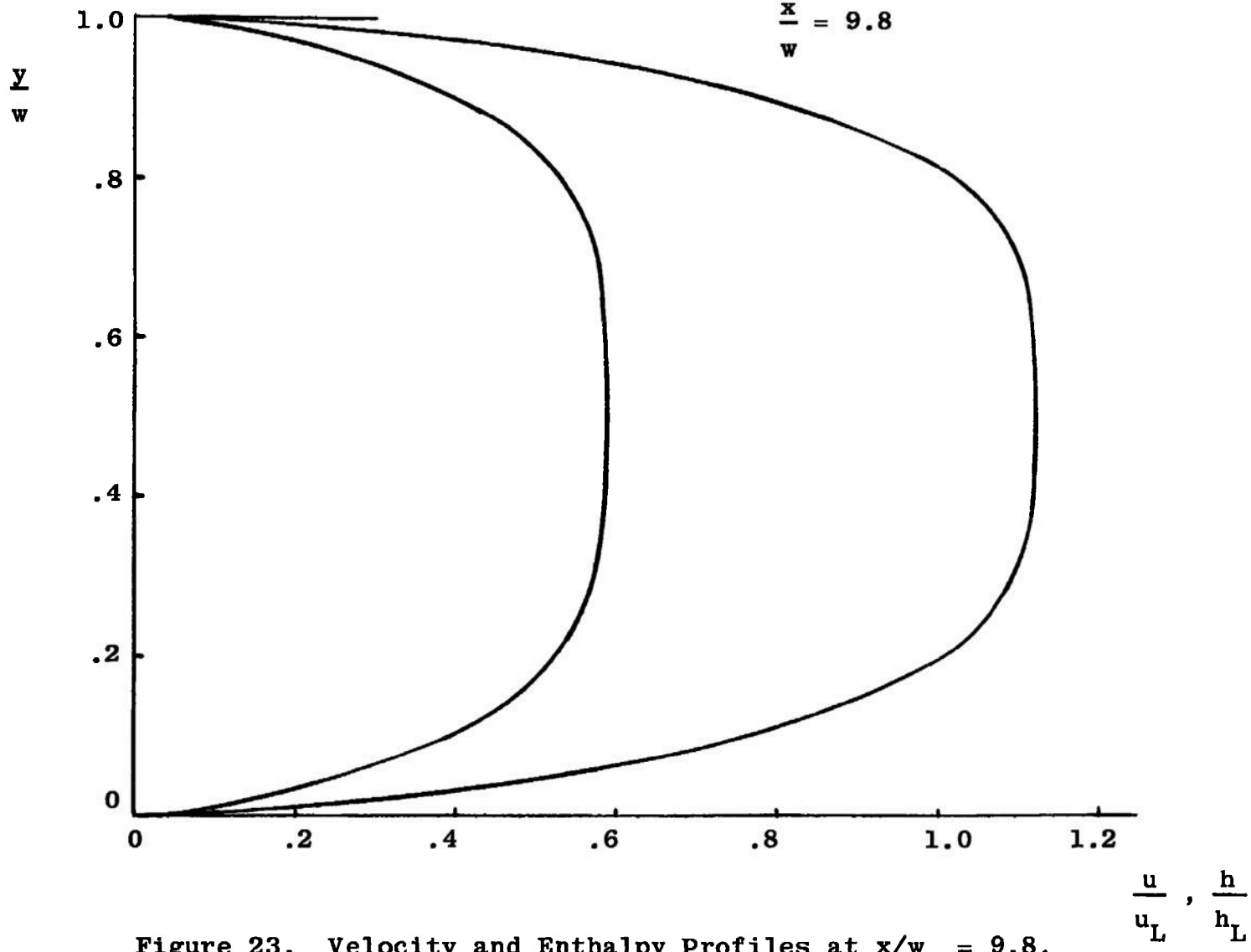

Figure 23. Velocity and Enthalpy Profiles at $x/w_o = 9.8$.

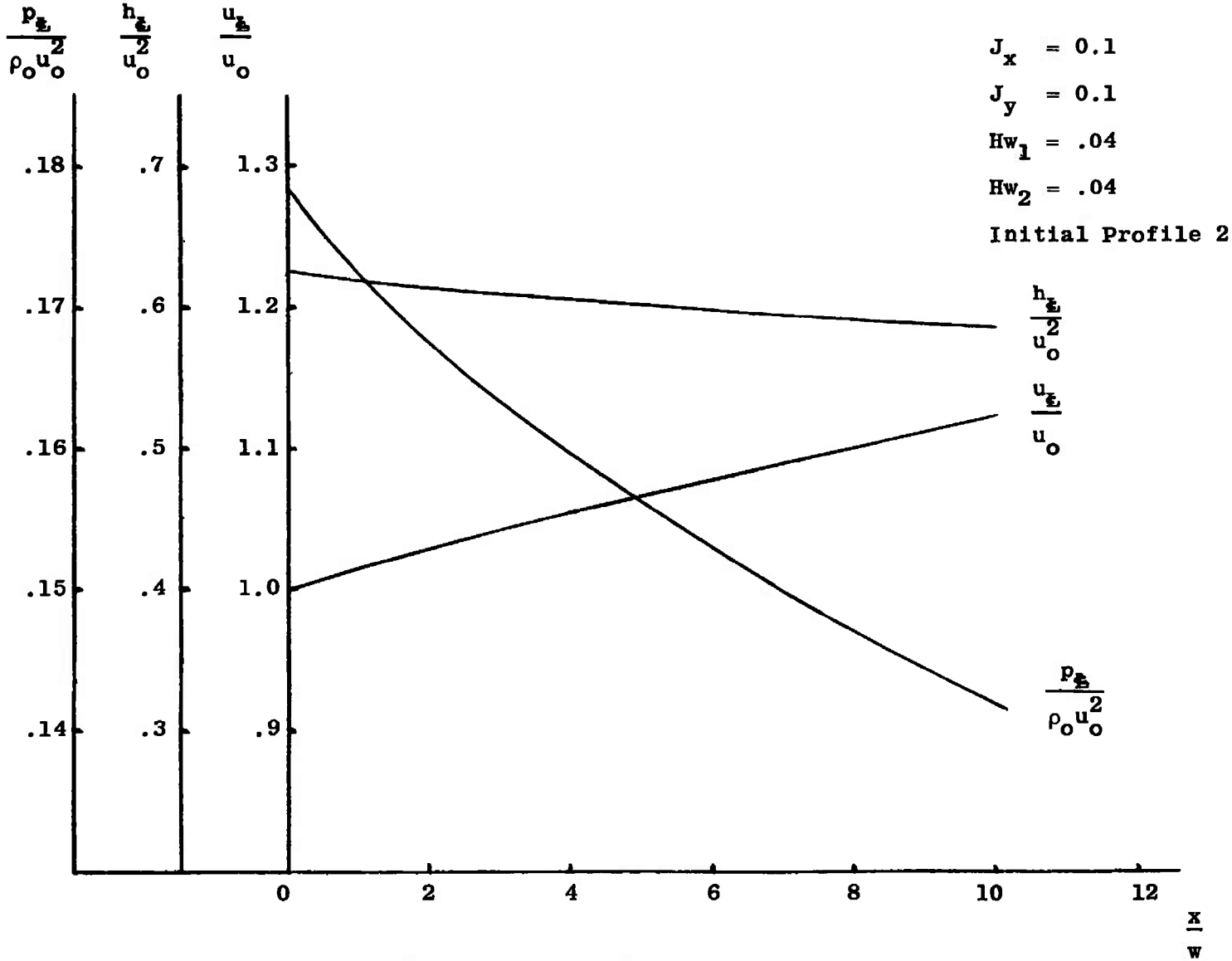

Figure 24. Centerline Distributions of Velocity, Enthalpy, Pressure.

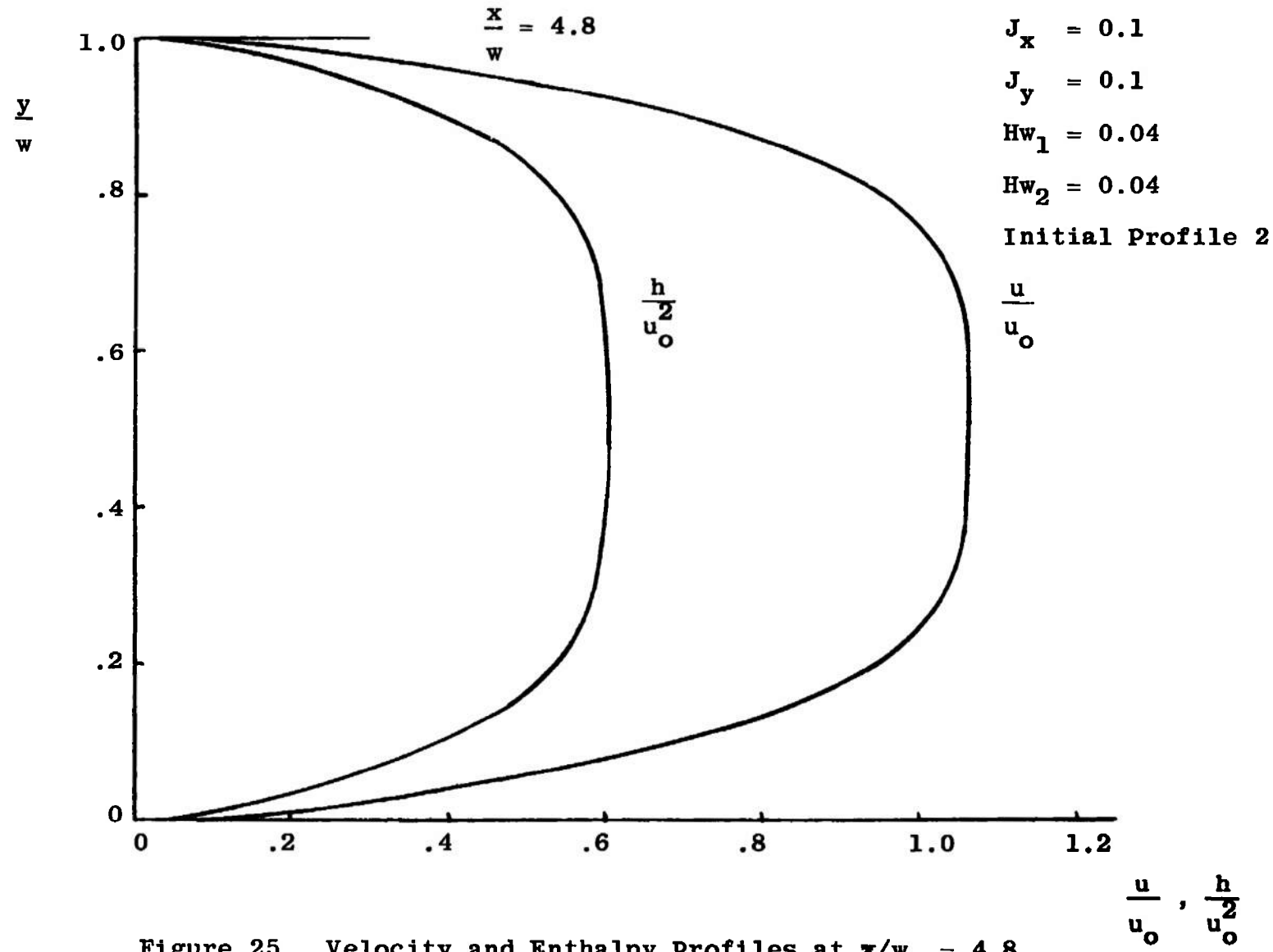

Figure 25. Velocity and Enthalpy Profiles at x/w_o = 4.8.

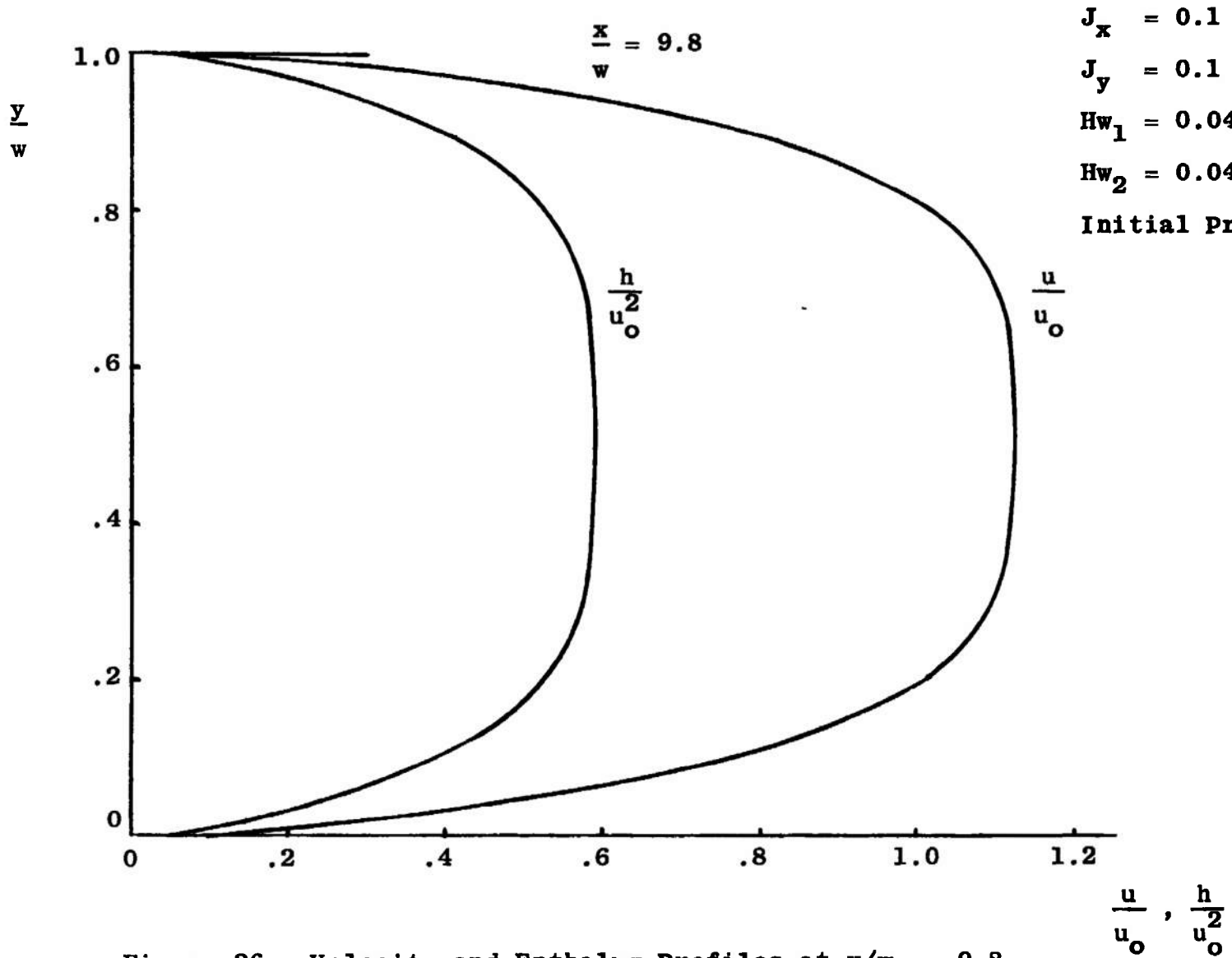

Figure 26. Velocity and Enthalpy Profiles at x/w_o = 9.8.

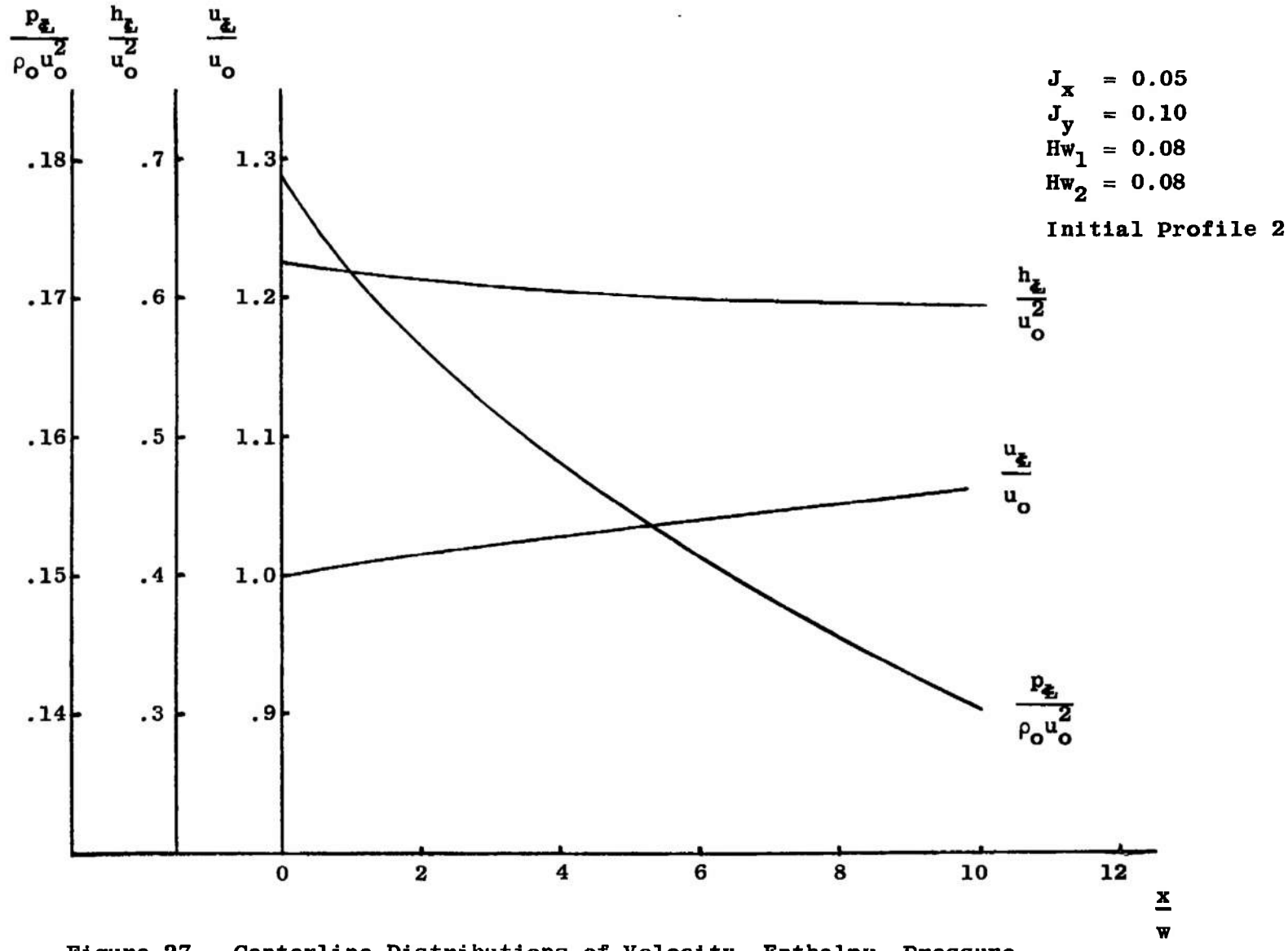

Figure 27. Centerline Distributions of Velocity, Enthalpy, Pressure.

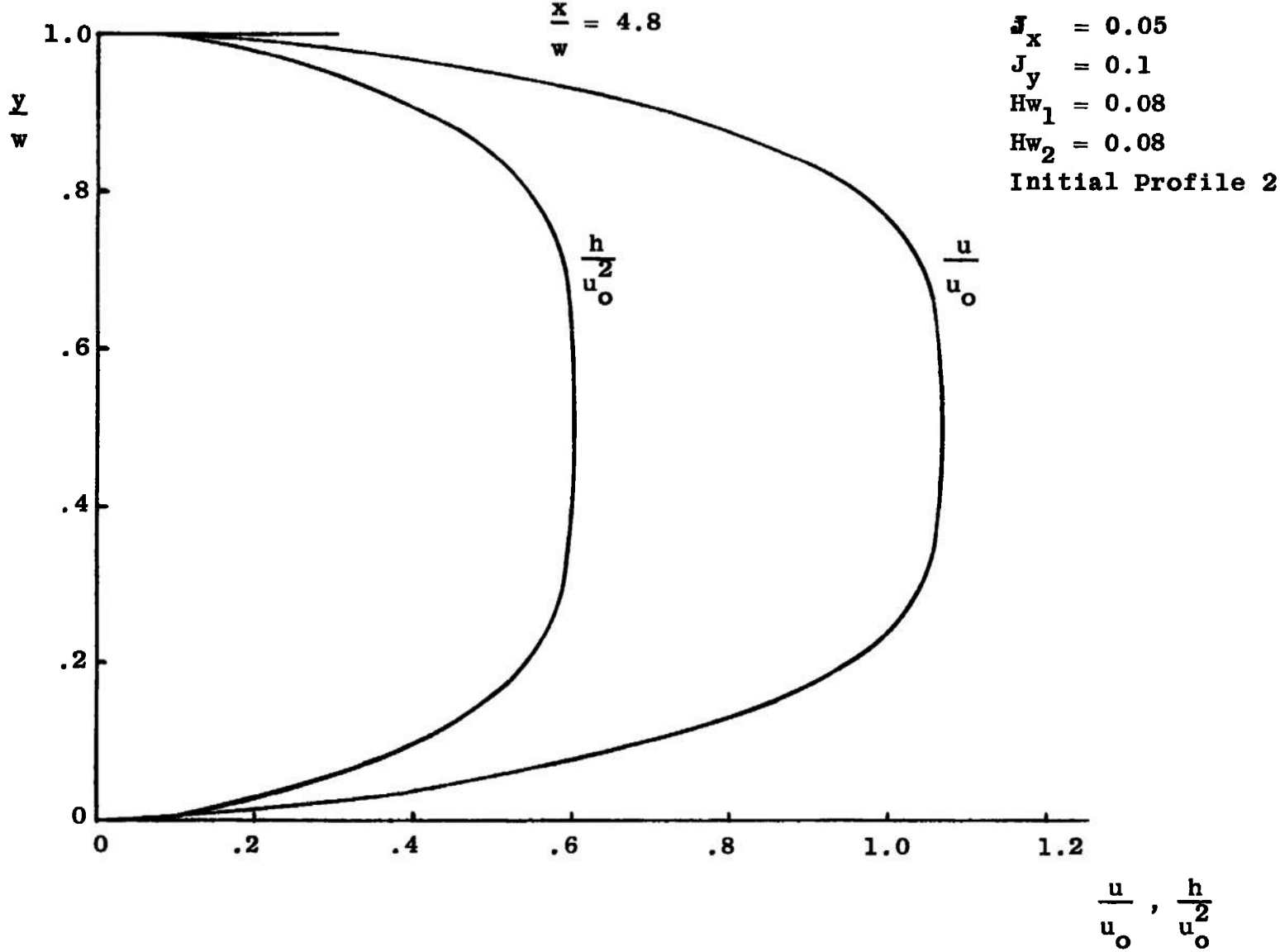

Figure 28. Velocity and Enthalpy Profiles at $x/w_o = 4.8$.

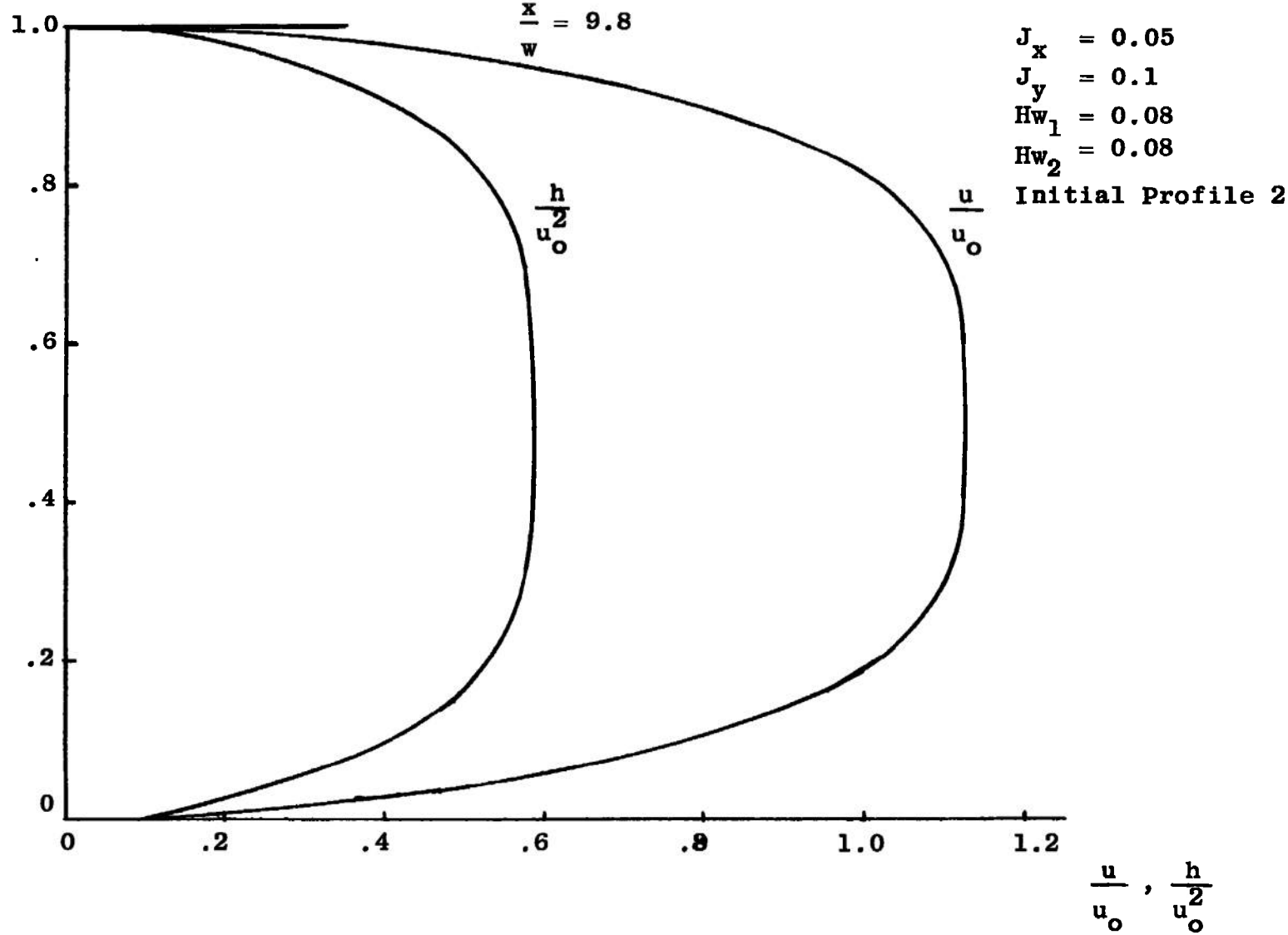

Figure 29. Velocity and Enthalpy Profiles at $x/w_o = 9.8$.

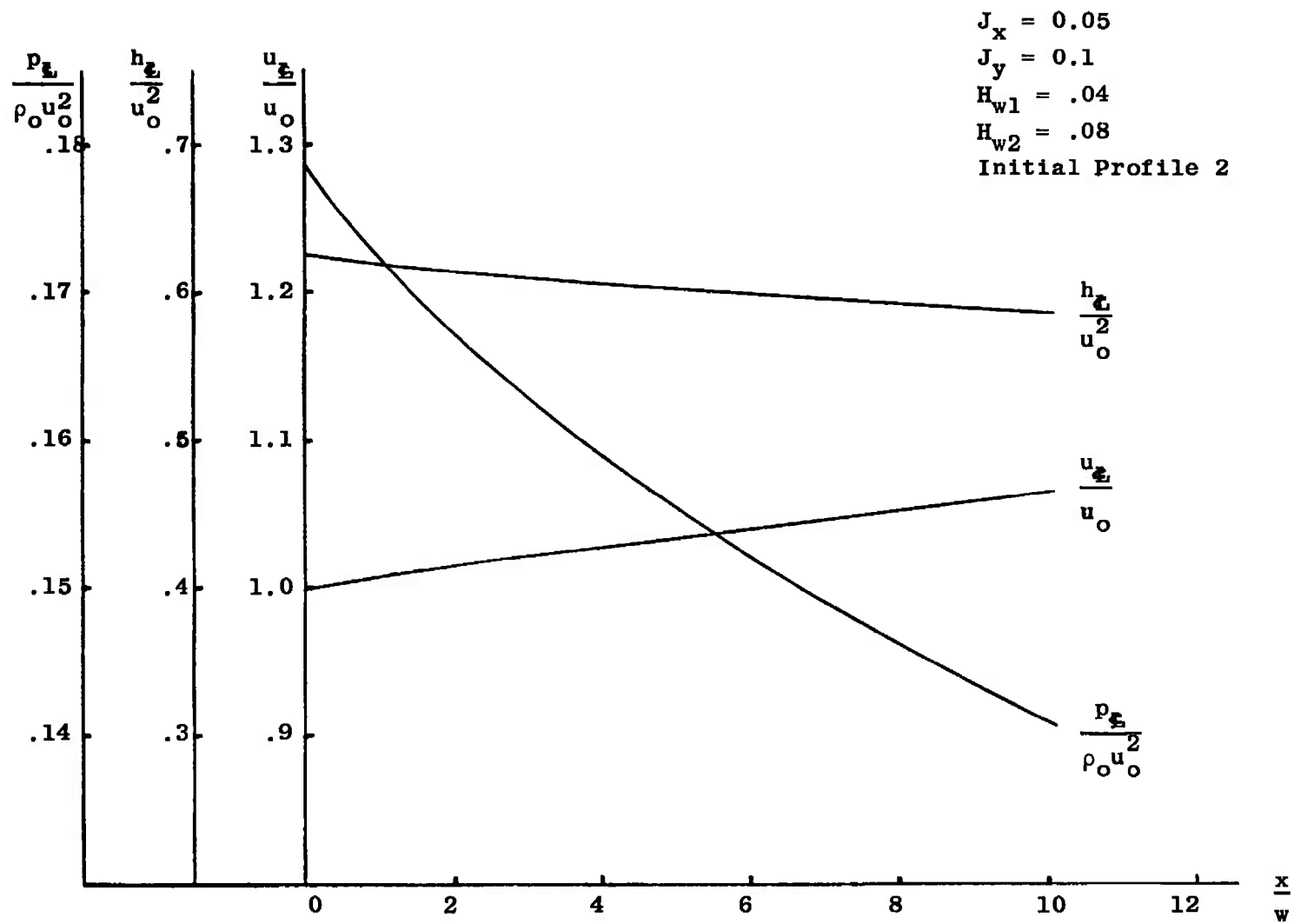

Figure 30. Centerline Distributions of Velocity, Enthalpy, Pressure.

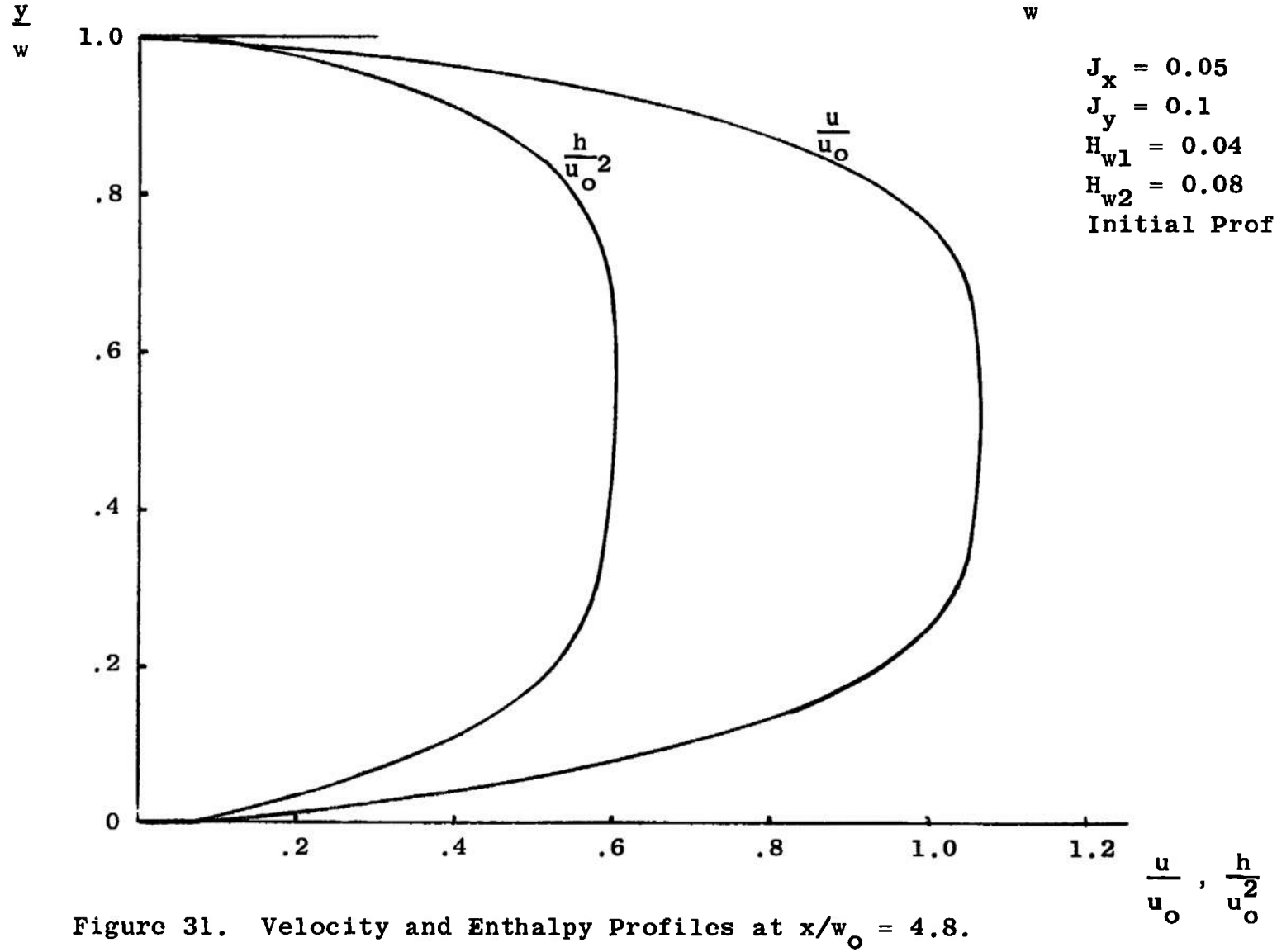

Figure 31. Velocity and Enthalpy Profiles at $x/w_o = 4.8$.

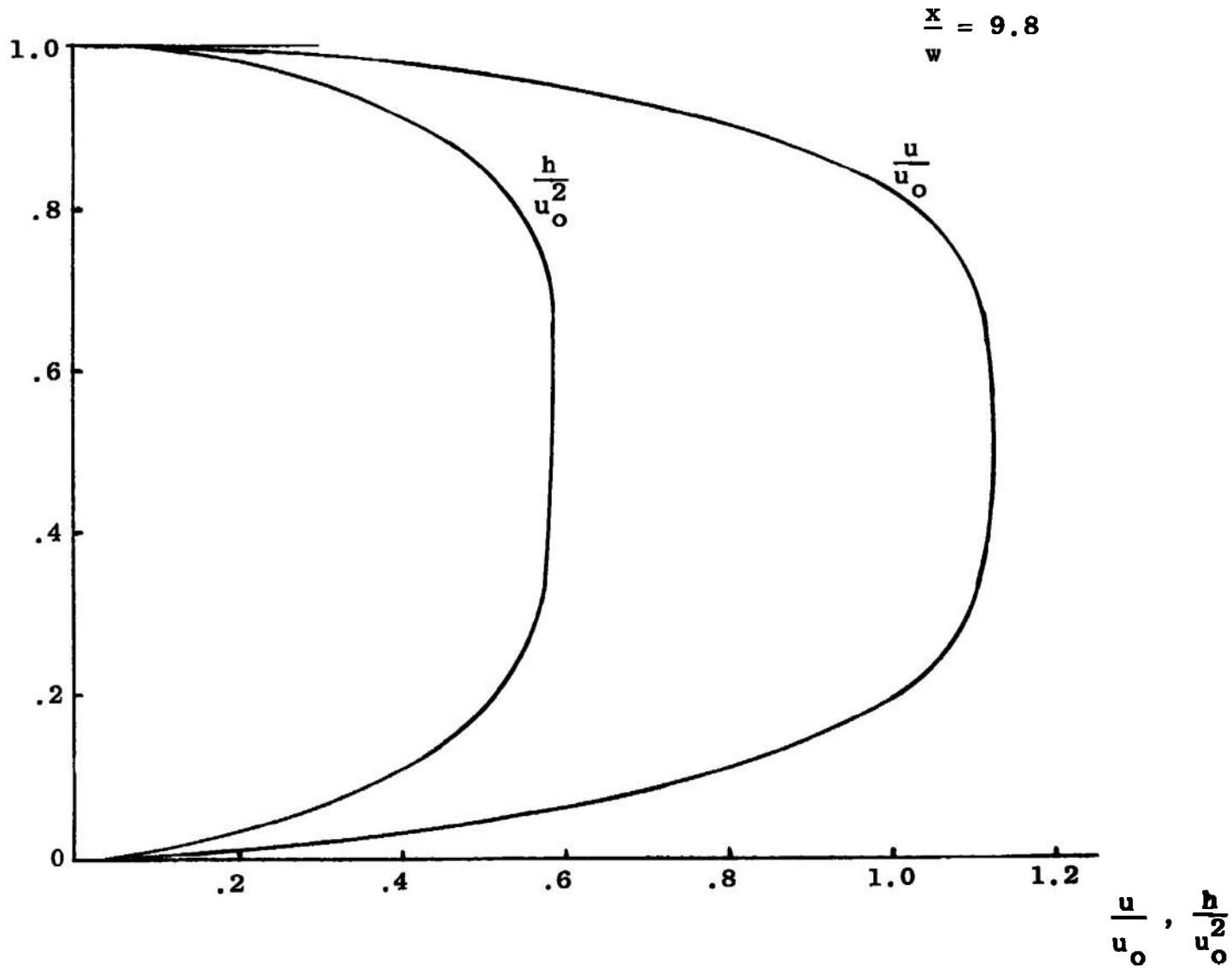

Figure 32. Velocity and Enthalpy Profiles at $x/w_o = 9.8$.

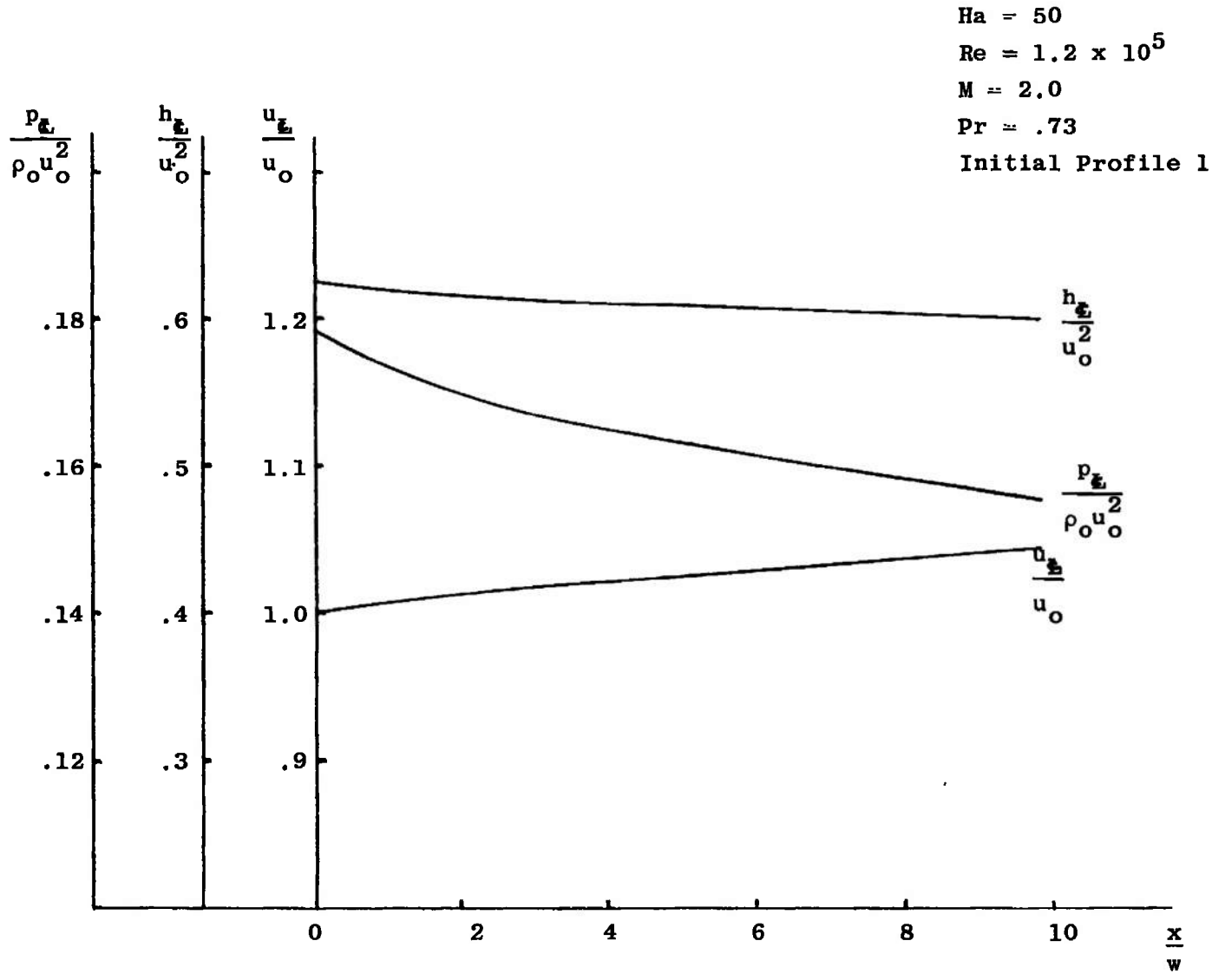

Figure 33. Centerline Distributions of Velocity, Enthalpy, Pressure.

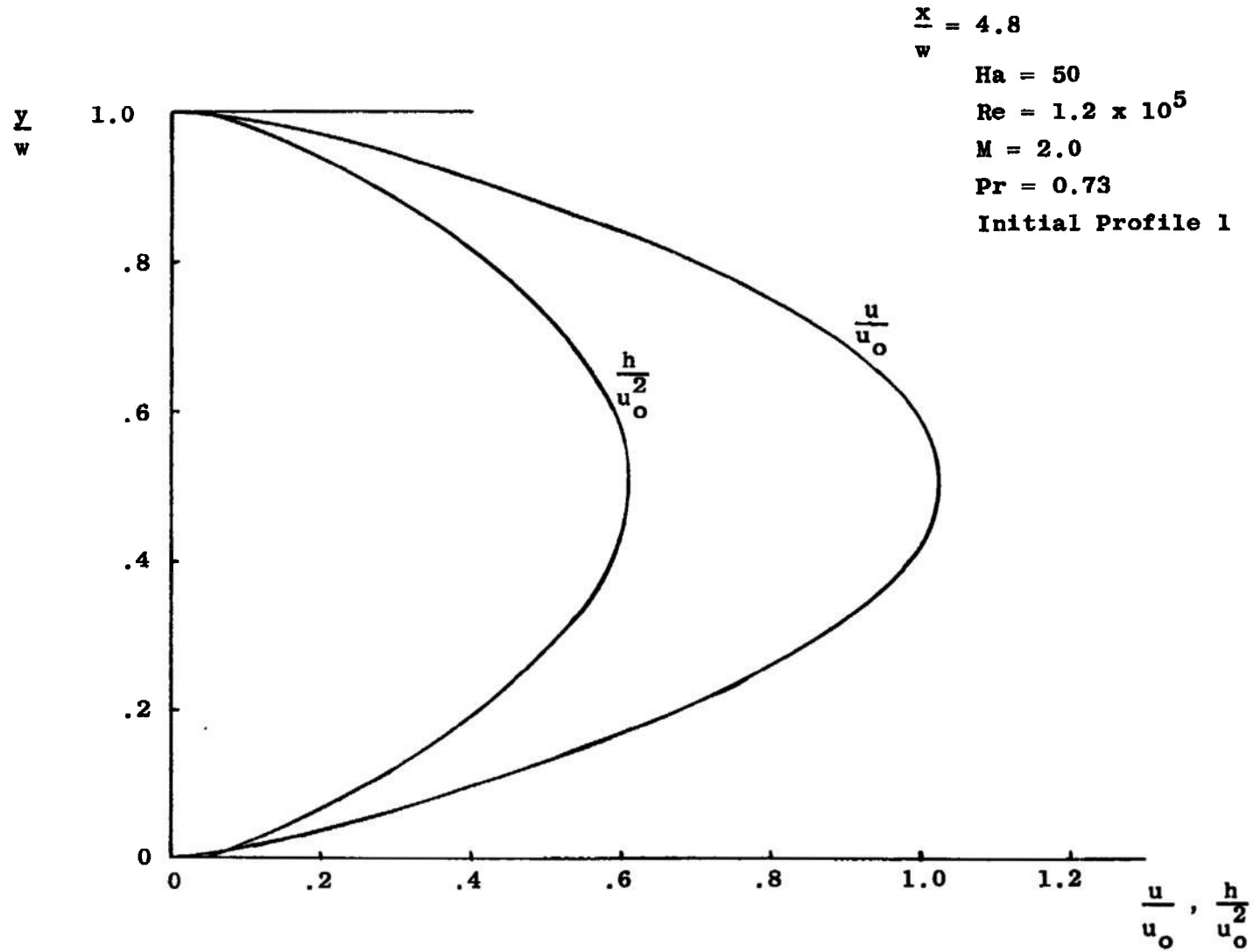

Figure 34. Velocity and Enthalpy Profiles at $x/w_o = 4.8$.

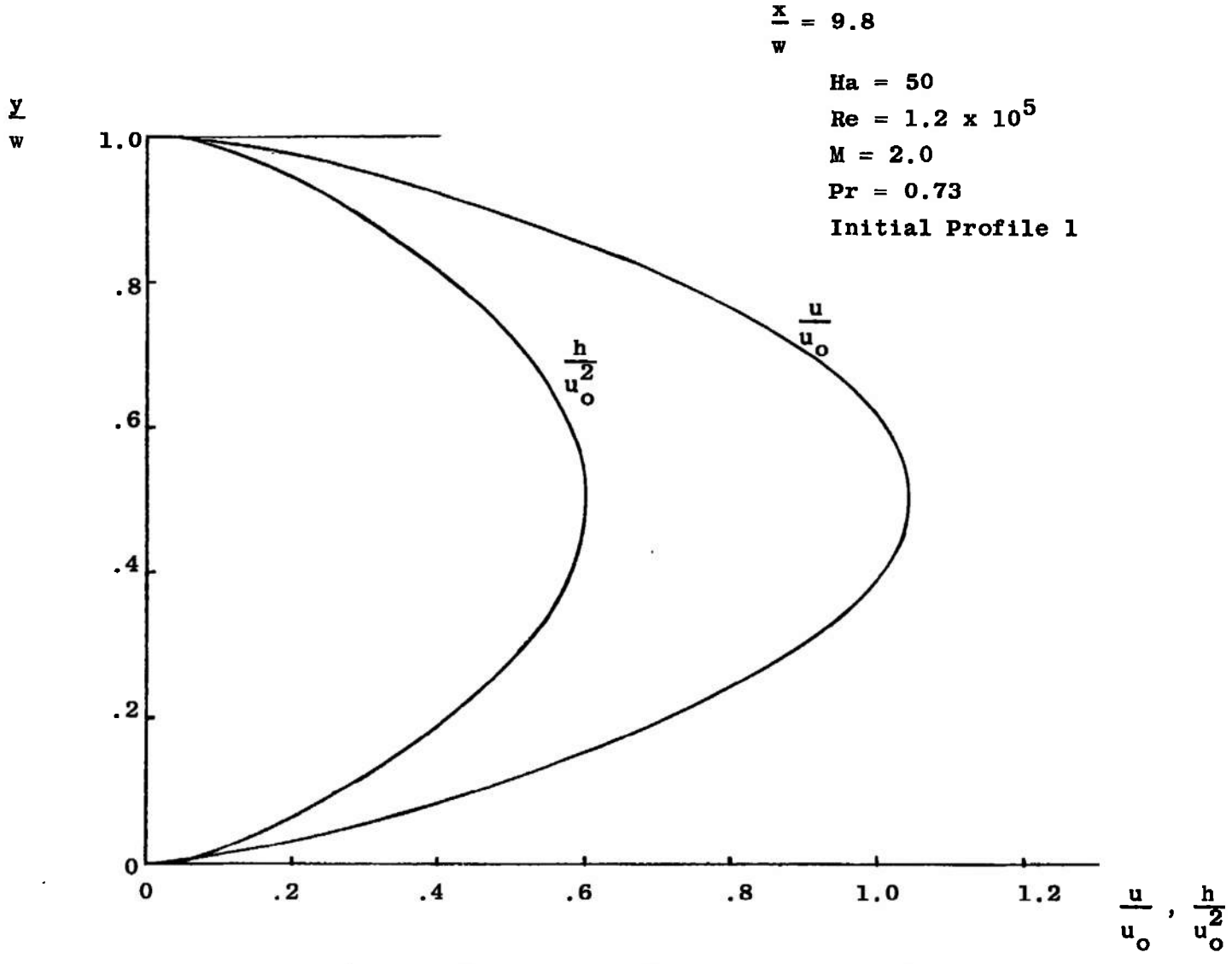

Figure 35. Velocity and Enthalpy Profiles at $x/w_o = 9.8$.

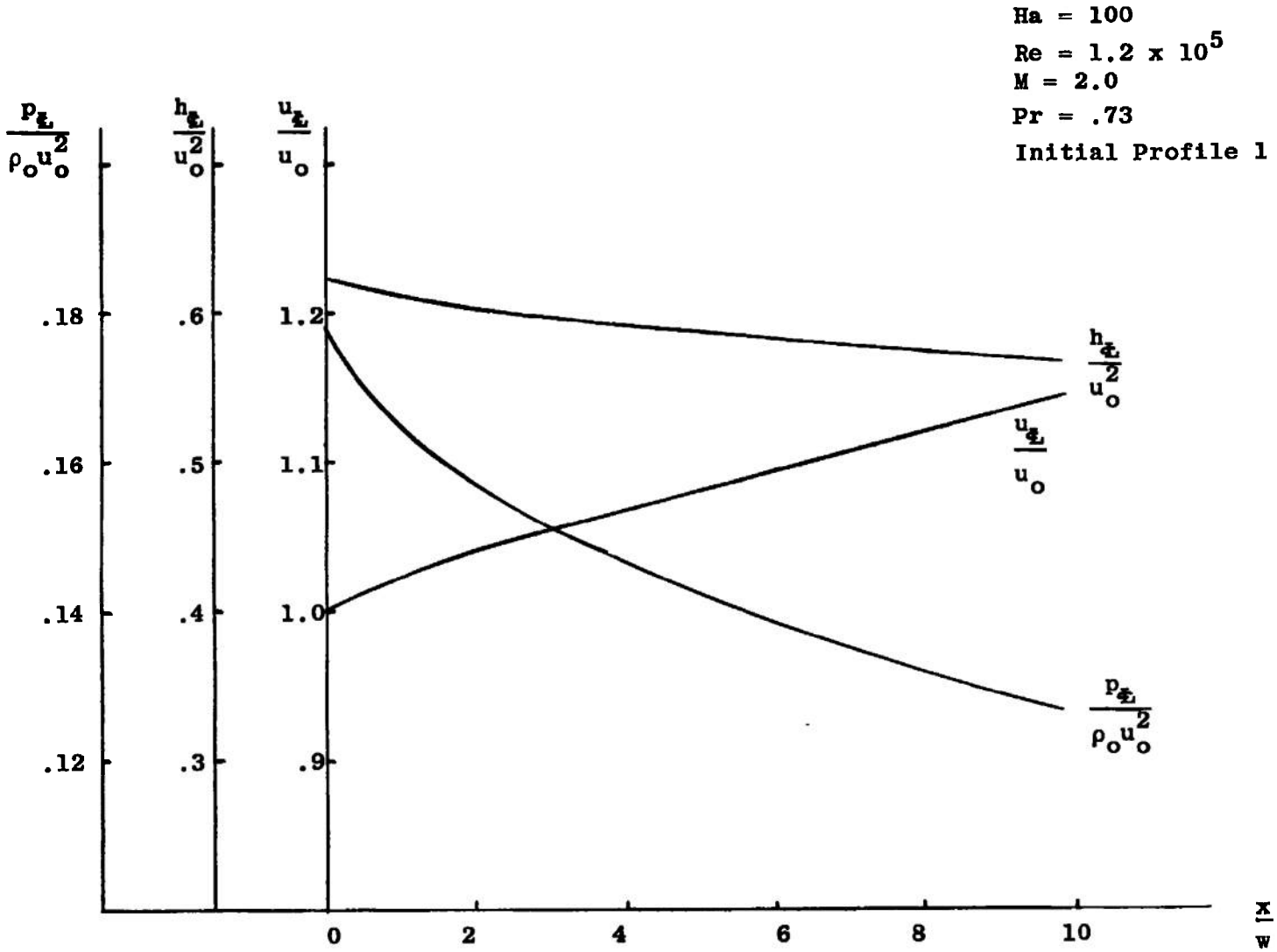

Figure 36. Centerline Distributions of Velocity, Enthalpy, Pressure.

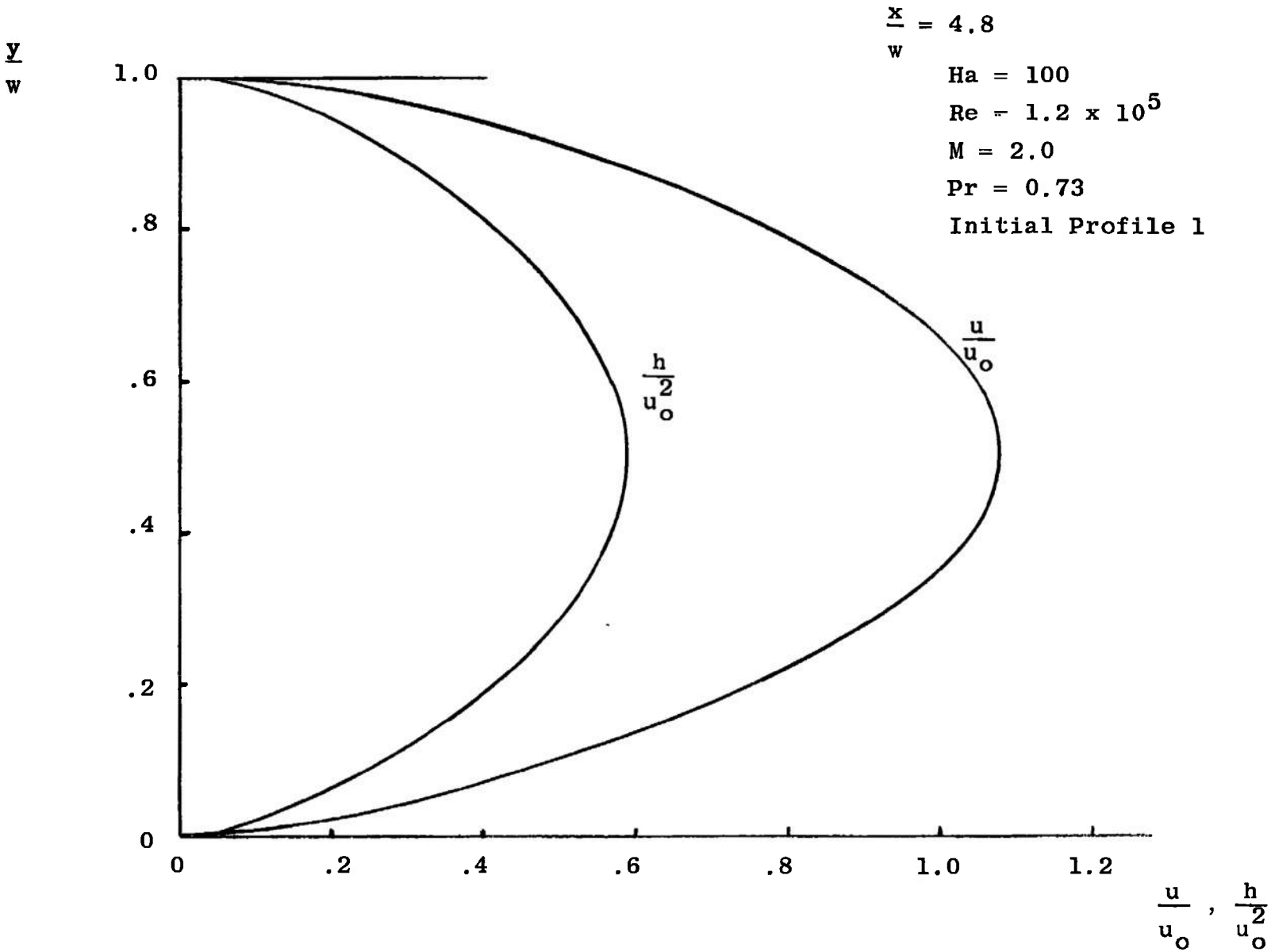

Figure 37. Velocity and Enthalpy Distributions at $x/w_o = 4.8$.

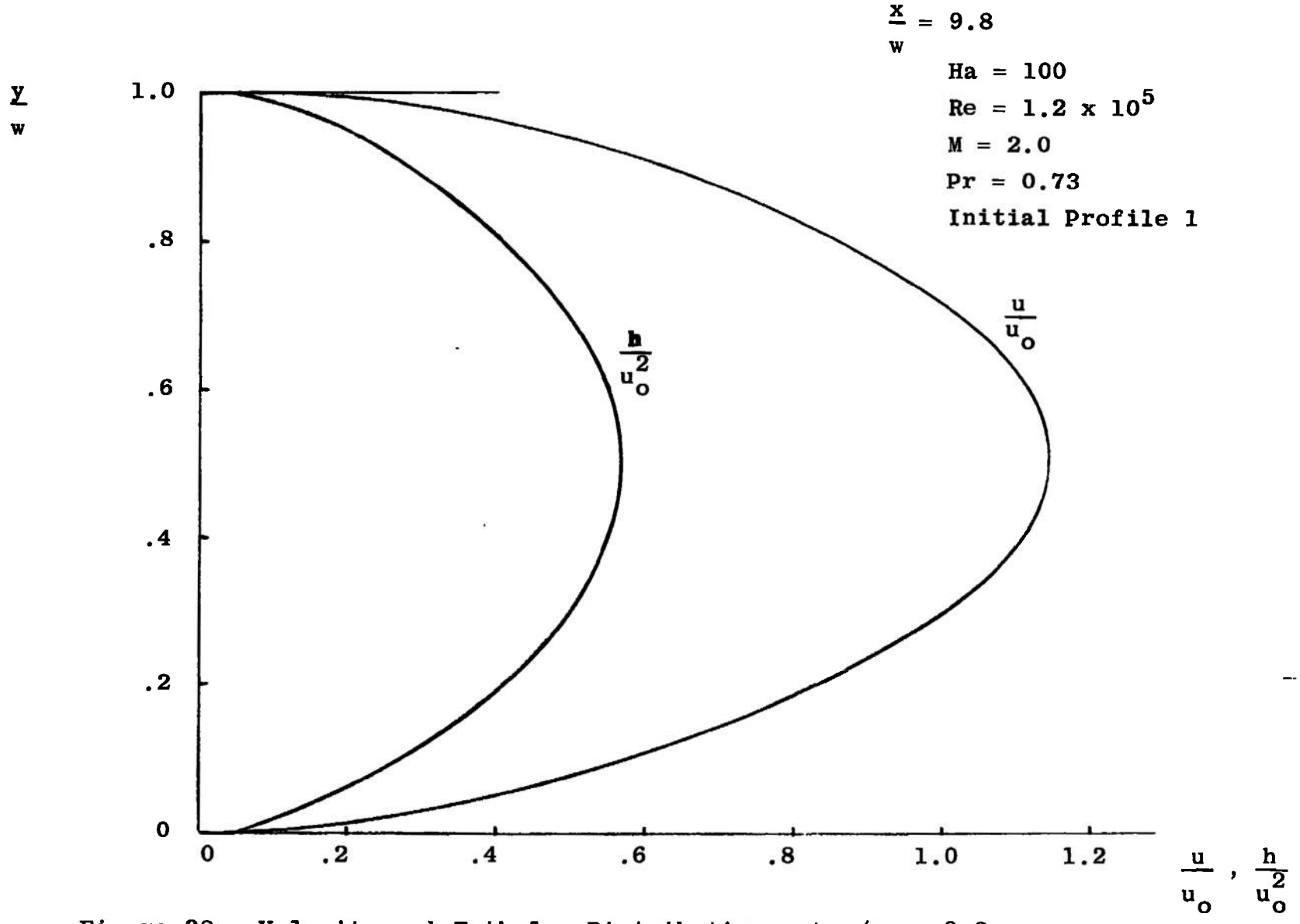

Figure 38. Velocity and Enthalpy Distributions at $x/w_o = 9.8$.

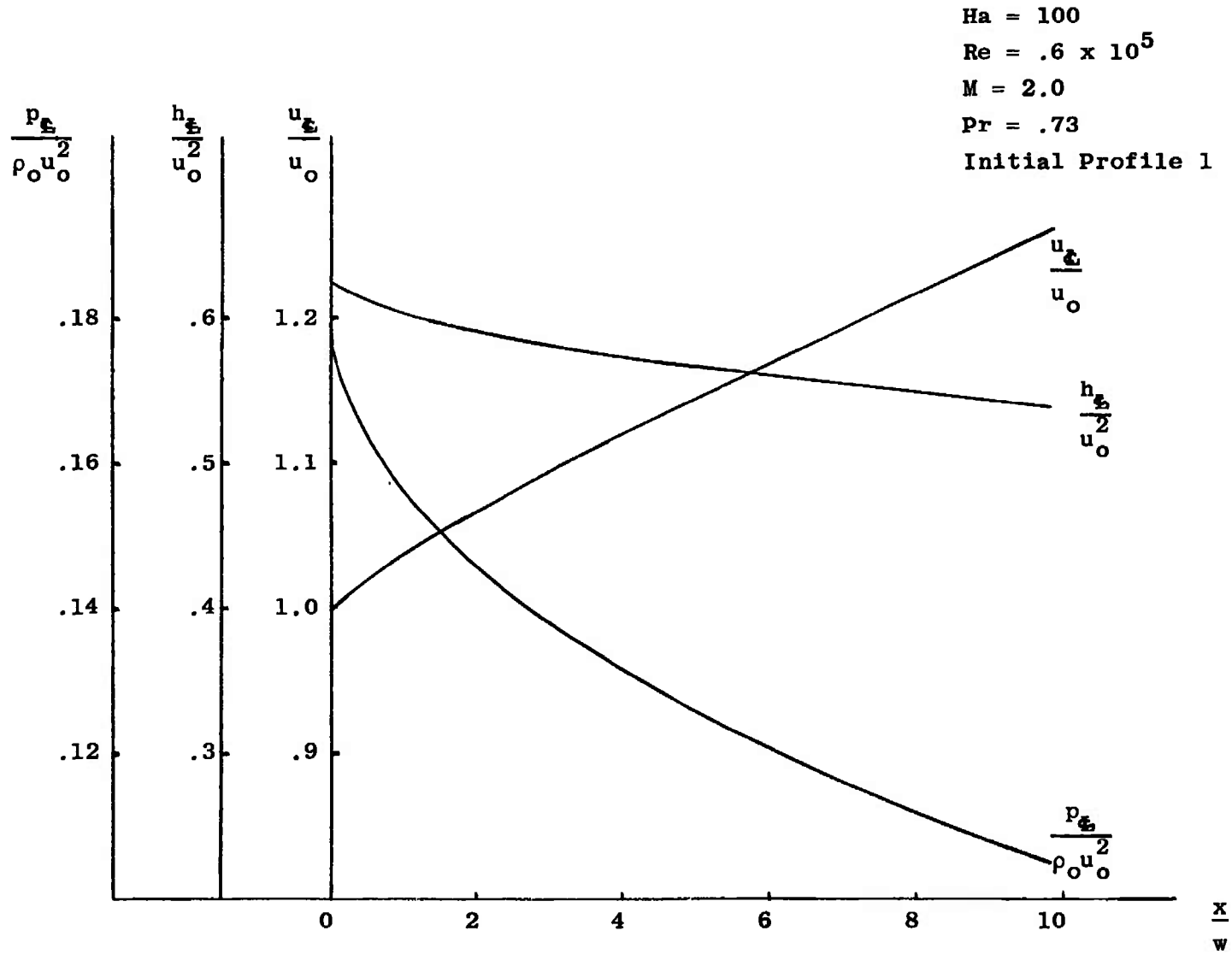

Figure 39. Centerline Distributions of Velocity, Enthalpy, Pressure.

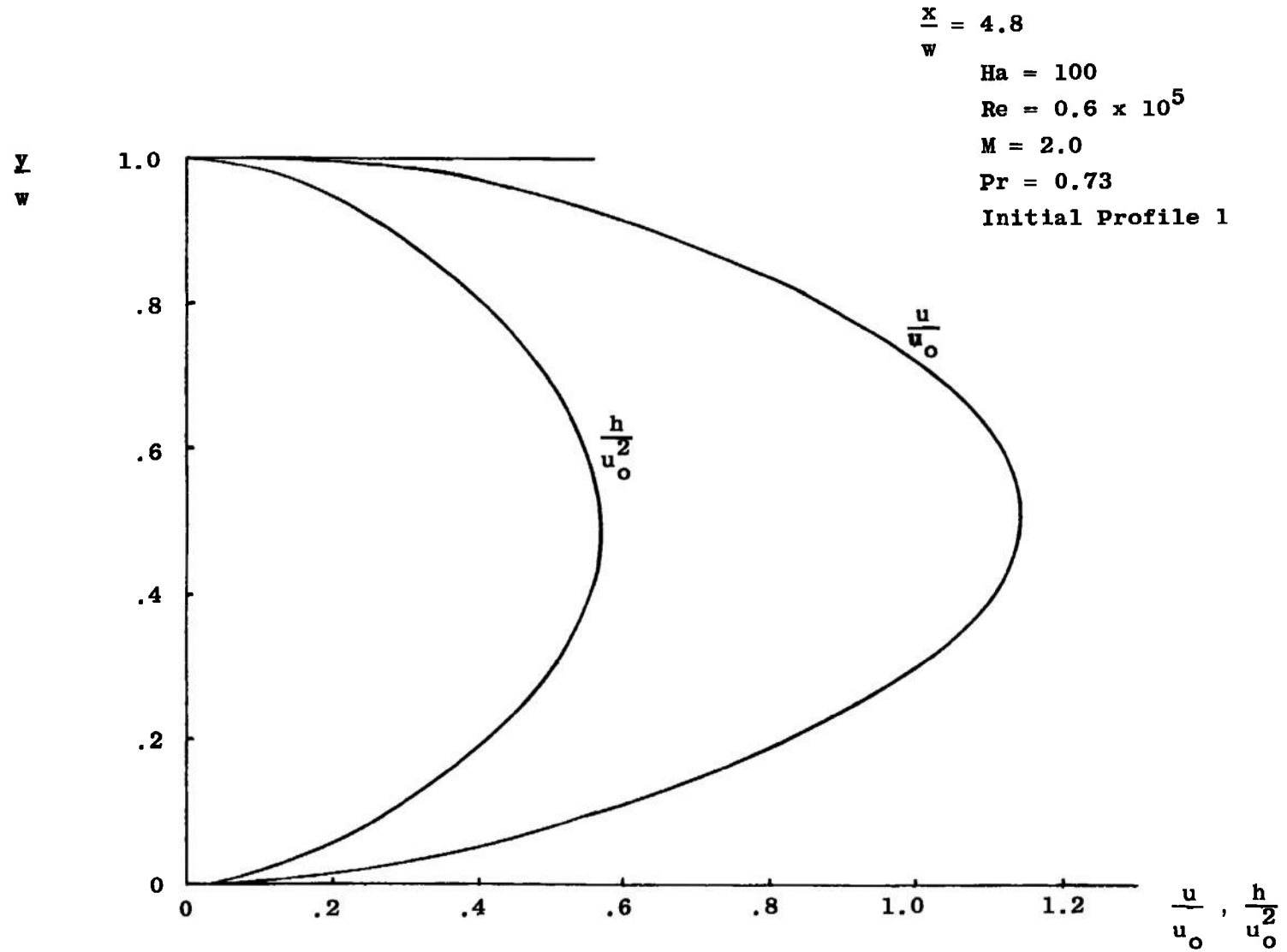

Figure 40. Velocity and Enthalpy Profiles at $x/w_o = 4.8$.

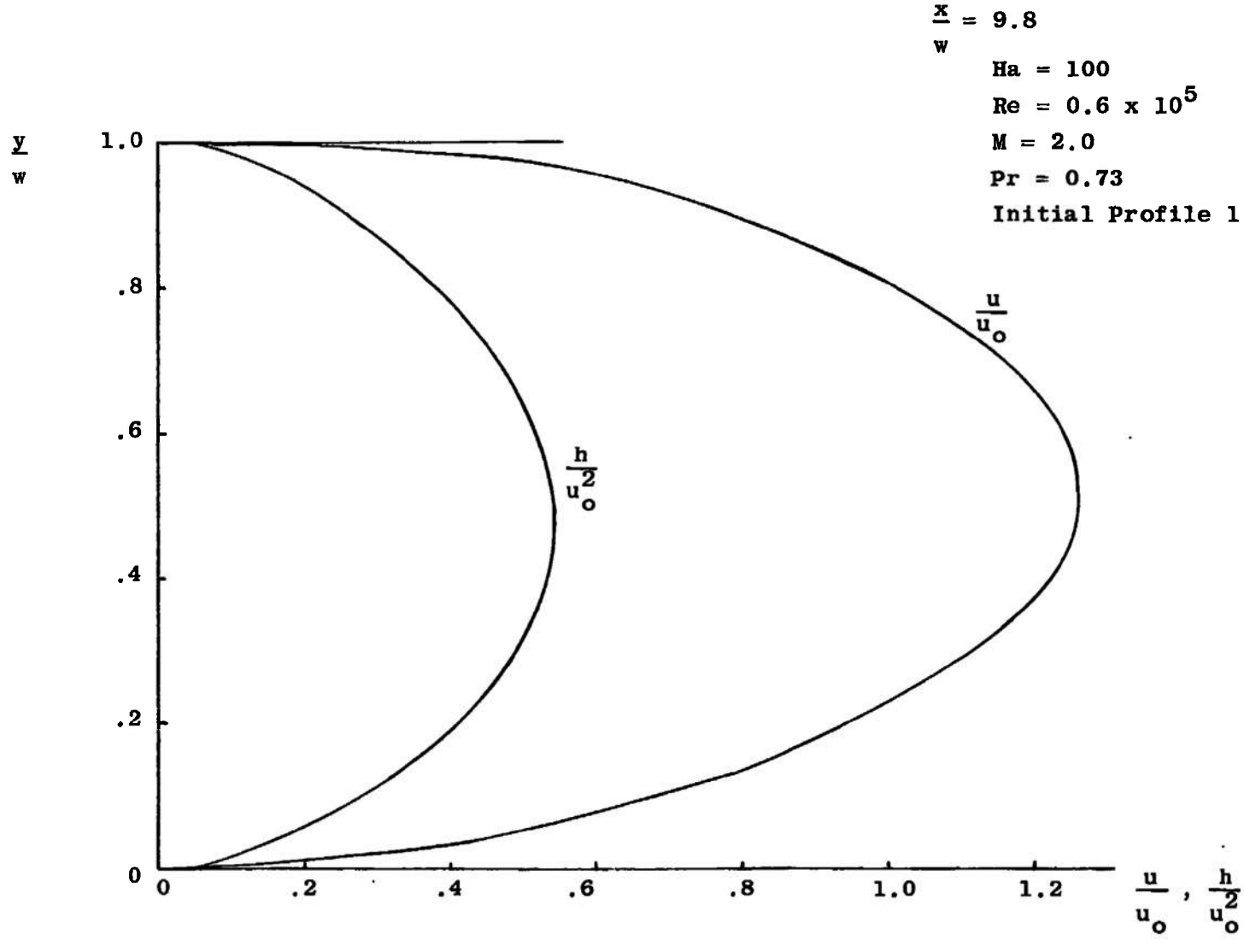

Figure 41. Velocity and Enthalpy Profiles at $x/w_o = 9.8$.

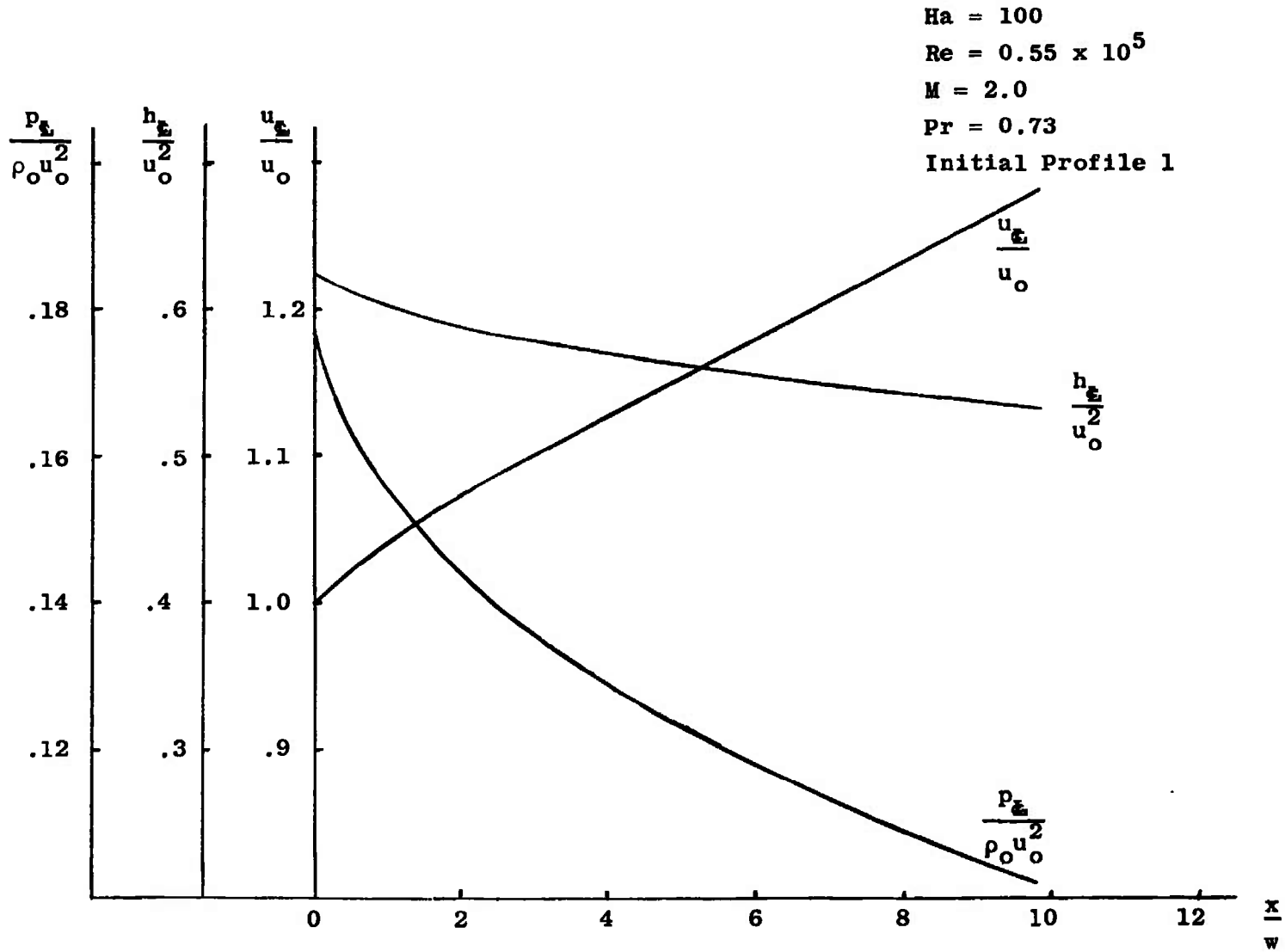

Figure 42. Centerline Distributions of Velocity, Enthalpy, Pressure.

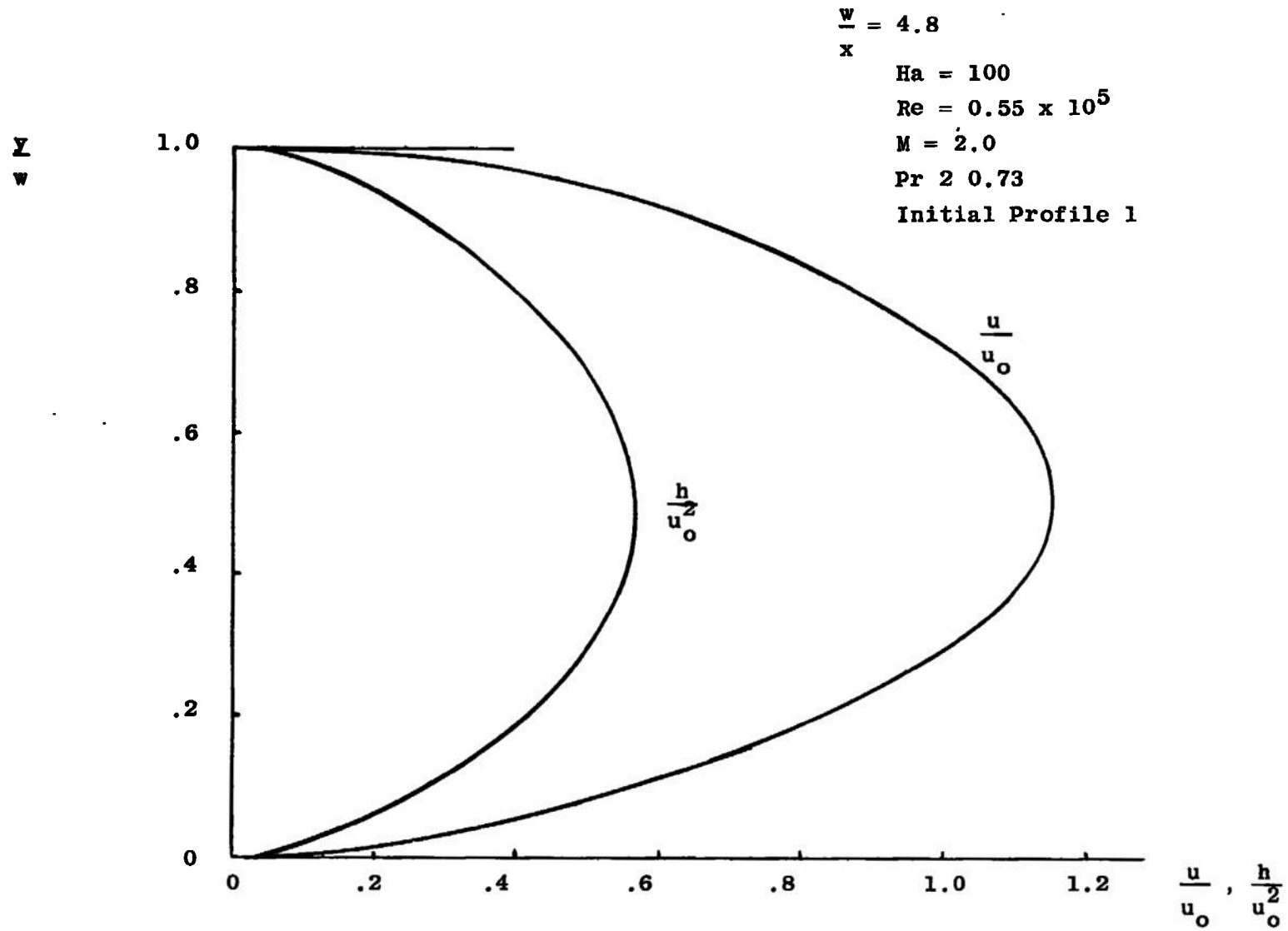

Figure 43. Velocity and Enthalpy Profiles at $x/w_o = 4.8$.

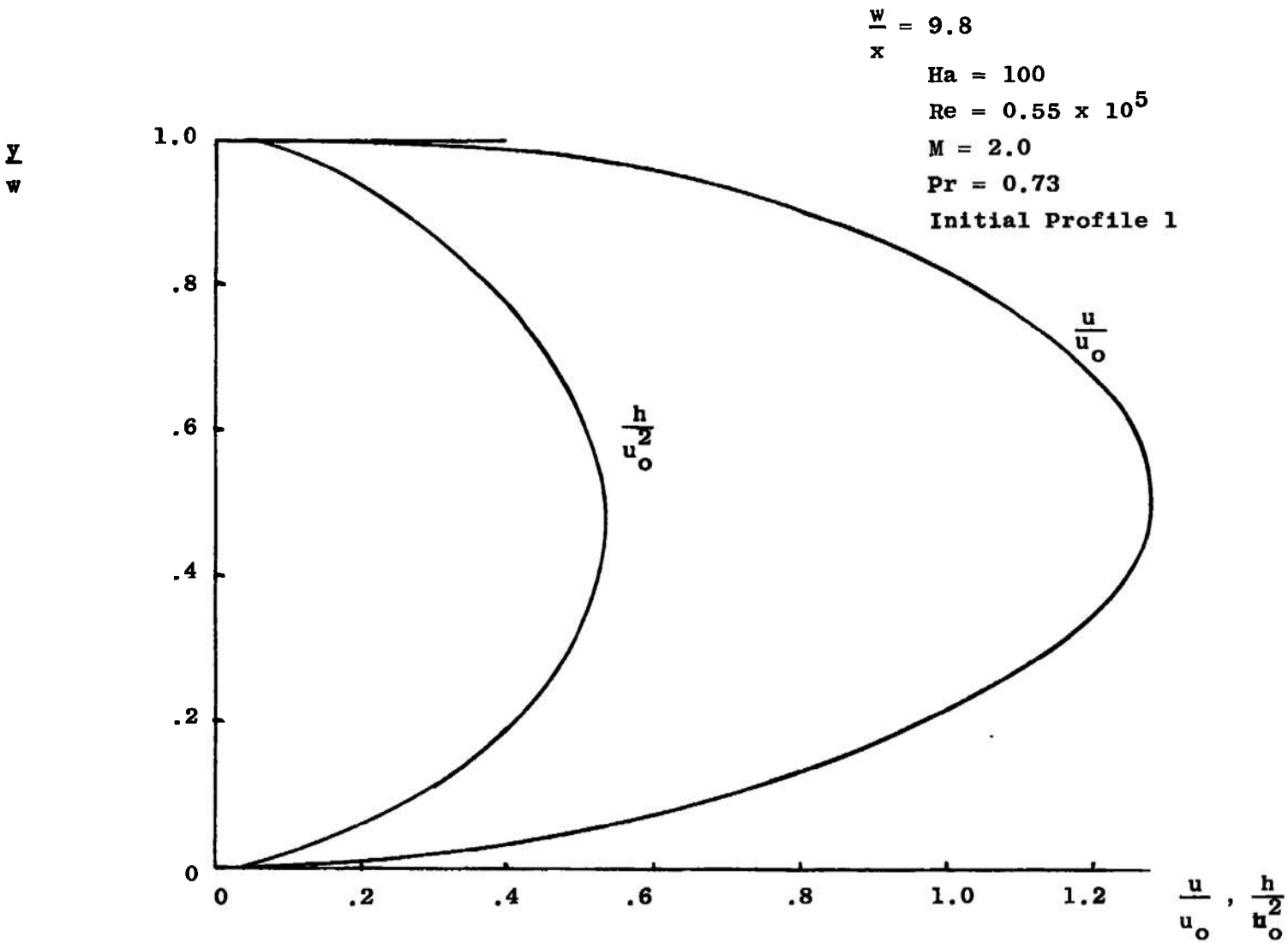

Figure 44. Velocity and Enthalpy Profiles at $x/w_o = 9.8$.

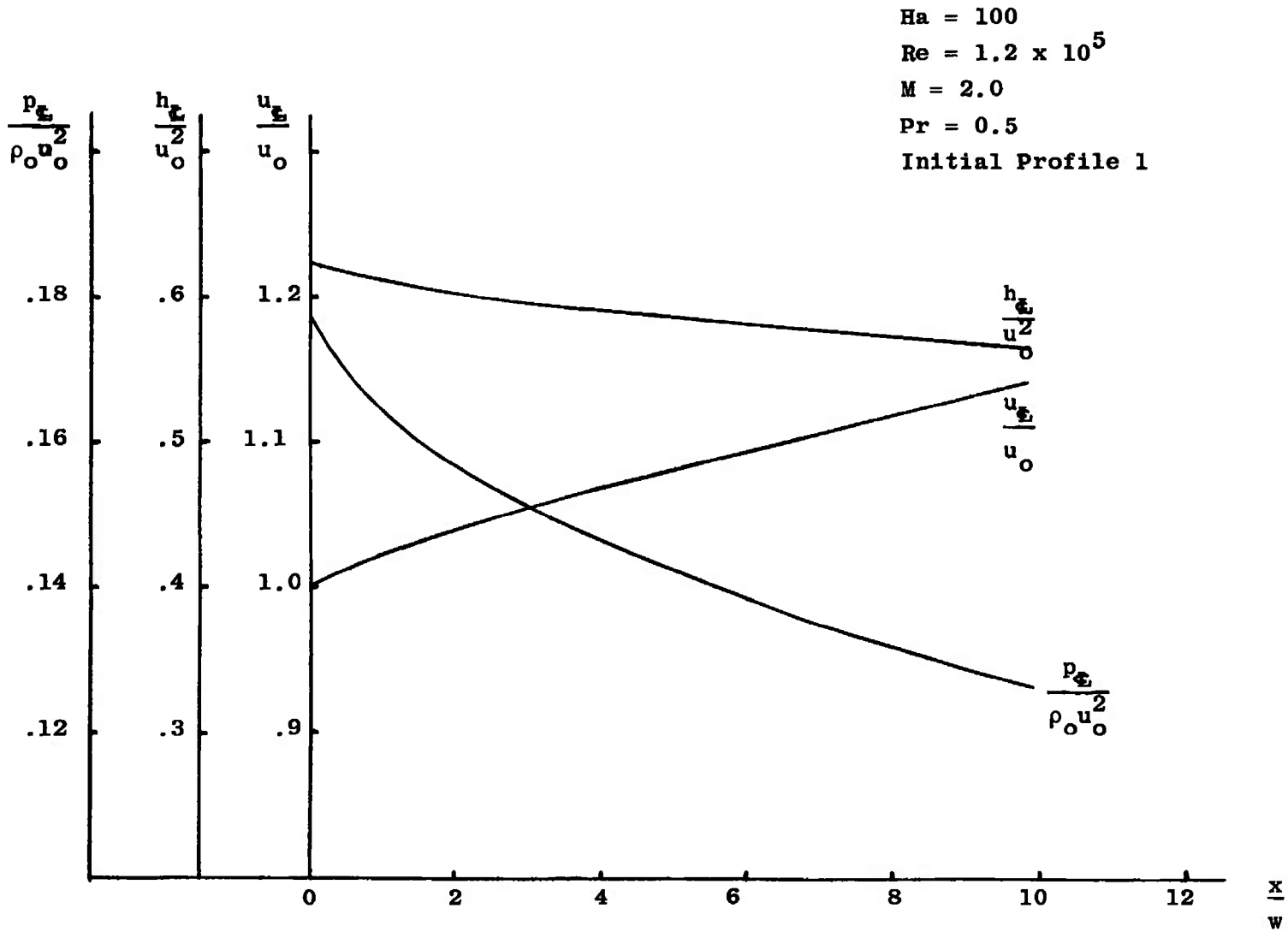

Figure 45. Centerline Distributions of Velocity, Enthalpy, Pressure.

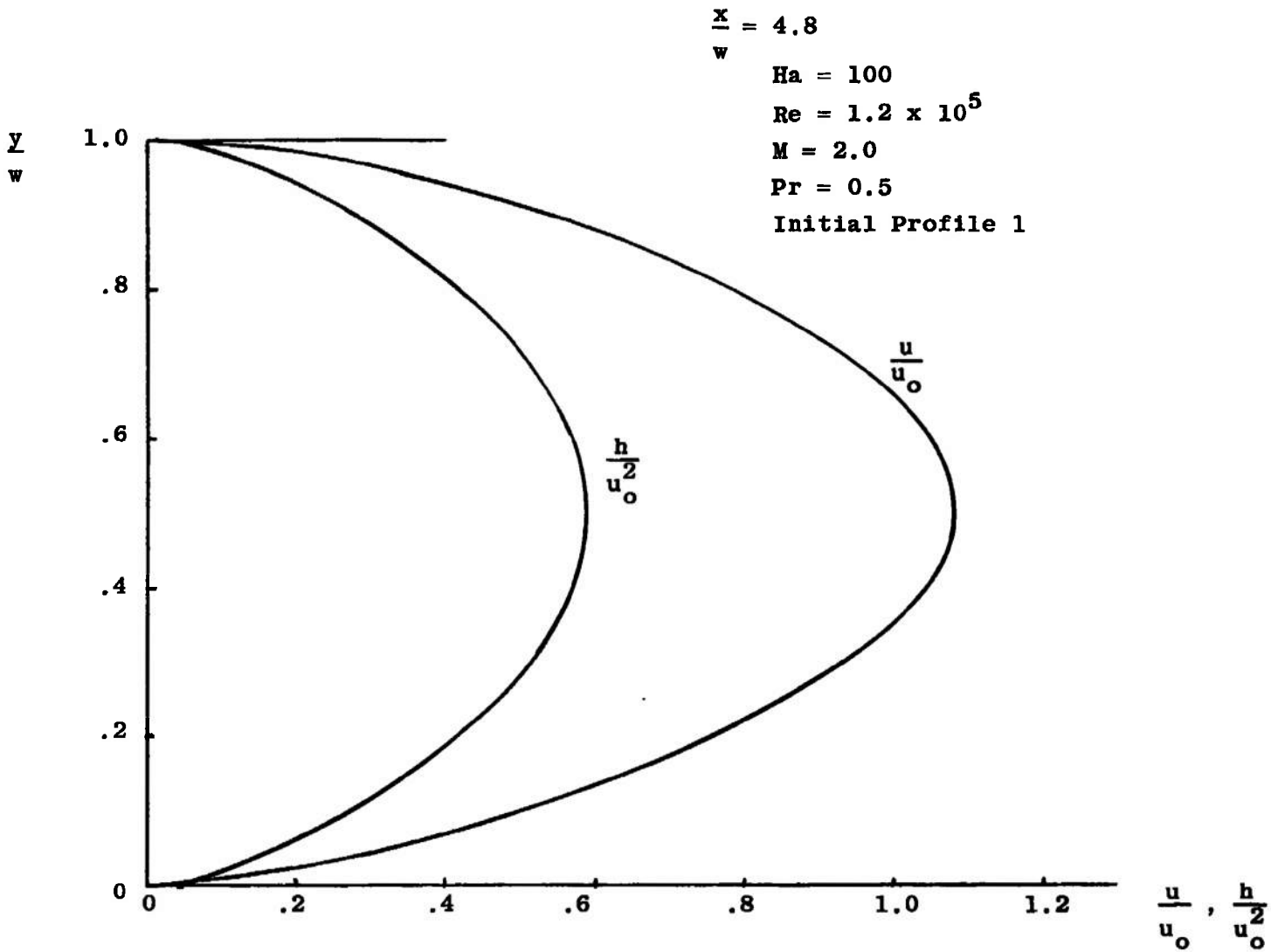

Figure 46. Velocity and Enthalpy Profiles at $x/w_o = 4.8$.

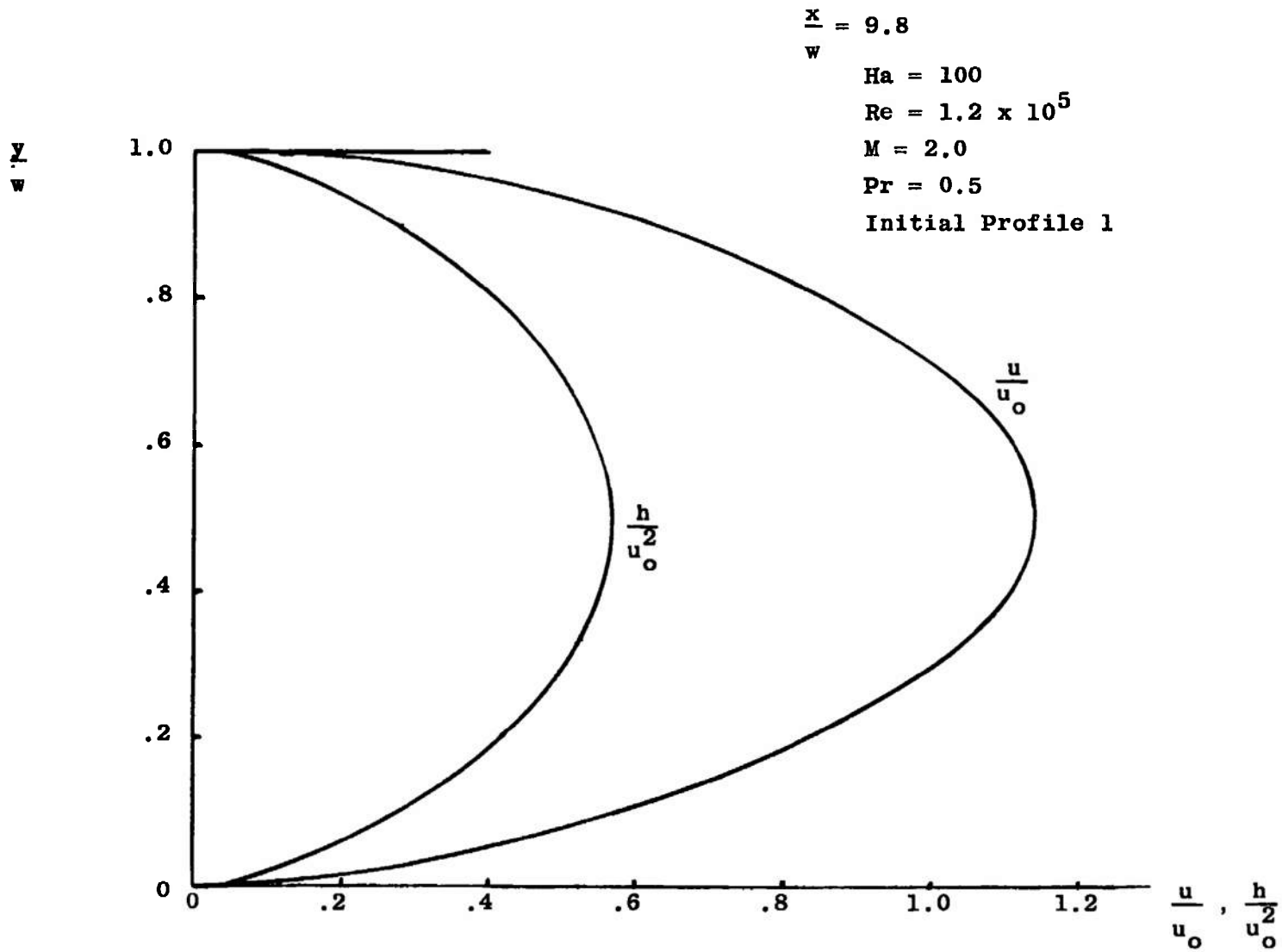

Figure 47. Velocity and Enthalpy Profiles at $x/w_o = 9.8$.

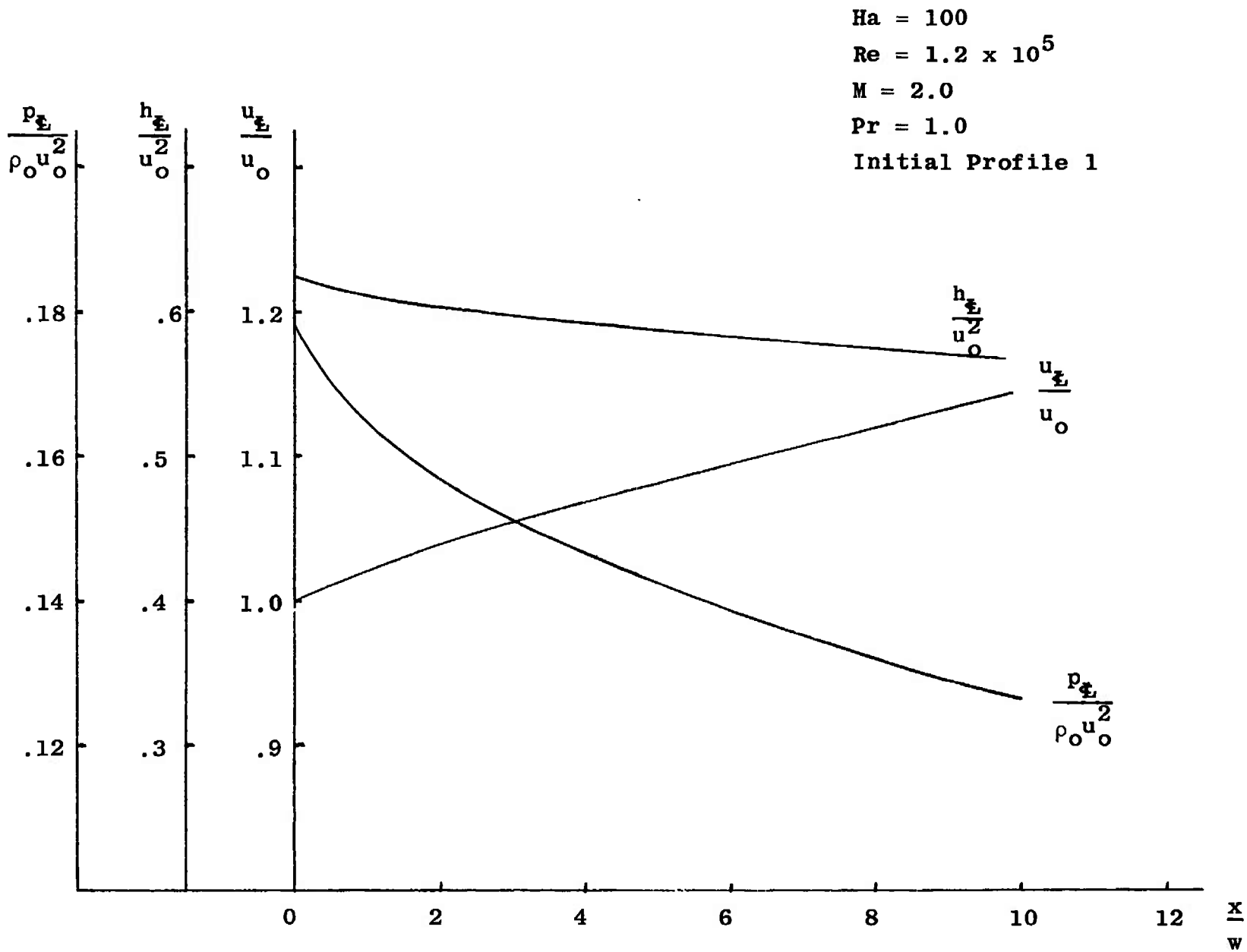

Figure 48. Centerline Distributions of Velocity, Enthalpy, Pressure.

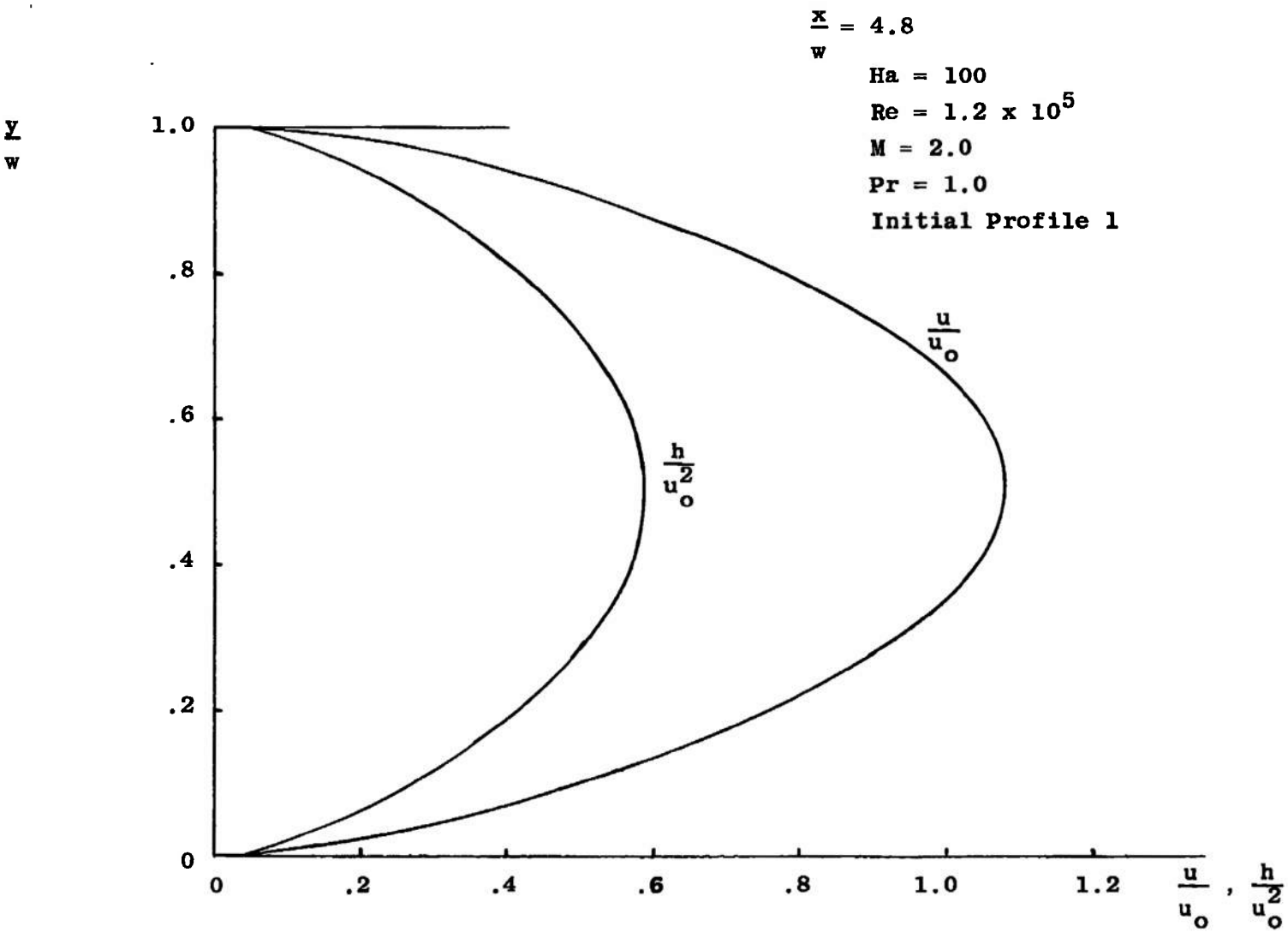

Figure 49. Velocity and Enthalpy Profiles at $x/w_o = 4.8$.

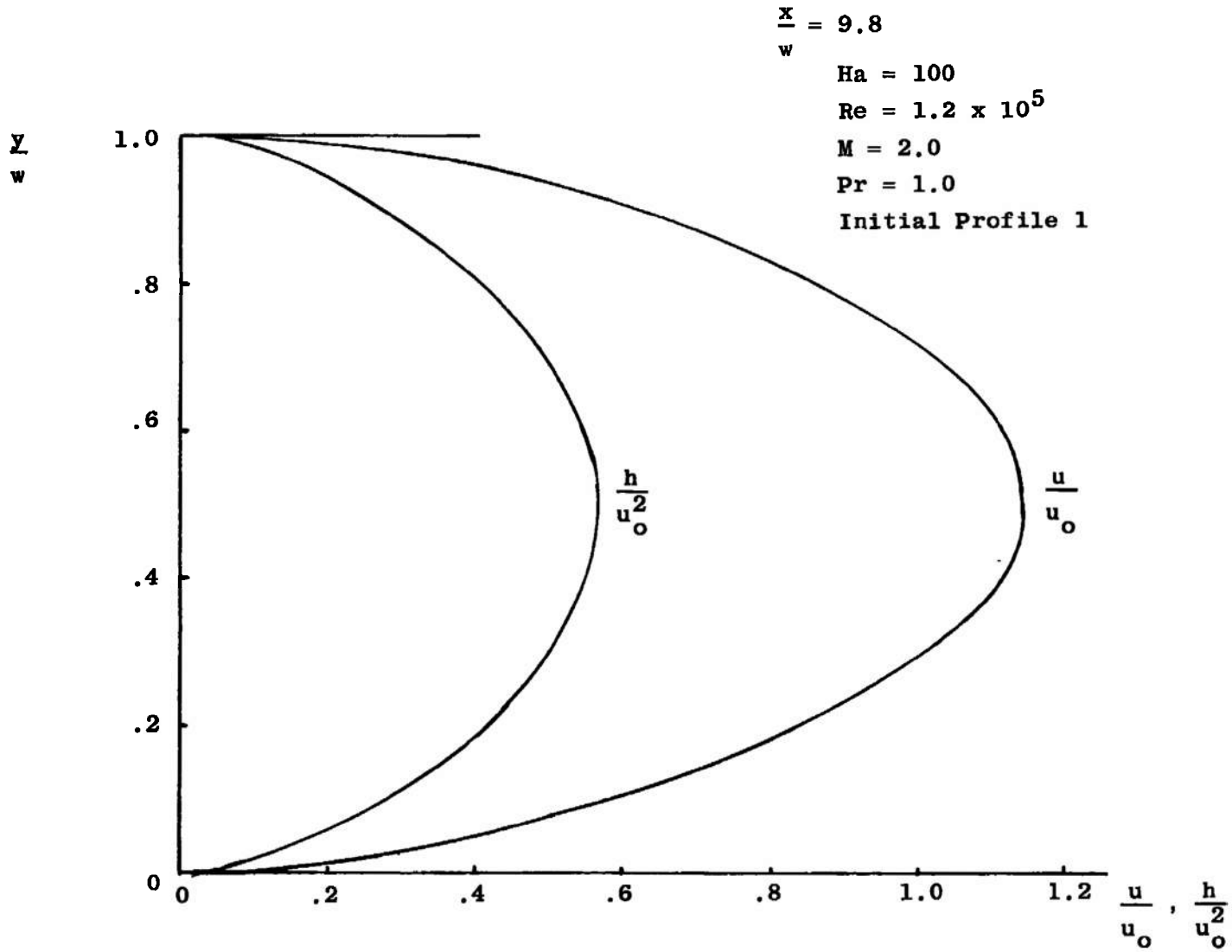

Figure 50. Velocity and Enthalpy Profiles at $x/w_o = 9.8$.

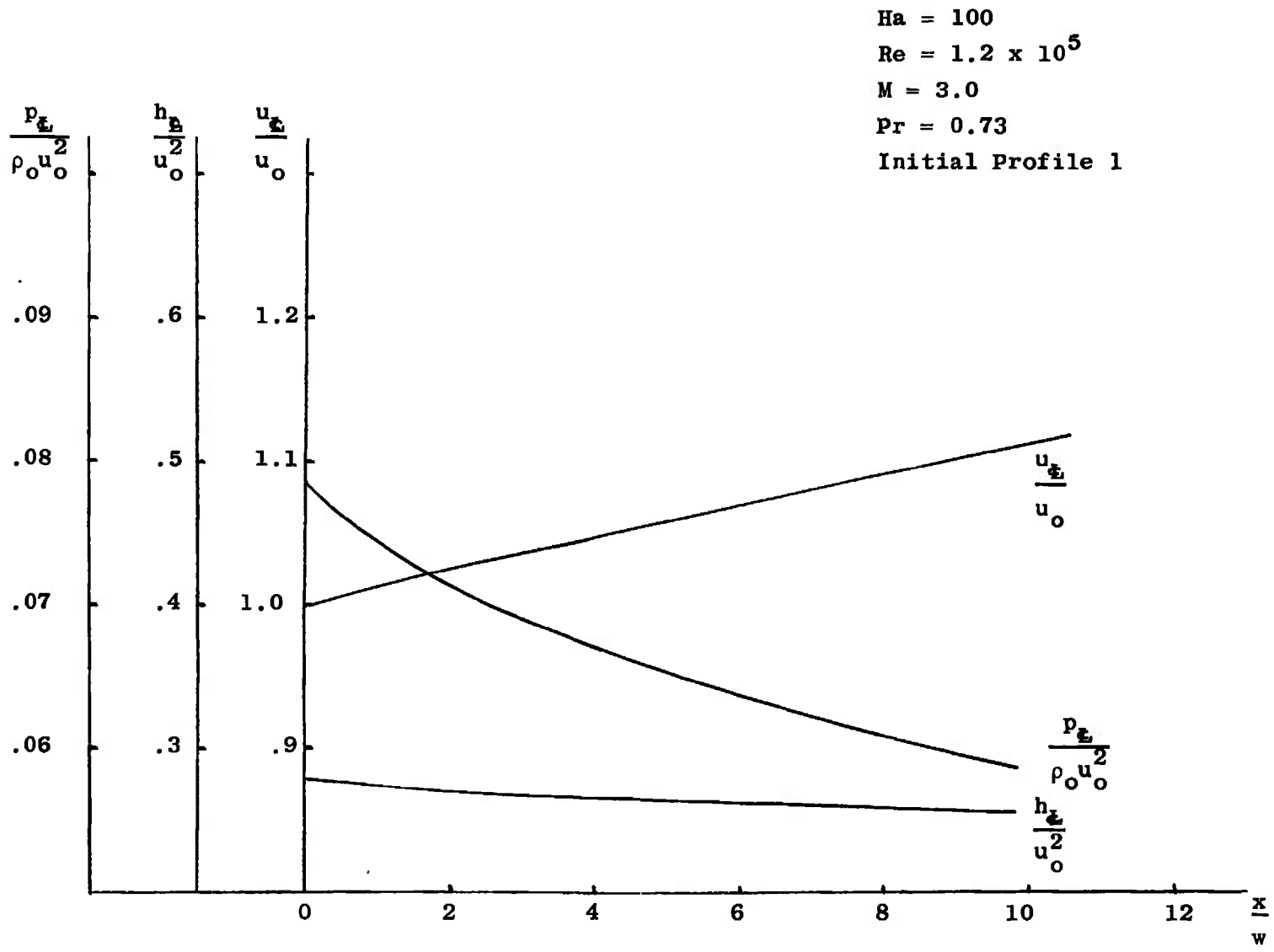

Figure 51. Centerline Distributions of Velocity, Enthalpy, Pressure.

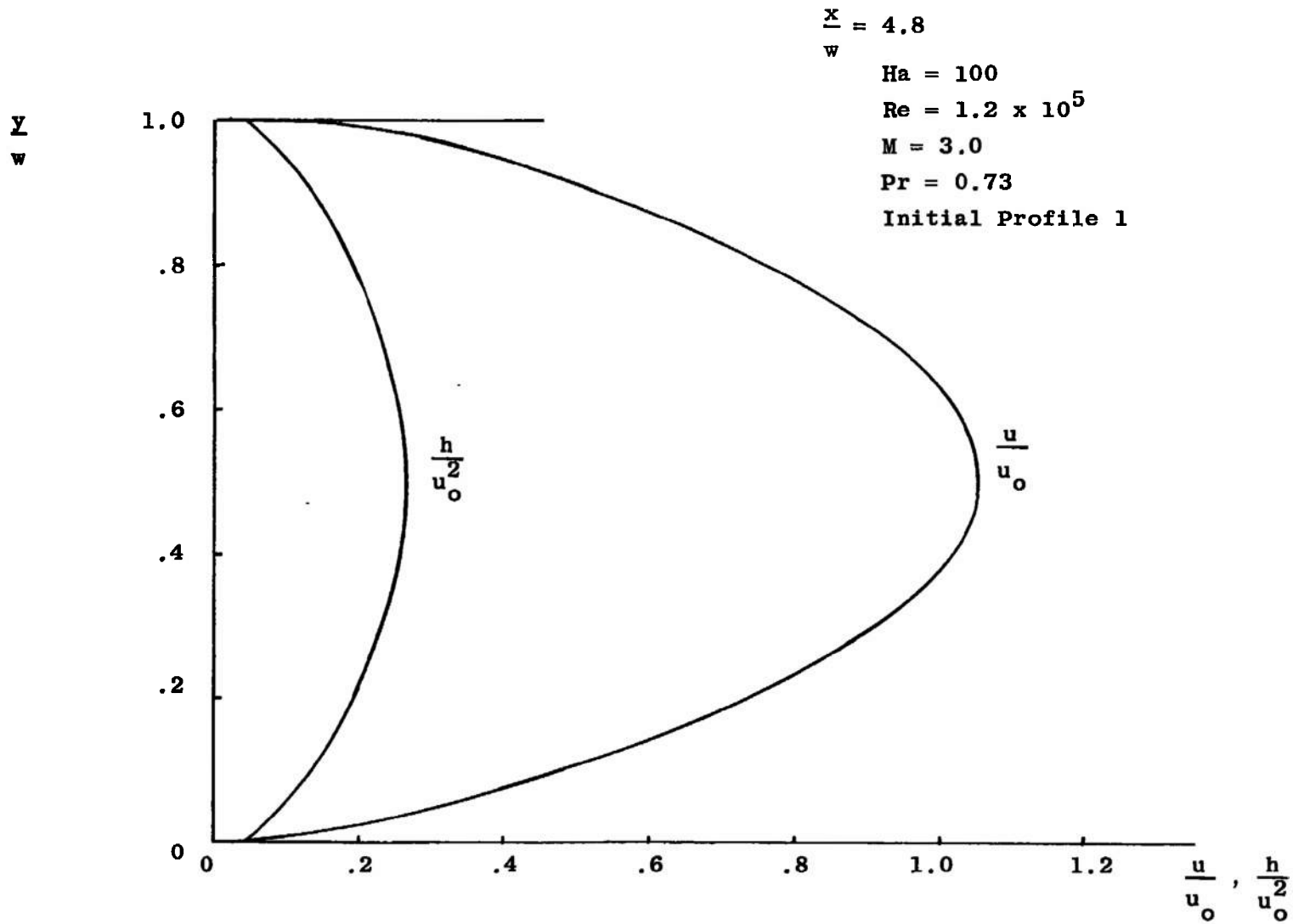

Figure 52. Velocity and Enthalpy Profiles at $x/w_o = 4.8$.

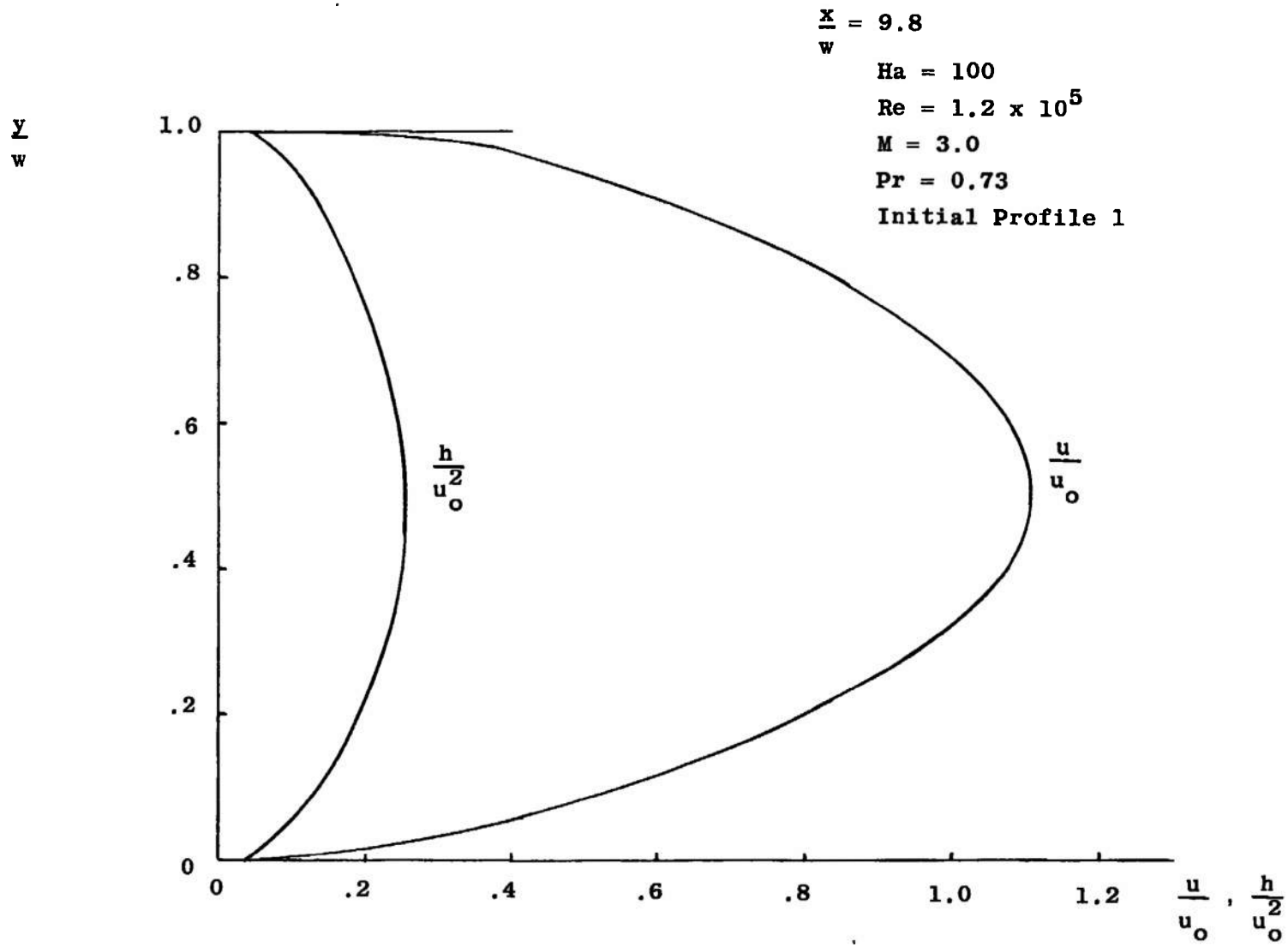

Figure 53. Velocity and Enthalpy Profiles at $x/w_o = 9.8$.

UNCLASSIFIED

Security Classification

DOCUMENT CONTROL DATA - R & D

(Security classification of title, body of abstract and indexing annotation must be entered when the overall report is classified)

1. ORIGINATING ACTIVITY *(Corporate author)*
The University of Tennessee Space Institute
Tullahoma, Tennessee 37388

2a. REPORT SECURITY CLASSIFICATION
UNCLASSIFIED

2b. GROUP
N/A

3. REPORT TITLE
INTERNAL MHD CHANNEL FLOWS INCLUDING HALL EFFECT AND VARIABLE FLUID PROPERTIES

4. DESCRIPTIVE NOTES *(Type of report and inclusive dates)*
Final Report November 26, 1969

5. AUTHOR(S) *(First name, middle initial, last name)*
William T. Snyder and James R. Maus, The University of Tennessee Space Institute

6. REPORT DATE
February 1970

7a. TOTAL NO. OF PAGES
88

7b. NO. OF REFS
18

8a. CONTRACT OR GRANT NO.
F40600-67-C-0001, Task I

b. PROJECT NO.
8950

c. Task 12

d. Program Element 6240533F

9a. ORIGINATOR'S REPORT NUMBER(S)
AEDC-TR-70-26

9b. OTHER REPORT NO(S) *(Any other numbers that may be assigned this report)*
N/A

10. DISTRIBUTION STATEMENT
This document has been approved for public release and sale; its distribution is unlimited.

11. SUPPLEMENTARY NOTES
Available in DDC.

12. SPONSORING MILITARY ACTIVITY
Arnold Engineering Development Center, AFSC, Arnold Air Force Station, Tennessee 37389

13. ABSTRACT

An analysis is presented of MHD channel flow with Hall effect and variable fluid properties. Because of the highly nonlinear nature of the governing conservation equations, a straight numerical analysis of the equations is followed based on the implicit finite difference method. The analysis considers the two-dimensional flow in the electric field plane in which the channel walls are electrode surfaces. Because of the presence of the Hall effect, a transverse pressure gradient is induced in the flow which necessitates the use of two equations of motion in the longitudinal and transverse directions. The analysis model employed is the so-called slender channel model in which the boundary layer forms of the equations of motion are applied across the entire channel width. Because the boundary layer equations are parabolic, it is possible to integrate the equations in a forward marching manner by starting with initially prescribed velocity and enthalpy profiles at the channel entrance.

DD FORM 1 NOV 65 1473

UNCLASSIFIED

Security Classification

14. KEY WORDS	LINK A		LINK B		LINK C	
	ROLE	WT	ROLE	WT	ROLE	WT
magnetohydrodynamics						
mathematical analysis						